



The
University
Of
Sheffield.

Statistically assessing forward-wise and inverse uncertainties in outdoor acoustics

Jordan Aaron Parry

A thesis submitted in partial fulfilment of the requirements for the degree of

Doctor of Philosophy

Department of Mechanical Engineering &

School of Mathematics & Statistics

07 November 2020

DECLARATION

I confirm that this is my own work and the use of all material from other sources has been properly and fully acknowledged.

Jordan Aaron Parry

ABSTRACT

Predicting outdoor sound in uncertain conditions is a difficult task and there are limited data and statistical research which enable us to relate accurately the variations in the conditions in the propagation path to the fluctuations in the received acoustical signal. This research aimed to create better understanding of the propagation of uncertainty, using both forward and inverse case studies, in varied conditions with widely accepted engineering models, so further improvements could be made in our academic understanding and to industrial practices.

The separation of the direction of uncertainty allows for more focus to be focused on each given condition. Firstly, the forward problem is approached by simplifying the model used and conditions in present, to better understand the statistical behaviour across evolving parameter uncertainties. A further study, inspired by current acoustical standards, evaluated whether improvements to data capture could be made by manipulating the physical way the data was obtained, in the presence of varying parameter uncertainties. The inverse problem was investigated for a very specific application of small arms fire, yet the methodology was expanded to show how powerful computationally cheap statistical methods can be used in investigating parameter interactions under given uncertainties, while also accurately inverting the desired parameters.

Investigations have proved successful in characterising, in general and for specific scenarios, the foundational uncertainties in outdoor sound propagation. Methods have been presented that allow for simple yet powerful study into the statistical behaviours of a wide range of outdoor sound propagation problems. Characterising uncertain acoustic data using statistical representations serves to be extremely beneficial, while a physical two-microphone method is shown to be theoretically efficient in negating a large proportion of the uncertainty present, while capturing acoustical data known to be useful for source localisation and characterisation. It is also shown in which direction research should be established in relation to military applications, after showing efficient ways in which computational models be applied to invert important parameters from readily obtainable data.

If one is to understand **the great mystery**, one must study all it's aspects...

TABLE OF CONTENTS

NONCLEMANTURE		i
B INTRODUCTION		1
A.I	Research objectives	1
A.II	Structure of thesis	2
A.III	Contributions to research	3
C FORWARD-WISE UNCERTAINTY		5
B.I	Investigating uncertain geometries effect on sound propagation in a homogeneous and non-moving atmosphere over an impedance ground	5
	Introduction	6
	Research methods	7
	Model development	7
	Simulation methods	9
	Results	10
	Exploring Φ and σ_g	10
	Simulation statistics	11
	Normality assumption	13
	Conclusions	13
	Appendix A: The effect of frequency range	15
	References	16
B.II	Pressure ratio and phase difference in a two-microphone system under uncertain outdoor sound propagation conditions	17
	Introduction	18
	Research methods	19
	The model	19
	Propagation of uncertainty	20

Results	20
Sound pressure amplitude ratio	20
Phase difference	21
Conclusions	25
Appendix A: Table of statistics	26
References	27

C INVERSE UNCERTAINTY28

C.I Outdoor acoustics: Estimation of gunfire over an acoustically soft impedance ground in a homogeneous atmosphere28

Introduction	29
Acoustical Methods	29
Acoustical Foundations	29
Gunshot Evaluation	30
Parameter Selection and Observations	31
Statistical Methods	32
Maximum Log-likelihood Estimation (MLE)	32
Bayesian Maximum a Posteriori (MAP)	32
Computational Error Analysis	33
Results	33
Broadband Analysis	33
Octave Filtering	34
Conclusion	35
References	35

C.II Pressure ratio and phase difference in a two-microphone system under uncertain outdoor sound propagation conditions36

Introduction	37
Research methods	38
Gun source evaluation	38
Acoustical predictions	39
Generating observed SPL	40
Statistical techniques	41
Maximum log-likelihood estimation (MLE)	41

Semi-Bayesian maximum a Posteriori (MAP)	42
Performance metrics	42
Results	43
Inference using broadband data	43
Visualisation of errors	43
Interactions of uncertainties	45
Inference using octave band data	47
Octave band visualisations	48
Conclusions	51
References	51

D CONCLUSIONS 53

D.I Key conclusions 53

D.II Future works 55

D.III Closing remarks 56

E BIBLIOGRAPHY 57

NONCLEMANTURE

List of Symbols

The list of symbols, with units where appropriate, as they appear chronologically. Symbols used twice for different parameters, or parameters that have multiple symbols, due to variations across different studies are marked with an asterisk (*).

r	Range between source and receiver	(m)
z_s	Source height*	(m)
k	Wavenumber	(–)
Q	Spherical wave reflection co-efficient	(–)
p_c	Complex sound pressure	(p)
p_{free}	Sound pressure (free field)	(p)
f	Frequency of sound*	(Hz)
Z	Normalised impedance	(Pasm ⁻¹)
ΔL	Excess attenuation	(dB)
ϕ	Porosity	(–)
α_∞	Tortuosity	(–)
\bar{s}	Median pore size	(m ²)
σ_s	Standard deviation of pore size	(m ²)
$\tilde{\rho}(\omega)$	Frequency dependent bulk dynamic density	(–)
$\tilde{C}(\omega)$	Bulk complex compressibility of the fluid	(–)
ω	Circular frequency*	(Hz)
η	Dynamic viscosity of air	(Pas)
ρ_0	Ambient density of air	(Pas)
γ	Ratio of specific heats	(–)
N_{Pr}	Pradntl number	(–)

P_0	Ambient atmospheric atmosphere	(Pa)
σ'_g	Thermal flow resistivity	(Pasm ⁻²)
σ_g	Effective flow resistivity	(Pasm ⁻²)
$z_b(\omega)$	Characteristic acoustic impedance	(Pasm ⁻³)
μ	Mean (average)*	(-)
Φ	Ratio of source/receiver height over range	(-)
σ	Standard deviation	(-)
s	Skewness	(-)
k_s	Kurtosis	(-)
M_o	Mode (average)	(-)
M_{dn}	Median (average)	(-)
N	Sample size*	(-)
$\overline{\mu_p}$	Average sound pressure amplitude ratio	(-)
$\overline{\mu_\omega}$	Average phase difference ratio	(-)
Δ	Uncertainty	(-)
ω	Frequency of sound*	(Hz)
s_h	Source height*	(m)
r_h	Receiver height	(m)
ϵ_s	Normally distributed error term	(dB)
$\mathcal{L}(\theta X)$	Likelihood function	(-)
$\ell(\theta X)$	Log-likelihood function	(-)
\widetilde{h}_s	Distribution of source heights	(m)
$\widetilde{\sigma}_g$	Distribution of effective ground impedances	(Pasm ⁻²)
r^*	Known true range	(m)
ϵ_r	Error between true and simulated range	(m)

A INTRODUCTION

A.1 Research objectives

Acoustics is the branch of physics which deals with sound waves, including their production, propagation & effects. The sub-branch of outdoor acoustics deals with the propagation of sound in the larger-scales of the outdoor environment. This expansion of the environment from smaller acoustic sub-branches gives rise to a multitude of influencing parameters, in which uncertainty can appear. This causes issues in the prediction, quantification and understanding of acoustics in the outdoors, with the knock-on effect of limiting the effectiveness of industrial practices in these conditions.

The objective of this research was to solidify the foundations of uncertainty in outdoor sound propagation problems; quantifying and explaining the underlying statistics and physics to enhance future research with a strong theoretical basis while also hoping to improve related practices. The immediate practices were motivated by the needs of the industrial sponsor (DSTL UK). Due to the lack of understanding of the fundamental statistical behaviours, various assumptions are applied along the narrative of this research, removing some of the more complex parameters defined earlier which may, or may not, be influential in combination with the presence of uncertainty. The thesis is structured around the logical order of the research, with separation into the respective forward or inverse statistical methodologies, rather than the chronological order of exploration.

The first steps in this research were to establish a strong foundation, asking how does uncertainty effect outdoor acoustics in the most fundamental form? The simplest case considered a 2-D geometry with a non-moving homogenous atmosphere present, removing all meteorological parameters that could possibly interfere with the acoustical study. This leaves only the geometry of the problem with the ground beneath the sound source and the sound receiver. The basic acoustical model (excess attenuation) defined the resulting interaction between a direct sound ray and a reflective ray from the impedance ground known for its ability to characterise the source. Once this case was established, it was asked whether slight variations in geometrical patterns propagate forward quantifiable statistical behaviours? This was studied over multiple impedance grounds with varying acoustical hardness, so results were applicable to many real-life variations **(Paper I)**.

Once a grasp of the fundamental uncertain nature of acoustics was studied, the problem moved from forward to inverse, with how well can parameters be inferred in simple but uncertain conditions? Inversion methods are complex, usually relying on intricate statistical ability to implement. The aim was to show how effective simplistic methods can be. A simple method relying on the maximisation of the likelihood function was applied, using both frequentist and Bayesian methodologies, to range a small handheld firearm. This source was analysed in an anechoic chamber to allow for accurate source data to be simulated. The model (excess attenuation) from **Paper I** was applied in **Paper III**, while a more realistic, but still simplistic, acoustical model (sound pressure level) was employed for more detailed investigations in **Paper IV**. The interactions between combinations of known, and unknown, parameters are studied to show the interactions present while ranging gunfire. The study also aimed to define these statistical methods and their implementations, so they could be applied for any acoustical source or initial conditions (**Paper III** and **Paper IV**).

With studies completed in either direction of uncertainty, the question of how uncertainty affects simple acoustical parameters was expanded to question slightly more complex acoustical output parameters. This led to the question of how, using a two-microphone model, uncertainty effected the phase difference and absolute sound pressure ratio in the presence of varying parameter uncertainties? This used the model (sound pressure level) from **Paper IV**, with additional calculations, combined with the methodology of forward propagation in **Paper I**. Sound level differences are used for acoustical calculations successfully at small scales, but specific research with these methods are lacking in outdoor scales. Varying impedance grounds and geometries, using the understanding developed from earlier studies, were investigated for greater understanding. The applicability of the two-microphone model in outdoor sound propagation was also investigated for the varying conditions (**Paper II**).

A.II Structure of thesis

This thesis is structured as interrelated collection of two published journal papers, one journal paper currently under review (as of 07 November 2020) and one peer-reviewed conference paper. The papers respective chronology is ignored and they are divided into two distinct statistical methodologies they embody: forward-wise and inverse problems.

Papers I, II, III and **IV** were completed within the University of Sheffield campus. **Paper I** and **II** form **Chapter B** while **Paper III** and **Paper IV** form **Chapter C** collectively. **Paper I** and **Paper II** are related by their statistical forward

methodologies. **Paper IV** is the logical progression of the smaller conference (peer-reviewed) **Paper III** that was given at the ICSTA 19'.

Paper I investigates the forward statistical behaviour that relate to using a simple acoustical model (excess attenuation) in the presence of uncertain geometries over a varied impedance ground in a non-moving homogenous atmosphere.

Paper II also investigates statistical behaviours going forward-wise in the presence of uncertain geometries over a varied impedance ground in a non-moving homogenous atmosphere, yet employs a two-microphone model to calculate more complex acoustic outputs (absolute pressure ratio/phase difference).

Paper III shows how a simple acoustical model (excess attenuation) can be combined with a simple Bayesian approach (Maximum A Priori) to the inverse problem of inferring the unknown range of a small firearm over a vegetative impedance ground.

Paper IV further describes how techniques related to maximisation of the likelihood function can be used with a realistic acoustical model (sound pressure level) to infer the unknown range of a small firearm, while describing how competing uncertainties inside other modelled parameters interact.

Finishing the thesis is the conclusions chapter. This includes a further discussion on the impact of the results of this research. Concluding remarks are made about where future study should be focused. A complete bibliography of all sources finishes the thesis, collecting referenced literature in the order of their appearance in the thesis.

A.III Contributions to research

Papers I-IV were written with multiple co-authors, specifically; Myself (**JP**), Kirill V. Horoshenkov (**KH**) and Duncan P. Williams (**DW**). The contributions made to each study can be broken down into the six categories; (i) conception & design, (ii) planning & implementation, (iii) data collection, (iv) analysis & interpretation, (v) writing and (vi) overall responsibility. **Table 1** shows, and acknowledges, where each author has made a contribution to any of **Papers I-IV** using the six defined categories.

Paper I	Paper II	Paper III	Paper IV
----------------	-----------------	------------------	-----------------

Conception & Design	KH; JP	JP; KH	JP	JP
Planning & Implementation	JP; KH	JP; KH	JP; KH	JP
Data Collection	JP	JP	JP; KH	JP; KH
Analysis & Interpretation	JP; KH	JP; KH	JP	JP; KH
Writing	JP; KH; DW	JP; KH	JP; KH; DW	JP; KH
Overall Responsibility	JP	JP	JP	JP

Table 1: Acknowledgements of contributions made to the papers included in this thesis.

B FORWARD-WISE UNCERTAINTY

B.1 Investigating uncertain geometries effect on sound propagation in a homogeneous and non-moving atmosphere over an impedance ground

Paper I – J. A. Parry, K. V. Horoshenkov and D. P. Williams. “Investigating uncertain geometries effect on sound propagation in a homogeneous and non-moving atmosphere over an impedance ground”. Applied Acoustics, 160 (March 2020).



Investigating uncertain geometries effect on sound propagation in a homogeneous and non-moving atmosphere over an impedance ground

Jordan A. Parry^{a,*}, Kirill V. Horoshenkov^a, Duncan P. Williams^b

^a University of Sheffield, Department of Mechanical Engineering, Sheffield, England, United Kingdom

^b Defence Science and Technology Laboratory (DSTL), Salisbury, England, United Kingdom

ARTICLE INFO

Article history:

Received 5 July 2019

Received in revised form 25 October 2019

Accepted 27 October 2019

Available online 14 November 2019

Keywords:

Outdoor sound propagation

Uncertainty

Impedance ground

Receiver geometry

Homogeneous atmosphere

Probability density function

ABSTRACT

Predicting outdoor sound in uncertain conditions is a difficult task and there are limited data which enable us to relate accurately the variations in the conditions in the propagation path with the fluctuations in the received acoustical signal. This paper investigates, through numerical simulations, the effect of uncertainties on sound propagation in a homogeneous atmosphere over an impedance ground. A simple Monte Carlo method is used to understand the effect of uncertainties in the source and receiver positions on the excess attenuation. The ratio of source/receiver height to the horizontal source/receiver separation is found to influence strongly the statistical distribution of the resultant excess attenuation spectrum. Impedance ground and level of uncertainty are found to be influential only for specific statistics while all samples were found to violate normality. These findings help to increase understanding of the role of uncertainties in outdoor sound propagation, accuracy of source characterization based on parameter inversion and at lower computational costs.

© 2019 Elsevier Ltd. All rights reserved.

1. Introduction

Predicting outdoor sound is a complex problem particularly when there is an uncertainty in the parameters involved. Comprehensive quantification of uncertainties in relation to outdoor acoustics remains challenging. One recent paper related to uncertainties in outdoor sound propagation concluded that uncertainties within the characteristics of the ground and atmosphere dominate uncertainties in the predicted sound pressure [1]. A subsequent paper by the same research team found that the impact of uncertainty from the range and source height were equal and that the temperature gradient was only influential at short ranges and at high frequencies [2]. Sound levels were found to be more accurately predicted in downwind situations compared to upwind. The authors also highlighted the importance of balancing the trade-off point between model complexity & computational effort.

The above work points out to the difficulties in isolating specific effects leading to outdoor sound measurement uncertainties and complexity of the interactions between key parameters many of which are not known. Complex models used in the case of inhomogeneous settings (e.g. atmospheric effects) can have better predic-

tion accuracy provided the values of the input parameters are accurately known [3]. However, there is a lack of data on the sensitivity of these models to some uncertainty in the input parameter values. In this respect, moving back to simpler models allows for a clearer understanding of the statistics which describe the uncertainties in predictions for sound propagation in homogeneous, and non-moving, atmosphere but with uncertain source position and ground conditions. Simpler models are able to accurately predict impedance of the ground and isolate this effect from the uncertainty in the source geometry.

Prediction of the ground effect on outdoor sound pressure from a point source at a known position is a reasonably routine matter. A considerable amount of work has been done to study this effect. Harriot and Hothersall investigated propagation, using multiple methods, over an impedance ground in an infinite plane, in a non-moving homogeneous atmosphere, while computational costs were also considered [4]. The specific geometry where source-receiver heights where 1 – 4 m across 50 m range at 1 kHz frequency created strong destructive interference between the direct and reflected waves. Accuracy in results was found to be highest for combinations of greater source-receiver heights or shorter source-receiver distances. More expansive methods were later applied by Kruse and Mellert [5]. They used a two-microphone method to measure errors due to an impedance ground under also under the assumption of a non-moving homogeneous atmosphere.

* Corresponding author.

E-mail addresses: JAParry1@Sheffield.ac.uk (J.A. Parry), K.Horoshenkov@Sheffield.ac.uk (K.V. Horoshenkov), DPWilliams@dstl.gov.uk (D.P. Williams).

For low impedance surfaces, acceptable accuracy was found at frequencies above 100 Hz, while higher flow resistivity grounds shown use of the predefined geometries may not be recommended for frequencies below 500 Hz. Although the results in Ref. [5] relate directly to the problem of sound propagation in the presence of an impedance ground, this work does not present any statistical data that can be used to characterise the uncertainty in the excess attenuation, especially in the case of large variability in the source position.

In general, the effects of uncertainty in key model parameters on prediction of outdoor sound propagation and acoustic source characterisation are greatly understudied. This becomes the motivation for our study with the primary question of this paper: How does an uncertainty in geometrical parameters affect the broadband excess attenuation of sound for a relatively simple source-receiver geometry? The excess attenuation is an important parameter which is routinely used to predict the influence of the ground, topography and meteorological conditions on sound pressure level at the receiver position [3]. Removal of other complexities to understand the effects will build stronger foundations to progress further developments for more complex research and application. Therefore, understanding of the effect of uncertainties on this parameter is of importance to several applications, which include environmental noise control, source characterisation and environmental monitoring.

The purpose of this paper is to study the effect of uncertainty in the range and source height on the statistical properties of the excess attenuation spectrum for a range of ground conditions. We structure the paper in the following manner. Section 2.1 details the acoustical model and ground effect, Section 2.2 details the statistical simulation setup, and Section 3 reviews the results from this simulation. Finally, Section 4 is our conclusions.

2. Research methods

2.1. Model development

2.1.1. Initial acoustic model

Let us assume that a sound wave radiated by a point source propagates above a porous ground in a homogeneous atmosphere. This means that the effects of atmospheric parameters such as wind and temperature gradients can be excluded, leaving only the geometrical parameters such as the source and receiver height and their horizontal separation. This geometric scenario is illustrated in Fig. 1. We assume that the problem is symmetrical, i.e. the sound pressure is predicted in an (x, z) co-ordinate system and the source and receiver are located at $(0, z_s)$ and (r, z) , respectively. The complex sound pressure at the receiver position is [3]

$$p_c = p_{free} \left[1 + Q \frac{R_1}{R_2} \exp(ikR_2 - ikR_1) \right], \quad (1)$$

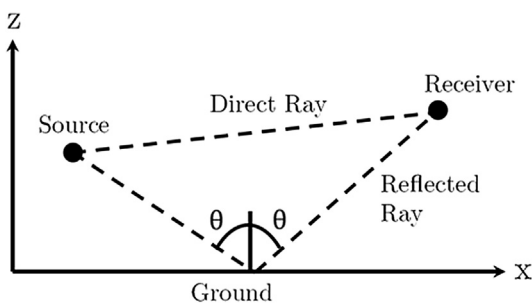


Fig. 1. Diagram of acoustical scenario with impedance ground and incident angle highlighted.

with

$$R_1 = \sqrt{r^2 + (z - z_s)^2}, \quad (2)$$

$$R_2 = \sqrt{r^2 + (z + z_s)^2}. \quad (3)$$

k and Q are the wavenumber and spherical wave reflection coefficient, respectively. p_{free} is the sound pressure in the absence of the impedance ground. The imaginary part of the wavenumber accounts for the attenuation in air. The reflection coefficient accounts for the proportion of the incident sound pressure reflected from the porous ground and any phase changes the reflected acoustic wave undergoes due to the ground effect. As detailed by Salomons in his book [6], the equation for the spherical wave reflection coefficient is

$$Q = \left(\frac{Z \cos \theta - 1}{Z \cos \theta + 1} \right) + \left(1 - \left(\frac{Z \cos \theta - 1}{Z \cos \theta + 1} \right) \right) F(w). \quad (4)$$

The angle θ is the incident angle as shown in Fig. 1. The function $F(w)$ is the boundary loss factor

$$F(w) = 1 + iw\sqrt{\pi} \exp(-w) \operatorname{erfc}(-iw), \quad (5)$$

and $\operatorname{erfc}(-iw)$ the complimentary error function

$$\operatorname{erfc}(z) = \frac{1}{\sqrt{2\pi}} \int_z^\infty \exp(-t^2) dt. \quad (6)$$

The parameter Z seen in Eq. (4) is the normalised impedance of the ground, which depends greatly on the ground characteristics. The sound pressure levels in the presence and absence of the ground are

$$p_c \rightarrow L_p = 10 \log_{10} \left(\frac{|p_c|^2}{2p_{ref}^2} \right), \quad (7)$$

$$p_{free} \rightarrow L_{p,free} = 10 \log_{10} \left(\frac{|p_{free}|^2}{2p_{ref}^2} \right), \quad (8)$$

respectively. Combining Eqs. (7) and (8) gives

$$L_p = L_{p,free} + \Delta L. \quad (9)$$

The term ΔL in Eq. (9) is the relative sound pressure level, or excess attenuation. This term can be expressed as

$$\Delta L = 10 \log_{10} \left| 1 + Q \frac{R_1}{R_2} \exp(ikR_2 - ikR_1) \right|^2. \quad (10)$$

This value physically represents deviation from the free field due to the influence of the ground. The excess attenuation can take positive and negative values that correspond to the constructive and destructive interference between the direct and reflected waves, respectively. The excess attenuation is used for a wide range of acoustics purposes, especially in outdoor acoustics, which is why it will be the predicted value in question during the analysis of the influence of the parameter uncertainties. Examples of possible excess attenuation spectra over different source/receiver geometries and impedance grounds are illustrated Fig. 2. Excess attenuation exhibits oscillatory behaviour as frequency increases and is greatly dependent on the geometrical parameters. However, in real cases the maximum value never exceeds 6dB. The difference in excess attenuation due to the acoustic hardness of the ground is both sensitive to the sound frequency and geometrical parameters. Direct analysis of the excess attenuation is rather complicated because the maxima and minima in this spectrum depend strongly on the problem geometry and ground properties. This makes it difficult to use the excess attenuation spectrum for the ground parameter inversion, source characterisation or for the inversion

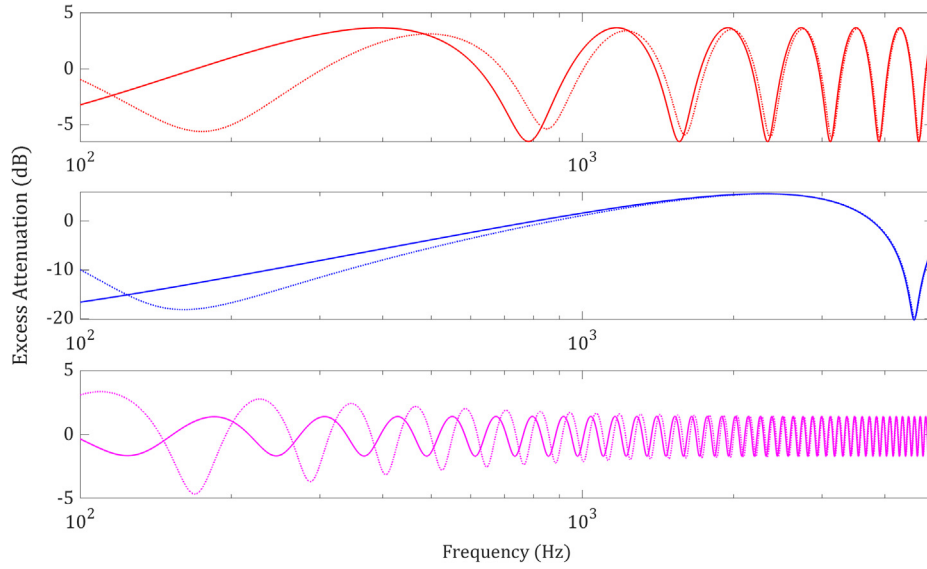


Fig. 2. Example excess attenuation spectrum. Top – source/receiver separation is 10m and source/receiver heights are 1.5m. Middle – source/receiver separation is 60m and source/receiver heights are 1.5m. Bottom – source/receiver separation is 10m and source/receiver heights are 4m. Solid line – acoustically ‘hard’ impedance ground. Dashed line – acoustically ‘soft’ impedance ground.

of the problem geometry acoustically. A question which this paper poses is: Can we adopt a statistical measure of sound pressure in the wave propagated above porous ground to quantify its variability due to some level of uncertainty in the problem geometry and ground properties? This paper attempts to answer this question using the probability density function for the excess attenuation of sound propagation above a porous ground in the presence of uncertainties, discovering from sampling methods.

2.1.2. Measuring impedance

The normalised impedance, Z , in the spherical wave reflection co-efficient (Eq. (4)) can be predicted with an acoustic model if the ground is assumed to be porous. The model used in this work was the one proposed by Dazel, Groby and Horoshenkov et al. [7]. This model calculates the acoustic properties of the impedance ground by considering the ground as a porous media with circular pores of non-uniform cross-section. This model assumes that the pore size is log-normally distributed. It requires four non-acoustical parameters to predict the ground impedance: (i) porosity (ϕ); (ii) tortuosity (α_∞); (iii) median pore size (\bar{s}); and standard deviation in the pore size (σ_s). If the median pore size in the ground is much less than the boundary layer thickness for all the frequencies of interest, then it has been shown that one can assume that $\alpha_\infty \sim 1$, $\phi \sim 1$ and $\sigma_s \sim 0$. In this case the only influential parameter is the median pore size, (\bar{s}).

In this work we use the Padé approximations for the frequency dependent bulk dynamic density, $\tilde{\rho}(\omega)$, and bulk complex compressibility, $\tilde{C}(\omega)$, in the equivalent fluid model to predict the acoustical properties of porous media with log normal distribution, with circular frequency ω . The bulk dynamic density can be approximated by

$$\frac{\tilde{\rho}(\omega(\epsilon_\rho))}{\rho_0} \simeq \frac{\alpha_\infty}{\phi} \left(1 + \epsilon_\rho^{-2} \tilde{F}_\rho(\epsilon_\rho) \right), \quad (11)$$

where

$$\tilde{F}_\rho(\omega) = \frac{1 + \theta_{\rho,3}\epsilon_\rho + \theta_{\rho,1}\epsilon_\rho}{1 + \theta_{\rho,3}\epsilon_\rho}, \quad (12)$$

is the Padé approximation to the viscosity correction function with $\epsilon_\rho = \sqrt{-\frac{i\omega\rho_0\alpha_\infty}{\phi\sigma_g}}$. In these approximations, the coefficients are real and positive numbers with $\theta_{\rho,1} = \frac{1}{3}$, $\theta_{\rho,2} = \sqrt{1/2}e^{\frac{1}{2}(\sigma_s \log(2))^2}$ and $\theta_{\rho,3} = \frac{\theta_{\rho,1}}{\theta_{\rho,2}}$. The equation for the bulk flow resistivity in the porous medium is

$$\sigma_g = \frac{\eta}{\kappa_0} = \frac{8\eta\alpha_\infty}{\bar{s}^2\phi} e^{6(\sigma_s \log(2))^2}, \quad (13)$$

with η being the dynamic viscosity of air and ρ_0 the ambient density of air. Likewise, the bulk complex compressibility of the fluid in the material pores can be equated as

$$\tilde{C}(\omega) = \frac{1}{\gamma P_0} \left(\gamma - \frac{\gamma - 1}{1 + \epsilon_c^{-2} \tilde{F}_c(\epsilon_c)} \right), \quad (14)$$

with

$$\tilde{F}_c(\epsilon_c) = \frac{1 + \theta_{c,3}\epsilon_c + \theta_{c,1}\epsilon_c}{1 + \theta_{c,3}\epsilon_c} \quad (15)$$

In the above two equations $\theta_{c,1} = \frac{1}{3}$, $\theta_{c,2} = \sqrt{1/2}e^{\frac{3}{2}(\sigma_s \log(2))^2}$, $\theta_{c,3} = \frac{\theta_{c,1}}{\theta_{c,2}}$.

The frequency dependant parameter is $\epsilon_c = \sqrt{\left(-\frac{i\omega\rho_0 N_{Pr}}{\sigma_g}\right)}$ with γ

the ratio of specific heats, N_{Pr} the Prandtl number and P_0 the ambient atmospheric pressure. Thermal flow resistivity is defined here as the inverse of the thermal permeability

$$\sigma'_g = \frac{\eta}{\kappa'_0} = \frac{8\eta\alpha_\infty}{\bar{s}^2\phi} e^{-6(\sigma_s \log(2))^2} \quad (16)$$

Combining Eqs. (11) and (14) predicts the characteristic acoustic impedance

$$z_b(\omega) = \sqrt{\frac{\tilde{\rho}_b(\omega)}{C_b(\omega)}}, \quad (17)$$

and complex wavenumber

$$k_b(\omega) = \omega \sqrt{\tilde{\rho}_b(\omega) C_b(\omega)}, \quad (18)$$

in a porous medium with log-normal pore size distribution.

2.2. Simulation methods

2.2.1. Parameter uncertainties

To create uncertainty in our desired parameters, random distributions around some true value of interest are generated. The context of true (known) value is that the user may know the true value, whereas our computational model only sees a random number generated from the distribution that was created from the known value. The uncertainty is varied by manipulating the widths of the distributions in proportion to the true value.

Uniform distributions are used to denote uncertainty around a parameter. The uniform distribution denoted $U[a, b]$, is a flat, or square, distribution between a lower and upper limit, being a and b here respectively. It is common practice to use uniform and normal distributions to simulate error. However, this paper is investigating the systemic uncertainty in the modelling process. Therefore, a flat uncertainty distribution for an input parameter is used so that any parameter value between the bounds is assumed as equally probable. This form of uncertainty is analogous to an observer knowing bounds of a parameter but no other knowledge. It should be noted that the distribution is non-normal by nature. The probability density function (PDF hereon) of the continuous uniform distribution is written as

$$f(x) = \begin{cases} \frac{1}{b-a} & \text{for } a \leq x \leq b, \\ 0 & \text{for } x < a \text{ or } x > b. \end{cases} \tag{19}$$

In this study, distributions around some parameter, say y , with the true known true value, y^* , are generated via

$$y \sim U((0.95 \times y^*), (1.05 \times y^*)) , \tag{20}$$

$$y \sim U((0.8 \times y^*), (1.2 \times y^*)) . \tag{21}$$

$$y \sim U((0.65 \times y^*), (1.35 \times y^*)) . \tag{22}$$

This creates a proportional uncertainty of $\pm 5\%$, $\pm 20\%$ and $\pm 35\%$ around the true value, respectively. These percentages are chosen to simulate a gradual decrease in the precision of an estimate by an observer, i.e. 5% shows confidence in the chosen interval whereas 35% shows a lack of thorough belief, allowing the value to be within a larger probability distribution interval. Due to the adopted nature of uniform probability distribution our true value is always the mean value as $\mu = \frac{1}{2}(a + b)$. These distributions are applied to simulate uncertainty in source/receiver height and range.

2.2.2. Sampling methods

The propagation of uncertainty, along with its related effects, is analysed using a basic Monte Carlo method. This simple Monte Carlo method generates a probability density function, or PDF, by repeatedly sampling from the parameter distributions described in the previous section and then inputs the generated parameter values, along with known parameters, into the excess attenuation model (Eq. (10)) over 10,000 runs. Within the context of uncertainty, it assumed that our model for this purpose of use is perfect. Therefore, no error term is included as it is assumed that the model output is precisely the real-life answer produced by the input parameters given.

The frequency range of 100Hz– 5kHz is used. In this simulation, 1000 frequency points are used, with each point used for the 10,000 main runs to cover equidistantly this broadband frequency range. The frequency range of 100 Hz – 5 kHz was adopted as a balance between computation costs, ability to measure outdoor sound pressures accurately and frequency composition of the sound pressure spectra radiated by realistic sources (see Figures 1.2, 1.3 and 9.25 in Ref. [3] and Figure 3.12 in Ref. [6]). The choice of frequency

range can be important and needs to fit a given application. Appendix A presents data from Monte Carlo simulation showing the effect of the adopted frequency range on the statistical distribution of the excess attenuation against an expanded frequency range.

In order to understand better the ground effect on the uncertainty four types of ground are studied: soft (35 kPam^{-2}); medium (500 kPam^{-2}); hard (2000 kPam^{-2}) and effectively rigid ($20,000 \text{ kPam}^{-2}$). The adopted values of the flow resistivity represent experimental data of real-life impedance grounds [8]: urban grass, sports field, gravel and concrete respectively. It is convenient to adopt a dimensionless parameter when dealing with the problem geometry. An obvious dimensionless parameter is the logarithm of the ratio of source/receiver height over range

$$\Phi = \log_{10} \left(\frac{R_h}{R} \right). \tag{23}$$

This parameter controls the problem geometry and its values are listed in Table 1 for a range of source/receiver height and range combinations. The maximum true value of height is 4 m due to knowledge that our model would not be as reliable for higher source/receiver positions because of the progressive effect of the wind and temperature gradients. The source height takes the same true value as the receiver height in these simulations for simplicity.

2.2.3. Statistical analyses

Statistical analysis accompanies the results from the Monte Carlo simulations. Visually, simulation results are displayed via histograms which present the probability density of the excess attenuation for a given uncertainty in the input parameters. Histograms are generated from the sample data by grouping the data into a number of bins. Since bin width is important, Scott's method [9] is used to choose a sensible number of bins to be generated from each sample. This method assigns bins based on the sample standard deviation and sample size. This became more important when filtering into octave bands as each band's sample size is different due to the sliding octave band width which increases with frequency.

Statistical moments calculated from the simulated data for the excess attenuation accompany our analysis. Four key moments in this analysis are: mean (μ); standard deviation (σ); skew (s); and kurtosis (k_s) while the mode (M_o) and median (M_{dn}) averages are also investigated. These moments allow us to quantify the behaviour of the probability density function for the excess attenuation presented in the histograms. One behaviour that can be described as normality. Normality is a key check with the validity of many statistical tests dependent on this assumption. It has been reviewed that around half of scientific literature articles published contain at least one error, highlighting the need for more validation in future works [10]. Such statistical procedures, especially those commonly used by non-statistical acousticians, such as; correlation, regression, analysis of variance and other such parametric

Table 1
Values of Φ and their geometrical parameter combinations.

Height (m)	Range (m)	Φ
1	200	-2.301
1	100	-2
2	100	-1.699
3	100	-1.523
4	100	-1.398
2	25	-1.097
3	25	-0.921
2	9.5	-0.677
3	8.3	-0.442
4	6.6	-0.218
2	2	0

tests are based on the assumption that the data is normally distributed, or more specifically, that the population that has been sampled from is a normal distribution [11].

Normality can be tested using various methods and tests, but the *Anderson-Darling test (A-D test)* will be used on simulated samples [12]. This test confirms whether the sample came from a population of a given distribution i.e. the normal distribution. It is a modification of *Kolmogorov-Smirnov test*, but gives more weight to the tails. The A-D test makes use of the specific distribution in calculating critical values. The A-D test statistics, A , is defined as

$$A^2 = -N - S, \tag{24}$$

where

$$S = \sum_{i=1}^N \frac{(2i-1)}{N} [\ln F(Y_i) + \ln(1 - F(Y_{N+1-i}))]. \tag{25}$$

N is the sample size, F is the cumulative distribution function (CDF) of the specified parameter distribution (the normal distribution in our case), and Y_i are ordered from smallest to largest. A^2 is then compared to the known *critical value* (C_v) for a given distribution, or the normal distribution for this paper's purpose (calculation of this value is outside the scope of this paper). If $A^2 < C_v$ then the null hypothesis (H_0) is accepted, and the data is assumed to follow a normal distribution (normality is not violated). If $A^2 > C_v$, then the null hypothesis is rejected and the alternative hypothesis (H_a) is accepted at a given significance level ($\alpha \leq 0.005$), allowing us to state the sample does not follow the normal distribution and normality is violated.

The values of the statistical moments are calculated from the simulated broadband and octave band excess attenuation data to be analysed. The median is defined as the middle point value of the data. The mean, or expected value $E(y) = \mu$, of the data is calculated by

$$\mu = \frac{1}{N} \sum_{i=1}^N y_i, \tag{26}$$

where y_i is a data point in the excess attenuation spectrum and N is the total number of data points. These two averages usually are in a similar position in a symmetric distribution. The sample standard deviation, a measure of how much data varies from the mean, is calculated as

$$\sigma = \sqrt{\frac{1}{N-1} \sum_{i=1}^N (y_i - \mu)^2}. \tag{27}$$

The skewness is a measure of asymmetry of data around the sample mean. For example, a perfect uniform distribution would have the value of 0, as would any other perfectly symmetric distribution such as the normal distribution. Negative and positive skewness mean that the sample data is *stretched* more to the left or right from the mean, respectively. As a general rule, data which has skewness of less than $|\pm 0.5|$ can be considered symmetrical. Data is highly skewed when skewness exceeds $|\pm 1|$. If the skewness is larger than 2, or smaller than -2 , then the data is strongly non-normal [12]. The skewness is calculated as

$$s = \frac{\sum_{i=1}^N (y_i - \mu)^3 / N}{\sigma^3}. \tag{28}$$

Kurtosis measures how outlier-prone, or how heavy-tailed or light-tailed the distribution is, in relation to a normal distribution. The kurtosis of a perfect normal distribution is 3, while the kurtosis of a perfect uniform distribution is 1.8. Distributions that are more, or less outlier-prone than the perfect normal distribution have kurtosis greater, or less, than 3 respectively. Kurtosis values between 1

and 5 are accepted for the assumption of normality [12], while values below 0 or greater than 7 would indicate a substantial departure from normality [12]. This final value is equated as

$$k_s = \frac{\sum_{i=1}^N (y_i - \mu)^4 / N}{\sigma^4}. \tag{29}$$

The median (M_{dn}) is found by locating the $(\frac{n}{2})^{\text{th}}$ point in the data set, where n is the number of points in the set. Since our data samples are an even number, the *middle value* between the two numbers that surround the $(\frac{n}{2})^{\text{th}}$ point is taken. The mode (M_o) is taken as the estimate that appears the most, also seen as the most likely value in the PDF (Figs. 3–6).

3. Results

The effect of ground impedance is well known to be greatly influential on the acoustical signal. However, the differences in the PDFs for the excess attenuation found for different values of Φ over the different ground types are not as pronounced as expected (see Figs. 3–6). Sample means and medians did not significantly differ across the range of the flow resistivity, σ_g . However, some statistical moments do show some consistent differences. This strongly suggests that the effect of the problem geometry on the excess attenuation statistics are dominant for this particular propagation model.

3.1. Exploring Φ and σ_g

Some differences do exist in the simulated PDFs for the different values of flow resistivity σ_g (see Figs. 3–6) and these behaviours are mirrored in the value of the statistical moments (see Tables 2 and 3). However, there is some consistency in the PDF for particular values of the parameter Φ . The most obvious differences between the results for different impedance grounds are for $\Phi < -2$. As σ_g is increased, the long smooth distribution has its deviation reduced by half between the softest and hardest impedance grounds (see Figs. 3 and 6 respectively). It is unclear what distribution these results follow. The PDFs presented in Figs. 3–6 appearing irregular and suggest some non-normality within the data.

When $-2 < \Phi < -1$ the PDF for the excess attenuation contains a clear peak which amplitude depends on the level of uncertainty in the adopted values of geometrical parameters. These data are associated with a strongly negative skewness and relatively large standard deviation (see Table 3). These peaks appear in the range of $0\text{dB} < \Delta L < 5\text{dB}$. A very small secondary peak emerges at $\Delta L \approx -5\text{dB}$, doing so more strongly as σ_g increases. The second peak in the PDF becomes clearly visible in the range of $\Delta L \leq -5\text{dB}$ when the ratio Φ increases for $\Delta L > -1$. The peaks' initial value changes depending on the value of σ_g , yet with no consistent pattern in relation to the change of σ_g . This peak directly relates to the mode (see Table 2), which makes the behaviour easier to describe. The amplitude of this second negative peak increases with an increase in the ratio Φ with its position moving progressively towards $\Delta L = -1\text{dB}$ for the lowest value of σ_g and to $\Delta L = -4\text{dB}$ for the highest value of σ_g .

For ratios $\Phi \approx 0$ the PDF of the excess attenuation spectrum appears increasingly bimodal, with the space between peaks increased, and the strength of the negative peak decreased, by the increase in σ_g . However, the increase in uncertainty and σ_g negates the second peak at the negative point, smoothing out the distribution.

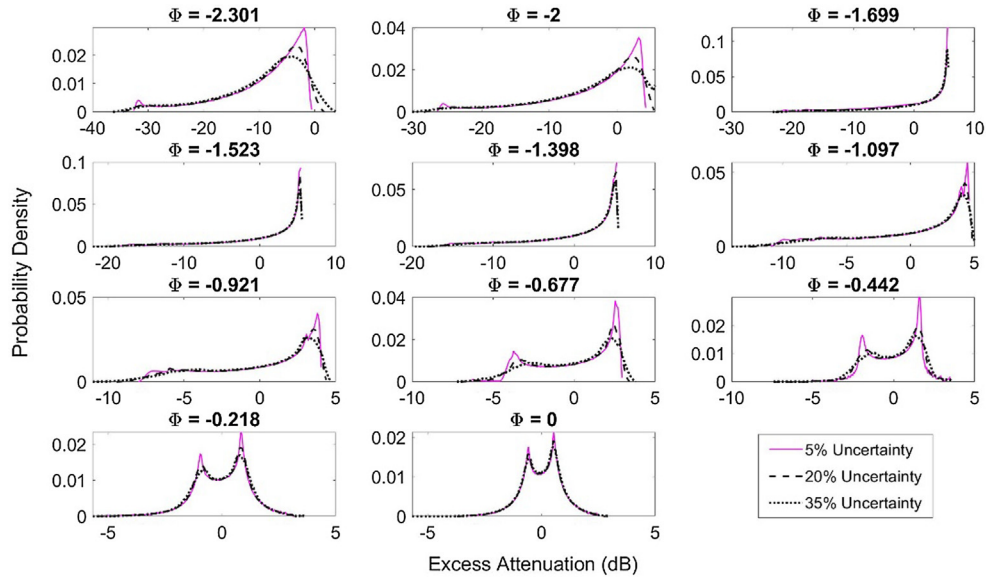


Fig. 3. The PDFs of excess attenuation spectra for a range of values of Φ and levels of uncertainties in the source/receiver coordinates. The flow resistivity of the ground is $\sigma_g = 35 \text{ kPasm}^{-2}$.

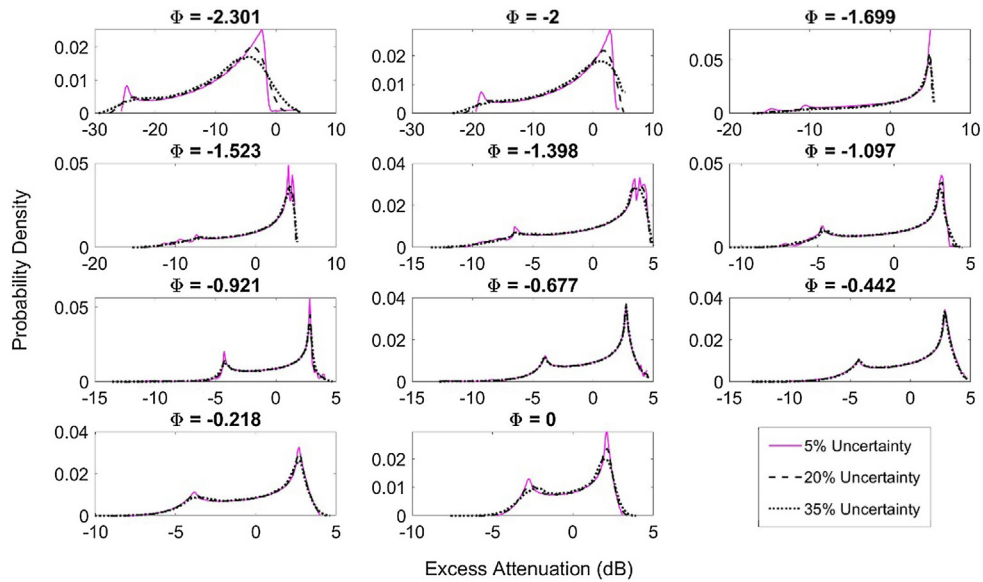


Fig. 4. The PDFs of excess attenuation spectra for a range of values of Φ and levels of uncertainties in the source/receiver coordinates. The flow resistivity of the ground is $\sigma_g = 500 \text{ kPasm}^{-2}$.

3.2. Simulation statistics

The statistics can be described by a number of *statistical moments*. It seems that the statistics for $\Phi < -2$ are inconsistent, and hard to describe in relation to combinations of differing values for Φ , σ_g and uncertainty.

Looking at the averages, the mean (see the 3rd column of Table 2) is the most stable and unaffected. For $\Phi > -1$, the mean is close to 0dB. For $\Phi < -2$ the mean is highly negative (see Table 2). This behaviour is seemingly unaffected by the change in the uncertainty level. As the ground becomes much harder, the mean for $\Phi < -2$ increases.

This suggests that the true mean of the population (the data set which each sample intends to replicate) is not strongly affected by the variation in Φ or σ_g . This is useful for shaping fitting distribution to data that require the use of the mean i.e. the normal distribution of $N \sim (\mu, \sigma^2)$.

The median (see the 4th column of Table 2) follows a similar behaviour to that observed for the mean while around 1dB higher. For a harder ground ($\sigma_g \geq 2000 \text{ kPasm}^{-2}$) it displays an oscillatory behaviour as a function of Φ . The increased median, in relation to the respective mean for a given Φ and σ_g is expected due to the negative skew.

The most repeated observed value, the mode (M_0) (see the last column of Table 2), is the average most effected by σ_g , Φ and uncertainty. The mode begins at 5dB when $\phi \approx -2$ which decreases to 2dB when Φ is decreased to zero. Each mode is reduced by 0.5dB per each increase in σ_g at every respective related value of Φ . Uncertainty does increase the mode for higher values of σ_g , with little difference seen between mode for the softest impedance ground. Modes when $\phi < -2$ show the greatest difference, with the lowest σ_g giving values between approximately $-5 < M_0 < 3$ while at the hardest impedance ground, the range of mode is halved and decreased to around

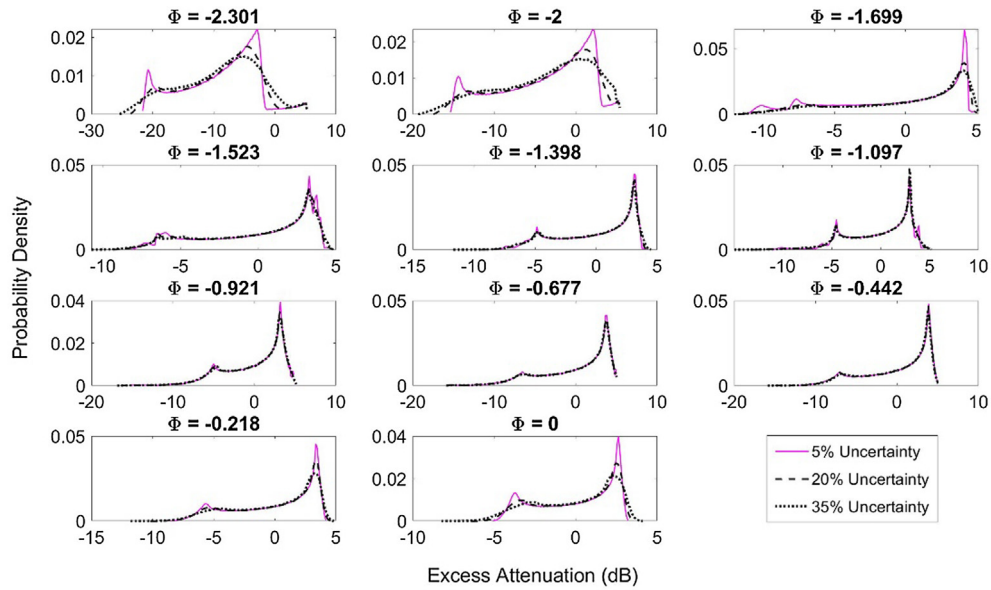


Fig. 5. The PDFs of excess attenuation spectra for a range of values of Φ and levels of uncertainties in the source/receiver coordinates. The flow resistivity of the ground is $\sigma_g = 2000 \text{ kPasm}^{-2}$.

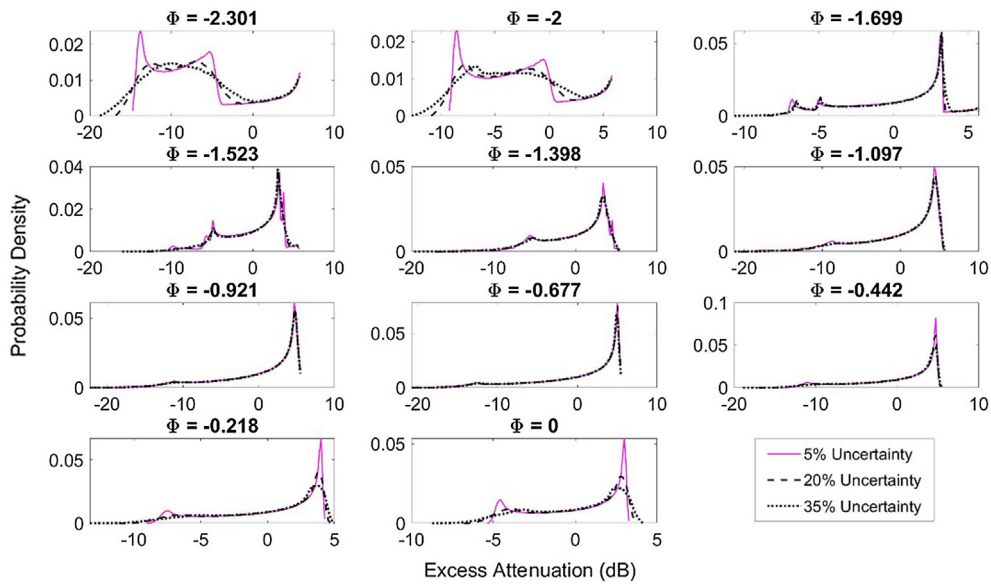


Fig. 6. The PDFs of excess attenuation spectrum for a range of values of Φ and levels of uncertainties in the source/receiver coordinates. The flow resistivity of the ground is $\sigma_g = 20,000 \text{ kPasm}^{-2}$.

$-13 < M_o < -7$. The increase from the median and mean was again an expected side effect of the negative skewness present in the samples. In the case of symmetric distributions, the mode quite often relates to parameter estimation techniques, highlighting the need for quantifying Φ and σ_g efficiently.

The second grouping of statistics (Table 3) are the higher moments such as the standard deviation (σ), skewness (s) and kurtosis (k_s). Behaviours for the increase/decrease in the varying control parameters ϕ , σ_g and uncertainty are clearer for these statistical moments than the earlier averages (Table 2).

The standard deviation is most effected by the value of σ_g and Φ (3rd column of Table 3). The standard deviation for the minimum value of $\Phi = -2.301$ has the maximum. As $\Phi \rightarrow 0$ the value of the standard deviation reduces consistently for all ground types. The standard deviation generally reduces with the increase in the value of σ_g for $\Phi < -1$. For $\Phi \approx 0$ the standard deviation slightly

increases with the increased flow resistivity of the ground. The effect of the geometrical uncertainty on the standard deviation is relatively small.

The skewness (4th column of Table 3) is seen to be consistently negative but increasing with the increasing value of Φ in the case of the softest ground ($\sigma_g = 35 \text{ kPasm}^{-2}$). As the value of σ_g increases to $20,000 \text{ kPasm}^{-2}$ this dependence changes and the skewness seems to have a clear minimum for $-1 < \Phi < 0.5$. For the flow resistivity values between these extreme ground cases the skewness behaves as an oscillatory function of Φ . The geometrical uncertainty does not affect this parameter significantly for $\Phi > -1.5$.

The behaviour of the kurtosis as a function of Φ (5th column of Table 3) shows a clear minimum around $-1 < \Phi < -1.5$ for the case with the softest ground. For the hardest ground this minimum becomes the maximum. For the cases with $35 < \sigma_g < 2000$

Table 2Collated sample averages from simulations for each combination of σ_g and Φ . Columns from left to right are for uncertainties from 5%, 20% and 35%, respectively.

σ_g	Φ	Mean (μ)			Mode (M_o)			Median (M_{dn})			
35 kPasm ⁻²	-2.301	-9.462	-9.469	-9.482	-1.905	-3.17	-4.099	-6.997	-7.109	-7.367	
	-2	-3.818	-3.844	-3.905	3.187	2.039	1.889	-1.304	-1.410	-1.654	
	-1.699	-1.074	-0.387	0.065	5.524	5.614	5.455	1.413	2.188	2.679	
	-1.523	0.217	-0.014	0.028	5.392	5.287	5.344	2.673	2.376	2.407	
	-1.398	0.108	0.017	0.026	5.068	5.167	5.068	2.322	2.207	2.192	
	-1.097	0.007	-0.059	-0.048	4.461	4.241	4.114	1.600	1.497	1.481	
	-0.921	-0.038	-0.045	-0.035	3.807	3.516	2.929	1.078	1.059	1.042	
	-0.677	-0.055	-0.055	-0.054	2.536	2.419	2.305	0.508	0.504	0.489	
	-0.422	0.021	0.019	0.012	1.562	1.48	1.302	0.252	0.250	0.247	
	-0.218	-0.007	-0.006	-0.002	0.84	0.808	0.802	0.105	0.108	0.109	
	0	0.013	0.012	0.009	0.54	0.547	0.511	0.068	0.065	0.064	
	500 kPasm ⁻²	-2.301	-9.327	-9.332	-9.343	-2.283	-3.804	-5.079	-7.381	-7.490	-7.739
		-2	-3.839	-3.864	-3.924	2.785	1.51	1.165	-1.866	-1.965	-2.198
-1.699		-1.025	-0.395	-0.007	4.996	4.876	4.897	0.814	1.505	1.954	
-1.523		0.038	-0.119	-0.078	4.089	4.246	4.246	1.664	1.446	1.475	
-1.398		-0.033	-0.089	-0.079	3.869	4.087	3.598	1.277	1.197	1.199	
-1.097		-0.095	-0.104	-0.097	3.094	3.156	2.975	0.748	0.744	0.758	
-0.921		-0.088	-0.092	-0.091	2.816	2.861	2.781	0.655	0.647	0.668	
-0.677		-0.089	-0.086	-0.083	2.767	2.741	2.773	0.746	0.753	0.762	
-0.422		0.023	0.014	0.009	2.86	2.917	2.862	0.932	0.924	0.904	
-0.218		-0.01	-0.006	-0.003	2.694	2.694	2.694	0.709	0.707	0.696	
0		0.012	0.011	0.01	2.122	2.129	1.925	0.672	0.677	0.689	
2000 kPasm ⁻²		-2.301	-8.884	-8.888	-8.894	-2.867	-4.481	-5.256	-7.623	-7.726	-7.96
		-2	-3.698	-3.723	-3.78	2.078	1.331	0.427	-2.333	-2.427	-2.636
	-1.699	-0.794	-0.294	0.004	4.153	4.148	4.112	0.566	1.063	1.434	
	-1.523	-0.059	-0.128	-0.095	3.285	3.255	3.25	1.02	0.924	0.966	
	-1.398	-0.087	-0.105	-0.097	3.113	3.146	3.07	0.806	0.793	0.809	
	-1.097	-0.151	-0.111	-0.109	3.007	2.943	3.016	0.715	0.801	0.825	
	-0.921	-0.097	-0.098	-0.101	3.179	3.113	3.074	1.016	1.015	1.012	
	-0.677	-0.097	-0.091	-0.088	3.804	3.683	3.855	1.333	1.331	1.319	
	-0.422	0.022	0.012	0.007	3.895	3.878	3.788	1.445	1.422	1.396	
	-0.218	-0.011	-0.006	-0.003	3.36	3.398	3.331	1.028	1.021	1.007	
	0	0.016	0.009	0.007	2.625	2.508	2.331	0.599	0.586	0.585	
	20,000 kPasm ⁻²	-2.301	-6.874	-6.870	-6.855	-13.779	-6.649	-9.912	-7.677	-7.746	-7.756
		-2	-2.941	-2.959	-2.993	-8.509	-7.561	-6.769	-3.131	-3.199	-3.296
-1.699		-0.019	0.002	0.037	3.129	3.246	3.198	0.87	0.951	1.048	
-1.523		-0.26	-0.123	-0.123	3.266	3.054	3.05	0.629	0.92	0.947	
-1.398		-0.178	-0.114	-0.117	3.403	3.418	3.215	1.032	1.151	1.158	
-1.097		-0.208	-0.114	-0.124	4.305	4.301	4.39	1.611	1.746	1.731	
-0.921		-0.103	-0.097	-0.106	4.691	4.717	4.732	1.990	1.992	1.972	
-0.677		-0.102	-0.092	-0.093	4.995	5.02	4.844	2.076	2.076	2.061	
-0.422		0.02	0.009	0.006	4.713	4.743	4.705	1.937	1.913	1.886	
-0.218		-0.011	-0.006	-0.003	4.011	3.87	3.654	1.311	1.304	1.287	
0		0.016	0.008	0.006	2.994	2.728	2.51	0.741	0.729	0.73	

kPasm⁻² this behaviour is complex and oscillatory. The geometrical uncertainty does not affect this parameter significantly.

3.3. Normality assumption

Normality is an assumption that needs to be taken seriously. When this assumption is violated, it becomes harder to draw accurate and reliable statistical conclusions [14]. In the case of higher-order statistical moments (Table 3) there is no visual indication that normality has been violated. However, the non-normal indicators are checked through the Anderson-Darling test which is applied to the simulation data from each combination of Φ , σ_g and uncertainty level. It is found that every single sample significantly ($p \ll 0.005$) rejected the null hypothesis that the sample was normal. This indicates that it is the data obtained violate the normality assumption.

This could indicate one of the following scenarios: (i) a certain combination of the frequency range over which the data are analysed, Φ and/or uncertainty create non-normal PDFs; (ii) the initial prior uniform distribution propagates through its non-normality; (iii) the acoustic prediction model is non-normal in itself. It is not of ease to state which the causes is nor is it any easier to prove. More investigation into the physics underpinning the interactions

between Φ , σ_g and acoustic wavelength, λ is required. It is also useful to investigate how great an effect the distribution of the uncertainty in unknown parameters is. This could be done by comparing simulation results from known prior distributions and using statistical test to investigate whether the final sample changes accordingly, yet this work lies outside the main scope of this work.

4. Conclusions

The effect of the impedance grounds on the statistics in the excess attenuation data was significantly related to the test statistic chosen. The mean and median values of the excess attenuation did not change significantly (within 1/100th of a dB) as the ground properties have changed from soft to hard. However, the mode and later statistical moments did differ in relation to the values of σ_g . The mode and standard deviation were most significantly affected by the change in σ_g . The deviation decreases in parallel with the increase of σ_g while the modes oscillatory behaviour around Φ had the range between the maximum and minimum modes decrease with the increase in σ_g . It is known that varying ground can make a very strong effect on the excess attenuation spectrum, but this shows a relatively small effect on mean, skewness and kurtosis when the model geometry is uncertain. In contrast, the modes

Table 3

Collated sample statistical moments from simulations for each combination of σ_g and Φ . Columns from left to right are for uncertainties from 5%, 20% and 35%, respectively.

σ_g	Φ	Std. Dev (σ)			Skewness(s)			Kurtosis (k_s)		
35 kPasm ⁻²	-2.301	7.661	7.768	8.011	-1.226	-1.171	-1.058	3.777	3.714	3.578
	-2	7.384	7.464	7.64	-1.284	-1.245	-1.17	3.92	3.873	3.77
	-1.699	6.987	6.649	6.431	-1.134	-1.318	-1.428	3.365	3.893	4.253
	-1.523	5.94	5.998	5.959	-1.332	-1.276	-1.291	3.85	3.705	3.786
	-1.398	5.54	5.564	5.537	-1.193	-1.172	-1.186	3.399	3.365	3.456
	-1.097	4.369	4.381	4.362	-0.84	-0.83	-0.859	2.456	2.474	2.616
	-0.921	3.51	3.512	3.51	-0.643	-0.658	-0.701	2.077	2.154	2.341
	-0.677	2.368	2.381	2.412	-0.452	-0.472	-0.511	1.87	1.963	2.143
	-0.422	1.539	1.559	1.596	-0.322	-0.35	-0.402	2.267	2.342	2.516
	-0.218	1.192	1.196	1.203	-0.485	-0.469	-0.441	3.644	3.644	3.571
	0	0.884	0.89	0.904	-0.263	-0.269	-0.306	3.369	3.469	3.71
	500 kPasm ⁻²	-2.301	6.778	6.891	7.151	-0.792	-0.749	-0.664	2.631	2.633
-2		6.322	6.409	6.604	-0.878	-0.849	-0.794	2.679	2.699	2.719
-1.699		5.724	5.381	5.216	-0.807	-0.963	-1.043	2.503	2.86	3.056
-1.523		4.502	4.532	4.506	-0.891	-0.874	-0.896	2.632	2.646	2.747
-1.398		3.955	3.974	3.971	-0.76	-0.757	-0.783	2.373	2.401	2.519
-1.097		3	3.022	3.057	-0.57	-0.576	-0.603	2.02	2.056	2.156
-0.921		2.83	2.85	2.889	-0.715	-0.711	-0.71	2.829	2.816	2.8
-0.677		3.123	3.123	3.119	-0.805	-0.801	-0.795	3.131	3.099	3.051
-0.422		3.166	3.163	3.138	-0.662	-0.679	-0.69	2.367	2.445	2.519
-0.218		2.738	2.734	2.725	-0.535	-0.546	-0.562	2.039	2.096	2.193
0		1.988	2.006	2.045	-0.378	-0.391	-0.43	1.789	1.869	2.05
2000 kPasm ⁻²		-2.301	6.18	6.296	6.559	-0.331	-0.317	-0.292	2.368	2.375
	-2	5.426	5.521	5.731	-0.57	-0.554	-0.529	2.164	2.22	2.305
	-1.699	4.601	4.303	4.219	-0.593	-0.713	-0.787	2.025	2.266	2.421
	-1.523	3.477	3.497	3.512	-0.616	-0.614	-0.646	2.036	2.073	2.178
	-1.398	3.096	3.121	3.159	-0.589	-0.593	-0.62	2.044	2.075	2.177
	-1.097	3.217	3.235	3.279	-0.763	-0.791	-0.794	2.853	2.913	2.934
	-0.921	3.663	3.674	3.689	-0.906	-0.906	-0.903	3.285	3.278	3.259
	-0.677	4.229	4.213	4.18	-0.906	-0.905	-0.898	2.927	2.925	2.9
	-0.422	4.077	4.069	4.036	-0.805	-0.814	-0.821	2.437	2.488	2.546
	-0.218	3.339	3.339	3.34	-0.62	-0.636	-0.665	2.039	2.111	2.247
	0	2.358	2.383	2.436	-0.433	-0.451	-0.499	1.767	1.858	2.06
	20,000 kPasm ⁻²	-2.301	5.636	5.732	5.94	0.715	0.639	0.49	2.591	2.523
-2		4.144	4.231	4.416	0.392	0.338	0.229	2.231	2.196	2.143
-1.699		3.311	3.354	3.423	-0.532	-0.554	-0.596	2.158	2.165	2.227
-1.523		3.564	3.588	3.642	-0.692	-0.779	-0.799	2.63	2.77	2.866
-1.398		3.958	3.967	4.007	-0.896	-0.94	-0.955	3.116	3.224	3.302
-1.097		5.068	5.049	5.062	-1.055	-1.098	-1.104	3.29	3.398	3.429
-0.921		5.488	5.481	5.464	-1.171	-1.172	-1.164	3.535	3.539	3.515
-0.677		5.642	5.615	5.571	-1.158	-1.155	-1.146	3.354	3.351	3.33
-0.422		4.987	4.983	4.957	-0.993	-1.005	-1.022	2.798	2.861	2.968
-0.218		3.864	3.872	3.89	-0.716	-0.74	-0.789	2.164	2.27	2.481
0		2.663	2.694	2.76	-0.487	-0.509	-0.568	1.806	1.914	2.153

dependence on both Φ and σ_g is crucial as common point estimation inference techniques, such as maximum likelihood methods, are directly linked to this statistic, thus an inaccurate estimation of the mode will hinder effective parameter estimations. These findings highlight the importance of removing such geometric uncertainties before making predictions or using excess attenuation data for parameter inversion. Inference work using more uncertain or complex models could also benefit from these findings, relying on the ability to either select arbitrary impedance values or save computation time drawing from these known PDF while have uncertainties, at minimum, present in the ground and receiver geometry. This would greatly reduce computational costs while having a likely negligible effect on accuracy.

The behaviour of the broadband excess attenuation PDF as a function of Φ is rather informative. When $\Phi < -1$ the PDFs contain a clear peak which amplitude depends on the level of uncertainty in Φ . These data are associated with a strongly negative skewness and relatively large standard deviation. For $\Phi < -2$ the PDF shifts in its entirety across the excess attenuation scale (x -axis) to around -5 dB, however has no obvious defined distribution, which is exacerbated across varying σ_g . For the ratio $\Phi \approx -1$ the standard deviation in the data, skewness and kurtosis reduce with a second peak becoming visible in the range of $\Delta L \leq -10$ dB. When the ratio Φ

increases above -1 , the second peak in the PDF at $\Delta L \leq 0$ dB becomes very pronounced. The amplitude of this peak increases with the increase in the ratio Φ and its position moves progressively towards $\Delta L = -1$ dB, converging the two peaks. The PDFs appear to become *bimodal* in nature due to the strength of this secondary peak. The convergence of the *negative peak* is hindered with both its increase in the related excess attention value (x -axis) and probability clue (y -axis), as well as the convincing appearance of a bimodal distribution, by the increase in σ_g and uncertainty. Being able to understand and/or control the PDF using this numerical value of Φ , solely and in combination with σ_g , will be of great use for future statistical methods to parameter inversion and may hint towards methodologies to use i.e. regression methods since interactions between parameters are likely to help prior selection while using Bayesian methods. The more pronounced bimodality at lower σ_g may also suggest reasoning to inaccuracies during measurement in low impedances i.e. convergence to wrong peak during calculation of the mean.

Most statistical inference is done via parametric methods i.e. assumes the observe data available follows a normal distribution. However, if normality is found to be violated, then the validity of the results gained using such methods is compromised [10–14]. None of the indicator statistics had values that indicated non-

normal behaviour, however the movement of the kurtosis values indicated some of the samples were acting peculiar. The Anderson-Darling tests that were performed were shown to extremely support the assumption that each sample violated normality, with substantial confidence ($p \ll 0.05$). It is unclear what caused these irregularities: the uniform sampling distribution or physical phenomena from Φ with the frequency bands themselves. Investigating the physics underpinning the interactions between Φ and λ , while comparing the effect of using normal and non-normal distributions to sample will hopefully recover the true reason. This also highlights the need to validate the normality assumption before progressing with statistical processes on a given data set, a process which is majorly overlooked.

Future research would require an investigation into a more complex sound propagation model that allows for meteorological effects. This would reveal how strong the influence of the geometrical uncertainties in relation to the influence of stochastic meteorological effects and ground effects. It would also reveal the relative *strength* of uncertainty in different input parameters on the excess attenuation. Regression methods on real data sets could also be used to investigate such behaviours as interaction effects etc. The parameter Φ could be used to strengthen the effectiveness of the regression either as an additional parameter or even instead of the receiver parameters. Investigating of the effect of a broader range of values of Φ on the excess attenuation statistics will also be of interest to expand current understanding. This may require a more complicated propagation model which includes a realistic ground topography, effects of buildings and vegetation in the propagation path. Investigation of a dimensionless parameter from a combination of Φ , σ_g and k to shape likelihood distributions would likely be successful. This could also be extended to other models to see if attributes of Φ remain constant. Finally, discovering the

cause of the non-normal behaviour in the predicted statistical moments for the excess attenuation is a key to better understanding of the capabilities and limitations in the statistical simulation of sound propagation in the presence of uncertainties. Performing rigorous normality tests for results from differing Φ and σ_g , both for broadband and narrowband samples, will be a step forward to discovering if they are true anomalies or a product of the non-normal input prior. We theorise it is possible that the extreme non-normality is a product of some interference patterns produced by certain values of Φ at relevant frequencies rather than prior parameter distribution being non-normal or normal.

Declaration of Competing Interest

The authors declare that they have no known competing financial interests or personal relationships that could have appeared to influence the work reported in this paper.

Acknowledgements

The author/s acknowledge the support of Defense Science and Technology Laboratory (Dstl) UK and EPSRC CASE studentship award to the University of Sheffield. The authors are also grateful to Prof. Jeremy Oakley from the Department of Mathematics and Statistics at the University of Sheffield for his useful comments on the statistical aspects of this work.

Appendix A. The effect of frequency range

The choice of frequencies in this paper is based on the fact that a majority of sources of outdoor noise emit efficiently frequencies of sound between 100 Hz and 5 kHz [3,6]. This range is sensible to

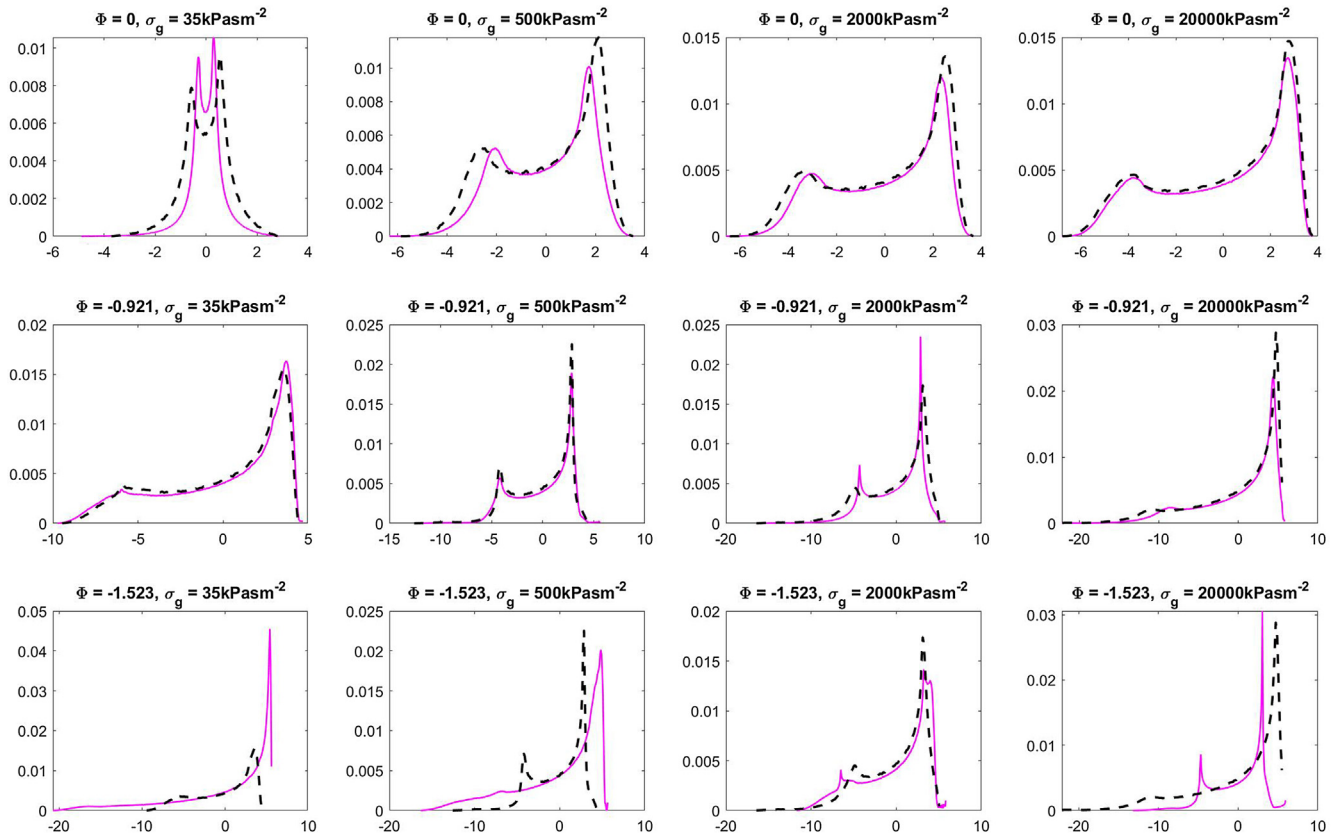


Fig. A1. The effect of the choice of the frequency range on the probability density function for the excess attenuation predicted with the adopted Monte Carlo simulation. The uncertainty is 20%. Black dashed line: frequency band 100 Hz – 5 kHz. Magenta: 25 Hz – 20 kHz. (For interpretation of the references to colour in this figure legend, the reader is referred to the web version of this article.)

find a balance between computational costs and accuracy in the statistical data attained from the Monte Carlo simulation.

The frequency ranges suggested in some popular prediction standards may differ from the range adopted in this paper. The ISO 9613 Part 2 standard [15] suggests that the calculations should be carried out in the octave bands between 63 and 8000 Hz. The Harmonoise prediction standard [16] suggests that this range should be between 25 Hz and 20 kHz.

The probability density functions for the excess attenuation presented (Fig. A1) illustrate the effect of the spectral width. This difference is between the 100 Hz – 5 kHz range and 25 Hz – 20 kHz range is not large, but noticeable dependent on Φ and σ_g . Therefore, it should be recommended to ensure that the spectrum of the source is properly captured in this type of analysis by adopting the right frequency range.

7. References

- [1] Pettit CL, Wilson DK. Uncertainty and stochastic computations in outdoor sound propagation. *J. Acoust. Soc. Am.* 2014;135(4).
- [2] Pettit CL, Wislon DK, Ostashev VE, Vecherin SN. Description and quantification of uncertainty in outdoor sound propagation calculations. *J Acoust Soc Am* 2014;136(3).
- [3] Attenborough K, Li KM, Horoshenkov KV. *Predicting Outdoor Sound*. CRC Press; 2006.
- [4] Hothersall DC, Harriott JNB. Approximate models for sound propagation above multi-impedance plane boundaries. *J Acoust Soc Am* 1995;97(2):918–26.
- [5] Kruse R, Mellert V. Effect and minimization of errors in in situ ground impedance measurements. *Appl Acoust* 2008;69(10):884–90.
- [6] Salomons EM. *Computational atmospheric acoustics*. Kluwer Academic Publishers 2001;5–27.
- [7] Dazel O, Groby JP, Horoshenkov KV. Asymptotic limits of some models for sound propagation in porous media and the assignment of the pore characteristic lengths. *J Acoust Soc Am* 2016;139(5):2463–74.
- [8] Attenborough K. Outdoor ground impedance models. *J Acoust Soc Am* May 2011;129(5):2806–19.
- [9] Scott DW. On optimal and data-based histograms. *Biometrika* 1979;66(3):605–10.
- [10] Ghasemi A, Zahediasl S. Normality tests for statistical analysis: a guide for non-statisticians. *Int J Endo Metab* 2012;10(2):486.
- [11] Curran PJ, Finch JF, West SG. 'Structural Equation Modelling: Concepts, Issues, and Applications' in *Structural equation models with non-normal variables: Problems and remedies*. Sage Publications Inc.; 1995. p. 56–75.
- [12] Field A. *Discovering Statistics Using SPSS*. London: Sage Publications Ltd.; 2009.
- [13] Stephens MA. EDF Statistics for Goodness of Fit and Some Comparisons. *J. Am. Stats. Assoc.* September 1974;69(346):730–7.
- [14] Elhan AH, Oztuna D, Tuccar E. Investigation of four different normality tests in terms of type 1 error rate and power under different distributions. *Turk. J. Med. Sci.* January 2006;36(3):171–6.
- [15] "ISO 9613-2:1996." ISO, 12 June 2017, <https://www.iso.org/standard/20649.html>.
- [16] "European Commission." CORDIS, <https://cordis.europa.eu/project/rcn/57829/factsheet/en>.

B.II Pressure ratio and phase difference in a two-microphone system under uncertain outdoor sound propagation conditions

Paper II – J. A. Parry, K. V. Horoshenkov and D. P. Williams. “*Pressure ratio and phase difference in a two-microphone system under uncertain outdoor sound propagation condition*”. Applied Acoustics, 170 (December 2020).



Pressure ratio and phase difference in a two-microphone system under uncertain outdoor sound propagation conditions



Jordan A. Parry^{a,*}, Kirill V. Horoshenkov^a, Duncan P. Williams^b

^a University of Sheffield, Dept. of Mech Engineering, Sheffield, England

^b Defence Science and Technology Laboratory, Salisbury, England

ARTICLE INFO

Article history:

Received 27 April 2020

Received in revised form 7 June 2020

Accepted 18 July 2020

Keywords:

Uncertainty

Outdoor acoustics

Microphone array

Sound pressure ratio

Phase difference

ABSTRACT

Predictions of outdoor sound propagation in uncertain conditions are a challenging task. Evidence suggests that using more than one receiver can reduce the effect of uncertainties. This paper studies via numerical simulations the effects of uncertainty in the source/receiver geometry and impedance ground condition on the sound pressure ratio recorded using the two-microphone method. A Monte Carlo method is employed to study the effect of uncertainties in the range and ground parameters. The range and frequency are found to be key parameters which control the resultant probability density function for the absolute sound pressure ratio and phase difference. The introduction of small uncertainty only matters if the uncertainty is present in the distance between the source and receiver. Uncertainties in the impedance ground are found to have a negligible effect. The sound pressure ratio is affected by the uncertainty more strongly at a shorter range. These findings pave the way to the development of more robust methods for outdoor acoustic source localisation and identification from two-microphone data.

© 2020 Elsevier Ltd. All rights reserved.

1. Introduction

The two-microphone method is used extensively in outdoor sound propagation to determine the ground impedance from acoustical data (e.g. [1]) for noise control (e.g. [2]) and source localisation (e.g. [3]). American National Standards Institute (ANSI) provides a standard method for determining the acoustic impedance of ground surfaces using the ratio between two close microphones to infer an impedance of an unknown ground using carefully obtained acoustical data [4]. The use of a sound pressure ratio or level difference between the two microphones cancels out troublesome interference patterns and source spectrum effect, allowing for more accurate predictions of the ground properties and environmental effects.

A key for the successful use of this method is the quality of the sound pressure measurements and microphone mismatch. While Harriot and Hothersall investigated the accuracy of the signal processing method in the presence of an uncertain ground, especially the interference patterns, the geometric and frequency ranges used in this standard are far too small to study whether these effects carried over into the larger geometries and/or more varied sound sources [5]. Kruse and Mellert [6] used the two-microphone

method to measure errors from uncertainties present in outdoor sound propagation over a wider frequency range. Errors were minimised at frequencies above 100Hz and 500Hz for acoustical soft and hard impedance grounds respectively, yet the study did not investigate the medium/longer ranges (>100 m) which are of common interest in outdoor acoustics and there is a limited statistical data on the sound pressure ratio and phase mismatch.

This study aims to increase the scale of the geometries used to assess the viability of the two-microphone method for the statistical analysis of outdoor sound propagation. One effect which has not been quantified yet, is the influence on geometrical uncertainties on the probabilistic measures of the sound pressure data obtained on a pair of microphones. The main research question here is: *How does the uncertainty in the sound/receiver position affect the absolute sound pressure ratio and phase difference between the two microphones used with this method?* These parameters are important in the understanding of outdoor sound propagation, with specific application to the inverse problems such as sources localisation, identification and ground property inversion. Other questions are also answered in the study such as; whether the two-microphone method is applicable for large scale studies and the computational efficiency that can be achieved with readily available hardware, having possible direct impact on the analysis of outdoor sound propagation methods used by industry and academia.

* Corresponding author.

E-mail addresses: JAParry1@Sheffield.ac.uk (J.A. Parry), K.Horoshenkov@Sheffield.ac.uk (K.V. Horoshenkov), DPWilliams@dstl.gov.uk (D.P. Williams).

This paper is structured in the following manner. Section 2.1 details the acoustical methods, such as the acoustical model and the physical representations of gathered outputs. Section 2.2 outlines the statistical methods applied to study the uncertainty. Section 3 presents and reviews the results from our simulations. Finally, Section 4 summarises the main findings of this study.

2. Research methods

2.1. The model

This study makes three key initial assumptions about the acoustical scenario: (i) non-moving homogenous atmosphere; (ii) a 2D (r, z) problem geometry with a point source; and (iii) a homogeneous impedance ground with well-defined acoustical characteristics between the source and receivers. The first assumption is used to understand the geometrical uncertainty in the absence of atmospheric effects. The 2D geometry is not a concern because it is used extensively and successfully for outdoor sound propagation modelling (e.g. [4]). The final assumption of the uniform ground is acceptable as prior works have shown that a relatively large variability in the ground does not significantly affect the interaction paths over the scales adopted in this study [7].

The American National Standard S1.18 method for determining an acoustic impedance of a ground [4] inspired this work. The ANSI S1.18 standard makes use of the ratio and corresponding level difference between the sound pressures obtained on two closely spaced receivers installed at the same range (r) from the point source. These two receivers are installed at two distinct receiver heights (h_r). This study uses the recorded pressure, and the ratios between these measures, at the receivers to establish; (i) the absolute pressure ratio and (ii) phase difference.

To calculate these values, it is first recounted that the sound pressure measured at a receiver from a source [8] can be equated to be

$$p = p_0 \left[1 + Q \frac{R_1}{R_2} \exp(ik(R_2 - R_1)) \right], \quad (1)$$

using the time convention $\exp(-j\omega t)$, where p_0 , k and Q are the reference sound pressure at 1 m from the source, wavenumber and spherical wave reflection coefficient, respectively. The distances R_1 and R_2 can be defined as

$$R_1 = \sqrt{r^2 + (z - z_s)^2}, \quad (2)$$

$$R_2 = \sqrt{r^2 + (z + z_s)^2}, \quad (3)$$

for given source (z_s) and the receiver (z) heights, respectively. R_1 and R_2 represents the directed and reflected path respectively. The spherical wave reflection coefficient (Q) accounts for the effect of the locally reactive impedance ground on the reflected rays. The equation for the spherical wave reflection coefficient is

$$Q = \left(\frac{Z \cos \theta - 1}{Z \cos \theta + 1} \right) + \left(1 - \left(\frac{Z \cos \theta - 1}{Z \cos \theta + 1} \right) \right) F(w). \quad (4)$$

The angle θ is the incident angle at which the reflected ray leaves the impedance ground, given as θ_A and θ_B in Fig. 1 for the different paths to each respective receiver. The function $F(w)$ accounts for the boundary loss factor and it is defined as

$$F(w) = 1 + iw\sqrt{\pi} \exp(-w^2) \operatorname{erfc}(-iw), \quad (5)$$

with $\operatorname{erfc}(-iw)$ being the complimentary error function

$$\operatorname{erfc}(z) = \frac{2}{\sqrt{\pi}} \int_z^\infty \exp(-t^2) dt. \quad (6)$$

The parameter Z in Eq. (4) is the normalised impedance of the ground, which is dependent on the acoustic properties of said ground. The impedance Z is determined using the model proposed by Horoshenkov et al. [6]. This model calculates the acoustic properties of the impedance ground by considering the ground as a porous media with pores of non-uniform cross-section, with the median pore-size \bar{s} .

In outdoor sound propagation studies, it is common to refer to the effective flow resistivity of the ground (σ_g). The acoustic impedance model proposed in [6] relates the effective flow resistivity to the median pore size as

$$\sigma_g = \frac{8\eta\alpha_\infty}{\bar{s}^2\phi} e^{6(\sigma_s \log 2)^2}, \quad (7)$$

where η is the dynamic viscosity of air. In the above equation it is common to set the values of porosity (ϕ) and tortuosity (α_∞) to unity and standard deviation in pore size (σ_s) to zero, because for a majority of outdoor ground types their influence on the value of effective flow resistivity is relatively small in comparison with that of the median pore size. This value will be used to determine the grounds effect on the interaction patterns between reflected and direct sound rays.

The complex sound pressure at the receiver positions A and B is

$$p_A = p_0 \left[1 + Q \frac{R_{1A}}{R_{2A}} \exp(ik(R_{2A} - R_{1A})) \right], \quad (8)$$

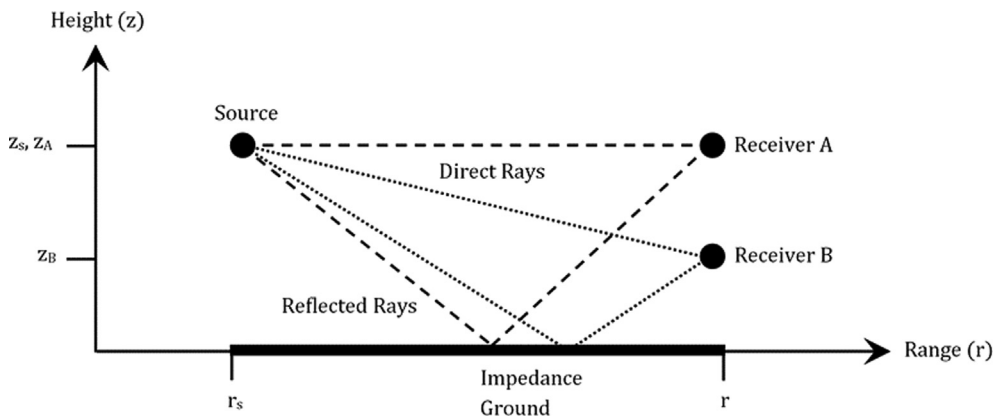


Fig. 1. Acoustic scenario of the two-microphone system in the (r, z) geometry.

$$p_B = p_0 [1 + Q \frac{R_{1B}}{R_{2B}} \exp(ik(R_{2B} - R_{1B}))], \tag{9}$$

where the distances are now dependent on the direct paths to the receivers A and B (R_{1A} & R_{1B}) and reflected from the ground paths (R_{2A} & R_{2B}). Using Eqs. (7) and (8), the sound pressure ratio between the signals recorded on receiver A and B, presented as an amplitude from hereon is

$$p_d = \frac{p_A}{p_B} \exp(i\phi_B - i\phi_A). \tag{10}$$

Two parameters in eq. (10) are of direct interest: (i) the ratio of the sound pressure amplitudes, $\mu_p = \frac{p_A}{p_B}$, and (ii) the phase difference, $\mu_\phi = \phi_B - \phi_A$. The uncertainty in the sound pressure amplitude ratio can alter the quality of the ground impedance inversion method [4], whereas the uncertainty in the phase difference would affect the accuracy of source localisation [3].

2.2. Propagation of uncertainty

The problem approached in this work is of a forward nature, with the uncertainty added into the model which we assume to be perfect i.e. the model would predict the exact result for a given set of parameters. It is assumed that there is a variability in the geometry and ground properties, specifically in: (i) the range (r); and (ii) the ground impedance which is controlled by the effective flow resistivity (σ_g). The heights of the source (z_s), receiver A (z_A) and receiver B (z_B) are assumed locked to 1.5m, 1.5m and 0.5m, respectively. The range (r) is varied from 100m to 500m, while the effective flow resistivity of the impedance ground takes the values of 100kPasm^{-2} and 2000kPasm^{-2} . These values for the impedance follow some published experimental data [10] that corresponds to acoustical soft (e.g. grassland) and hard grounds (rocks), respectively.

For these ground types the real and imaginary parts of the sound pressure spectra at receiver A for $p_0 = 1\text{Pa}$ are illustrated

in Fig. 2, which shows the real ((a) and (c) of Fig. 2) and imaginary ((b) and (d) of Fig. 2) parts of these spectra for a set of ranges. It is seen that the true spectra are all dependent on combinations of frequency (ω) and range (r) with visible differences between simulated results.

In this paper the sensitivity in the model to some uncertainty in the range (r) and effective flow resistivity of the ground (σ_g) is studied through a Monte Carlo simulation. The Monte Carlo method is sampling method, that repeatedly calculates a given value while allowing for uncertainty to be present in certain model input parameters. In this case, the model employed is the one previously defined in Eq. (10), predicting the sound pressure amplitude ratio and phase difference between the two receiver points.

The input parameters of the effective flow resistivity (σ_g) and range (r) are independently, and in combination, doped with uncertainty. This is done by replacing the true singular value with a parameter randomly sampled from the given distribution. The given distributions used in this study are uniform distributions, flat distributions around the true value, meaning that any value inside the distribution is equally likely to be selected before each run of the Monte Carlo simulation. The uncertainty is controlled by changing how wide the distribution is i.e. lower and upper bounds being proportionally within either 5% or 35% of the true value.

This process is repeated for 1000 runs, for each combination of uncertainties, where for ease of analysis the average of each simulation is taken giving us the average sound pressure amplitude ratio ($\overline{\mu_p}$) and average phase difference ($\overline{\mu_\phi}$) in the frequency range of 60Hz to 8kHz. These parameters are the main focus of the analysis presented in the following section. The analysis is carried out visually and statistically, where kernel density estimation is used to generate the probability density functions (PDFs) of the average sound pressure amplitude ratio ($\overline{\mu_p}$) and average phase difference ($\overline{\mu_\phi}$).

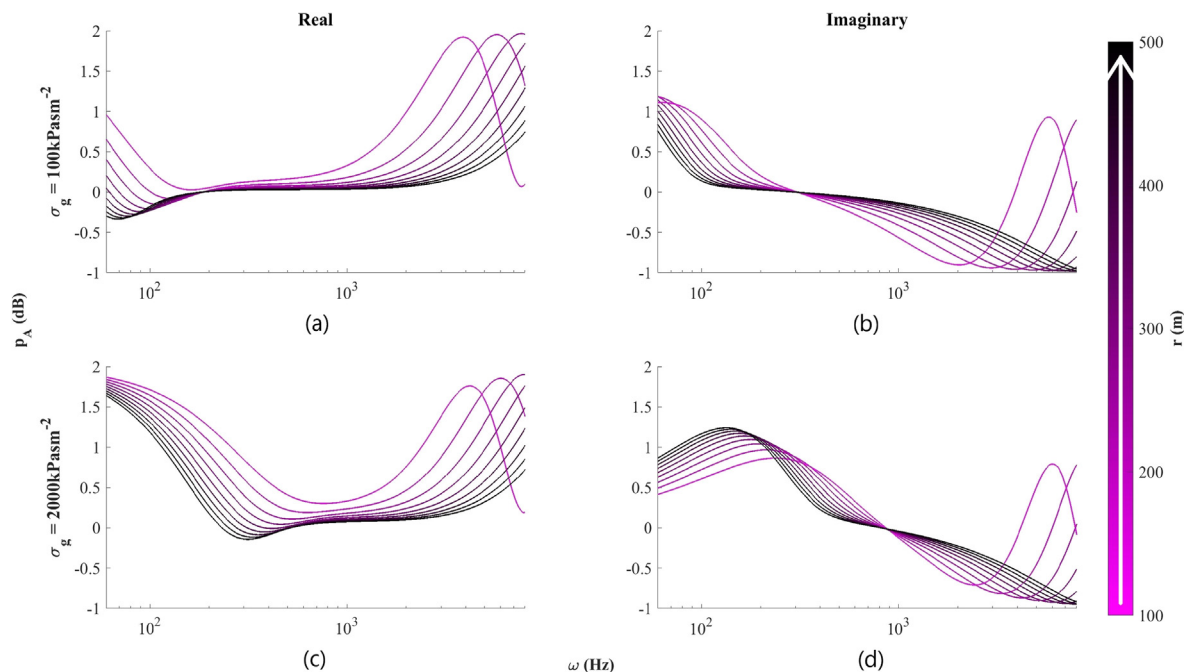


Fig. 2. Real (Left column) and Imaginary (Right column) parts of the sound pressure predicted at position A as a function of the range. Top and bottom rows show data for acoustically soft (100kPasm^{-2}) and hard (2000kPasm^{-2}) impedance grounds, respectively.

3. Results

3.1. Sound pressure amplitude ratio

Fig. 3 shows the spectra of the average sound pressure amplitudes predicted for sound propagation in the presence of a relatively soft ground. Four situations are considered: (i) the fixed values of the parameters ($\sigma_g|r$); (ii) uncertain value of the effective flow resistivity ($\Delta\sigma_g|r$); (iii) uncertain value of the range ($\sigma_g|\Delta r$); and (iv) uncertain values of the effective flow resistivity and range ($\Delta\sigma_g|\Delta r$). Here Δ stands for the parameter uncertainty. Two sets of results are presented: (i) for $\Delta = 5\%$ of the given true value ((a), (b), (c) and (d) of Fig. 3); and (ii) for $\Delta = 35\%$ of the given true value ((e), (f), (g) and (h) of Fig. 3). Fig. 4 presents a similar set of results for the case of hard ground. Figs. 5 and 6 present the probability density functions for the average sound pressure amplitudes taken over the whole frequency spectrum. These are shown for each of the given combinations of parameter uncertainties.

The results from the Monte Carlo simulation suggest that the effect to the average pressure amplitude ratio ($\bar{\mu}_p$) for any combination of small uncertainties ($\Delta = 5\%$) is relatively small, i.e. that this ratio predicted for these microphone locations is relatively immune to variations in the true value of range or flow resistivity of the ground. The effect of frequency on this ratio is dominant as suggested in Ref. [3]. Visually, the spectra only show discernible differences from the true spectra ((a) and (e) in Fig. 4) when the true range (r) is less than $\leq 150\text{m}$ and large uncertainty ($\Delta = 35\%$) is added to it ((d) and (h) in Fig. 4).

Statistically (see Table 1 in Appendix A) the mean of the average ratio of the sound pressure amplitudes ($\bar{\mu}_p$) increases from ~ 1.7 to ~ 2.9 as the range (r) increases. There is variation of ± 0.01 between the means for each hardness of the impedance ground which is controlled by the effective flow resistivity (σ_g). The standard deviation

of the average ratio of the sound pressure amplitudes ($\bar{\mu}_p$) decreases in line with the increase in range (r), with the deviation proportionally decreasing by 50% in the decrease from 500m to 100m.

The generated PDFs seen in Figs. 5 and 6, for soft impedance ($\sigma_g = 100\text{kPasm}^{-2}$) and hard impedance ($\sigma_g = 2000\text{kPasm}^{-2}$) grounds respectively, allow for better insight into the effect of the uncertainty and range. Range (r) is the strongest parameter for shaping these distributions, creating a strong peak at $\bar{\mu}_p \sim 3$. This peak is reduced and disappears as the range reduces from 500m to 100m resulting in a close to flat distribution (see the magenta distributions in Figs. 5 and 6).

The strength of the peak is reduced for all simulations with the acoustical hardening of the impedance ground is increased i.e. an increase in flow resistivity (σ_g). In this case the shape of the distribution and probability of other values (i.e. less than 3) do not change significantly. For the larger uncertainty ($\Delta = 35\%$) and at the shortest range (e.g. $r = 100\text{m}$) another peak appears in the PDFs at $\bar{\mu}_p \sim 1$ (see Fig. 6).

It is apparent that a PDF of the average ratio of the sound pressure amplitudes ($\bar{\mu}_p$) is not generally affected by smaller uncertainties or effective flow resistivity (σ_g). This mirrors the behaviours seen in a similar study into excess attenuation [7]. The range (r) and frequency (ω) shape the spectrum and PDF behaviours, with the range (r) being the dominant parameter which effect becomes more pronounced as the uncertainty increases.

3.2. Phase difference

Similar to the procedure reported in Section 3.1 the behaviour of the average phase difference spectra is studied over the four conditions: (i) the fixed values of the parameters ($\sigma_g|r$); (ii) uncer-

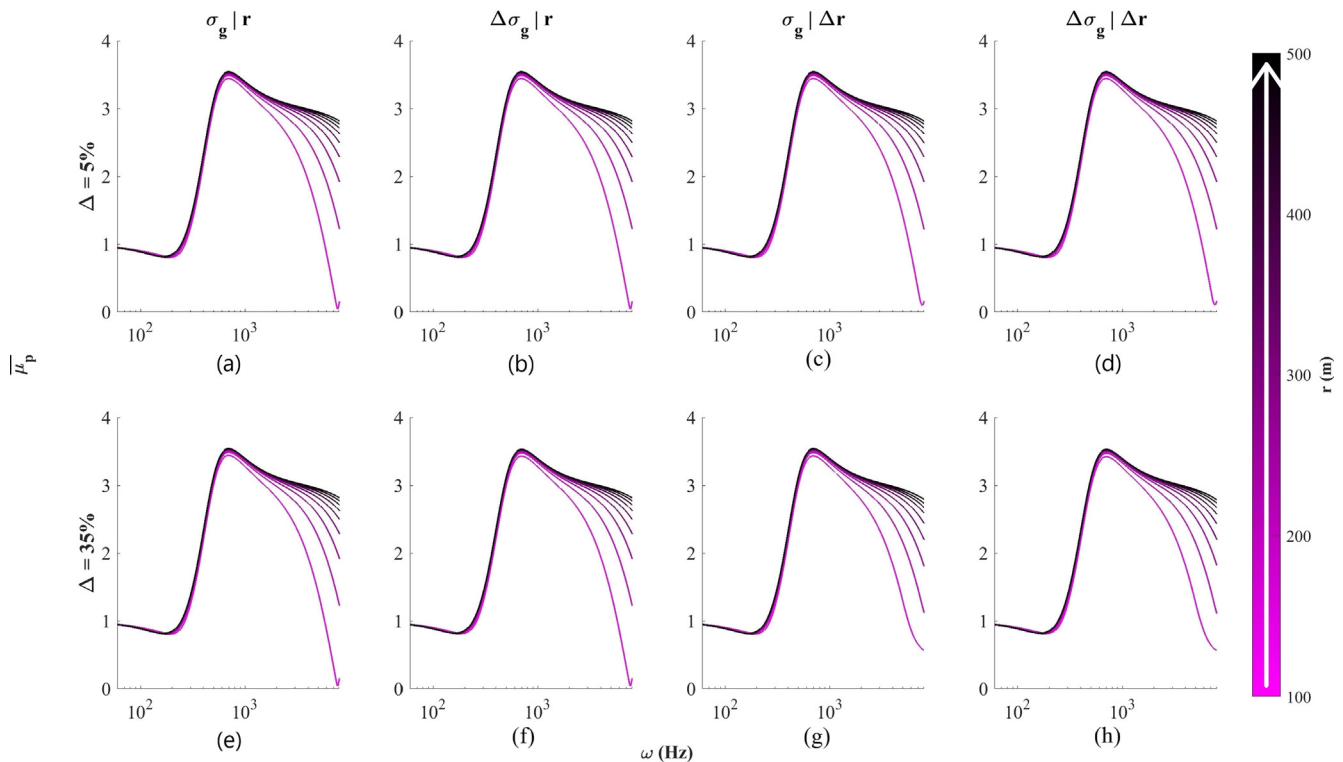


Fig. 3. Simulation results for the average ratio of the sound pressure amplitudes ($\bar{\mu}_p$), for an acoustically soft ground ($\sigma_g = 100\text{kPasm}^{-2}$), where each column defining the uncertainty present and range (r) is mapped to colour, from magenta (100m) to black (500m). Uncertainty (Δ) is at 5% in the first row and increased to 35% in the second row. (For interpretation of the references to colour in this figure legend, the reader is referred to the web version of this article.)

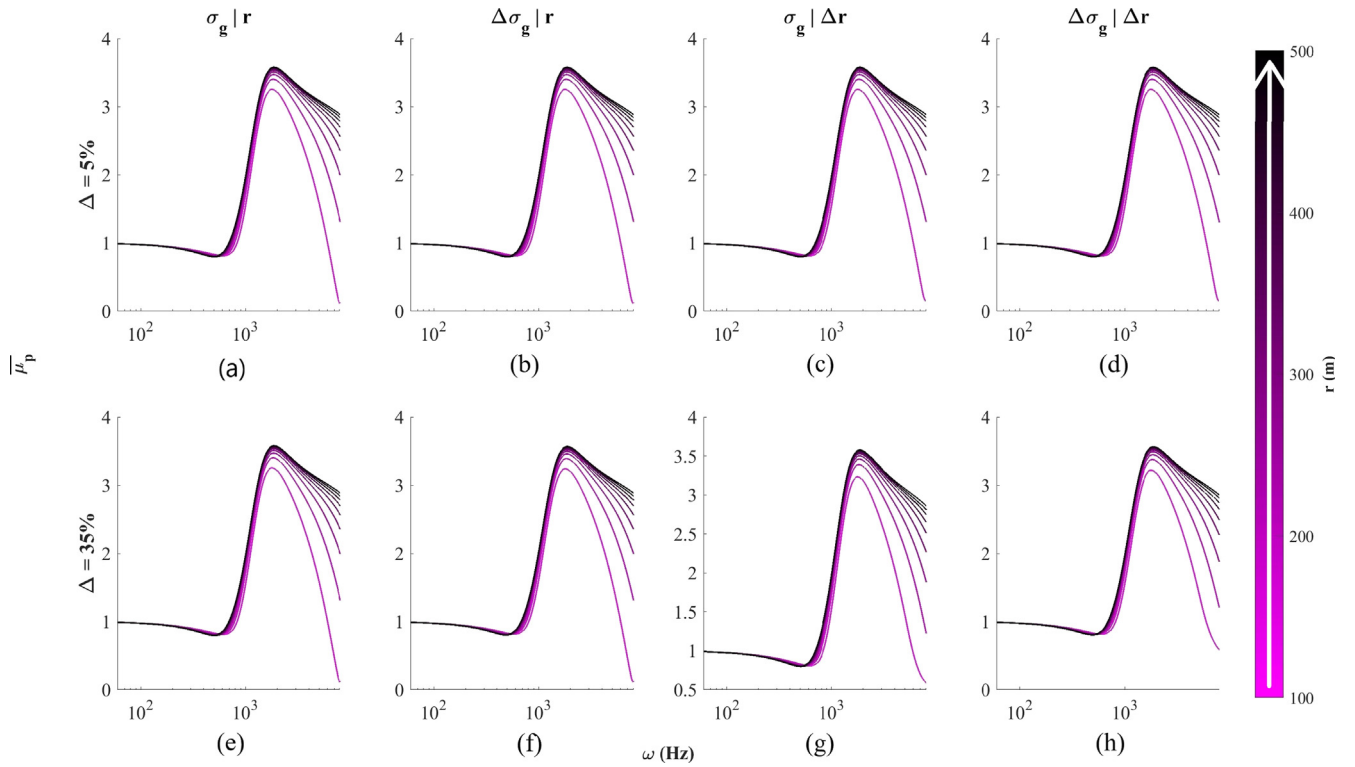


Fig. 4. Simulation results for the average ratio of the sound pressure amplitudes ($\bar{\mu}_p$), for an acoustically hard ground ($\sigma_g = 2000\text{kPasm}^{-2}$), where each column defining the uncertainty present and range (r) is mapped to colour, from magenta (100m) to black (500m). Uncertainty (Δ) is at 5% in the first row and increased to 35% in the second row. (For interpretation of the references to colour in this figure legend, the reader is referred to the web version of this article.)

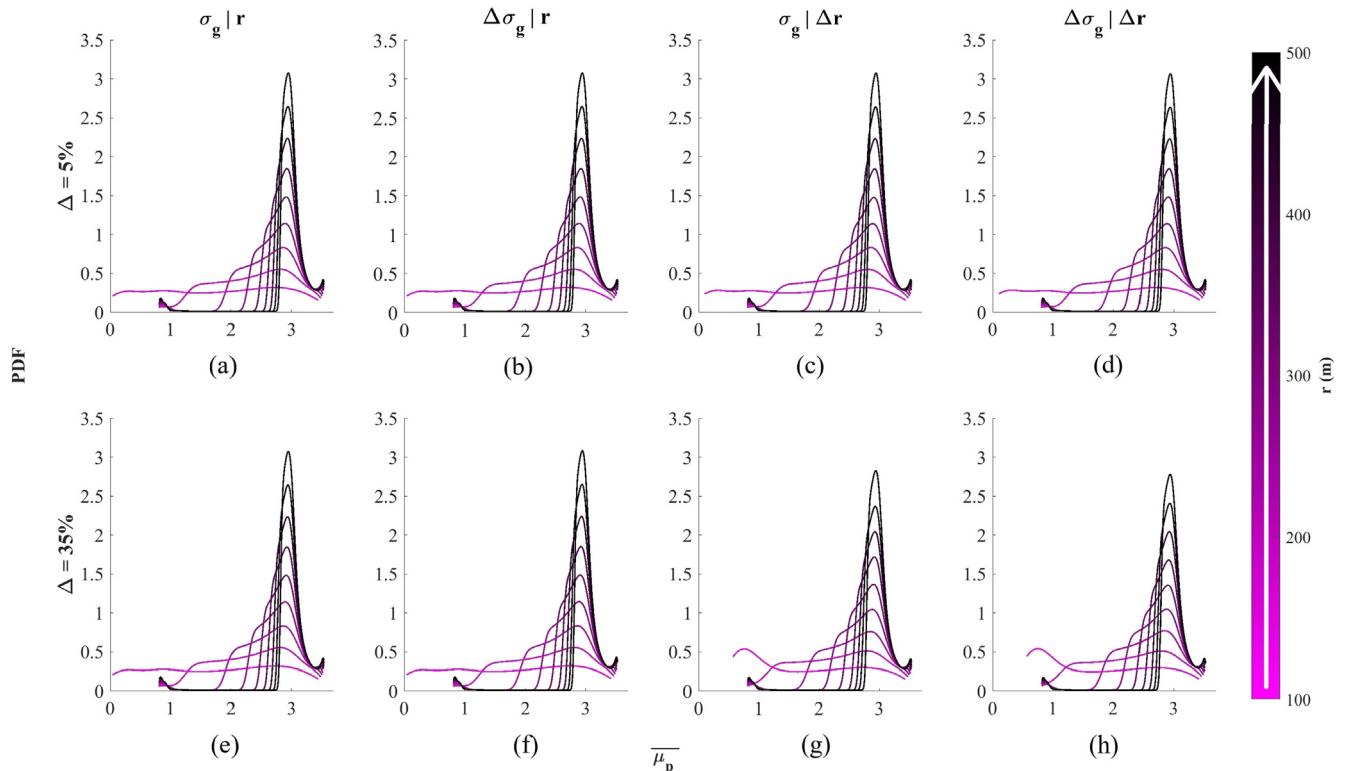


Fig. 5. PDFs for the average ratio of the sound pressure amplitudes ($\bar{\mu}_p$), for an acoustically soft ground ($\sigma_g = 100\text{kPasm}^{-2}$), where each column defining the uncertainty present and range (r) is mapped to colour, from magenta (100m) to black (500m). Uncertainty (Δ) is at 5% in the first row and increased to 35% in the second row. (For interpretation of the references to colour in this figure legend, the reader is referred to the web version of this article.)

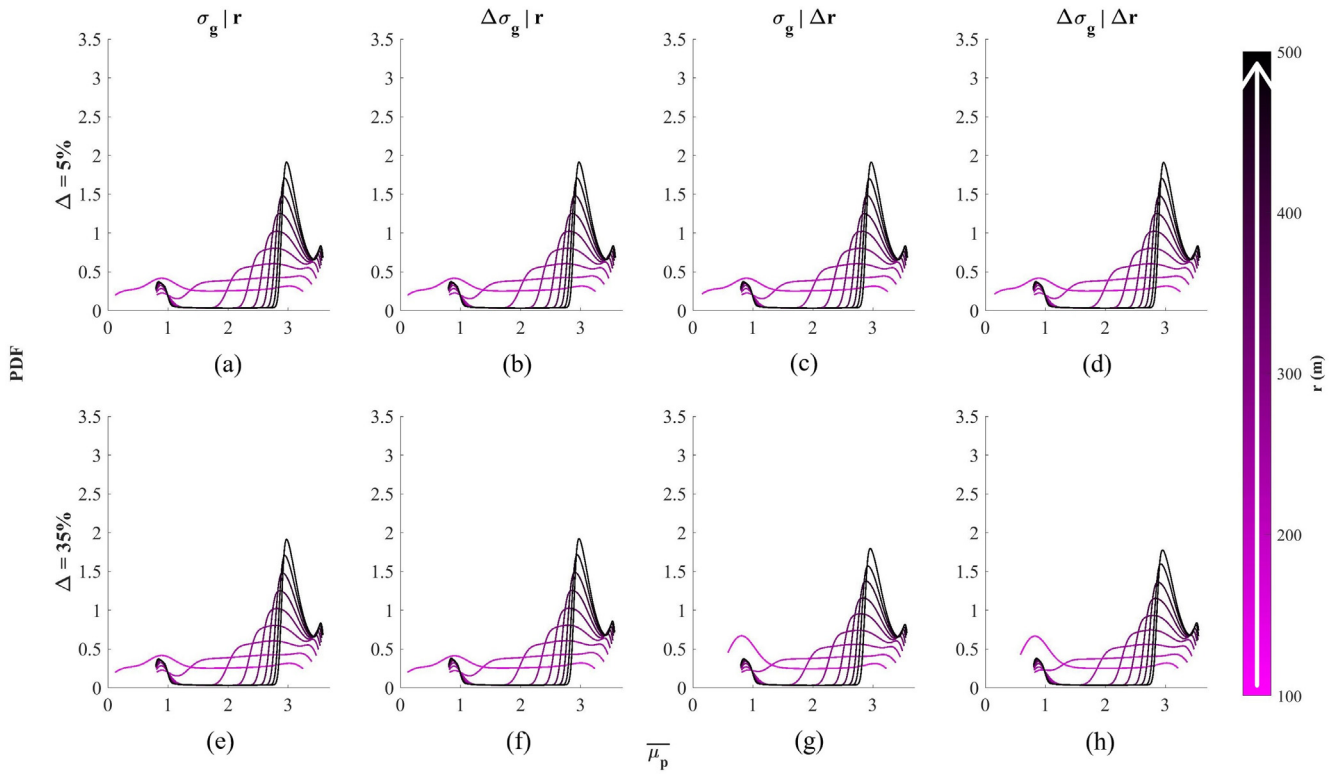


Fig. 6. PDFs for the average ratio of the sound pressure amplitudes ($\overline{\mu}_p$), for an acoustically hard ground ($\sigma_g = 2000\text{kPasm}^{-2}$), where each column defining the uncertainty present and range (r) is mapped to colour, from magenta (100m) to black (500m). Uncertainty (Δ) is at 5% in the first row and increased to 35% in the second row. (For interpretation of the references to colour in this figure legend, the reader is referred to the web version of this article.)

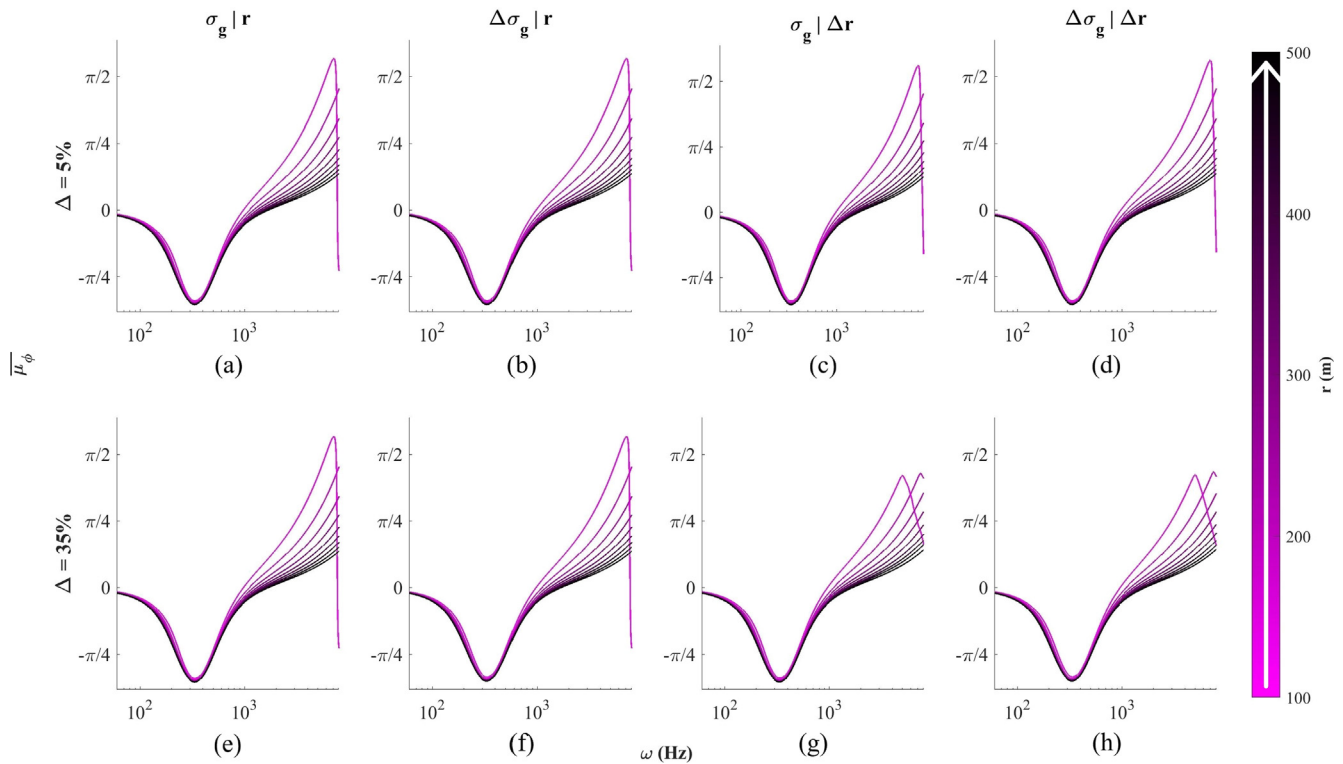


Fig. 7. Simulation results for the average phase difference ($\overline{\mu}_\phi$), for an acoustically soft ground ($\sigma_g = 100\text{kPasm}^{-2}$), where each column defining the uncertainty present and range (r) is mapped to colour, from magenta (100m) to black (500m). Uncertainty (Δ) is at 5% in the first row and increased to 35% in the second row. (For interpretation of the references to colour in this figure legend, the reader is referred to the web version of this article.)

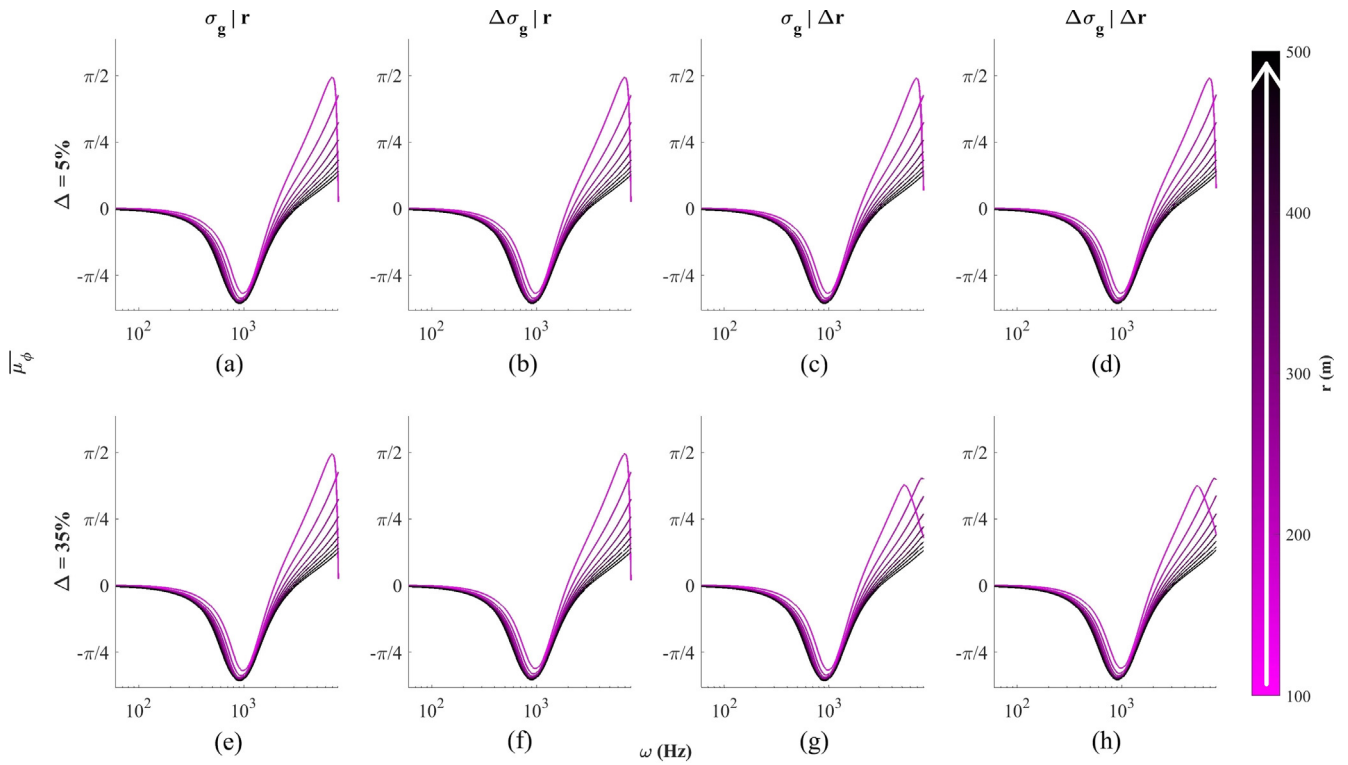


Fig. 8. Simulation results for the average phase difference ($\bar{\mu}_\phi$), for an acoustically hard ground ($\sigma_g = 2000\text{kPasm}^{-2}$), where each column defining the uncertainty present and range (r) is mapped to colour, from magenta (100m) to black (500m). Uncertainty (Δ) is at 5% in the first row and increased to 35% in the second row. (For interpretation of the references to colour in this figure legend, the reader is referred to the web version of this article.)

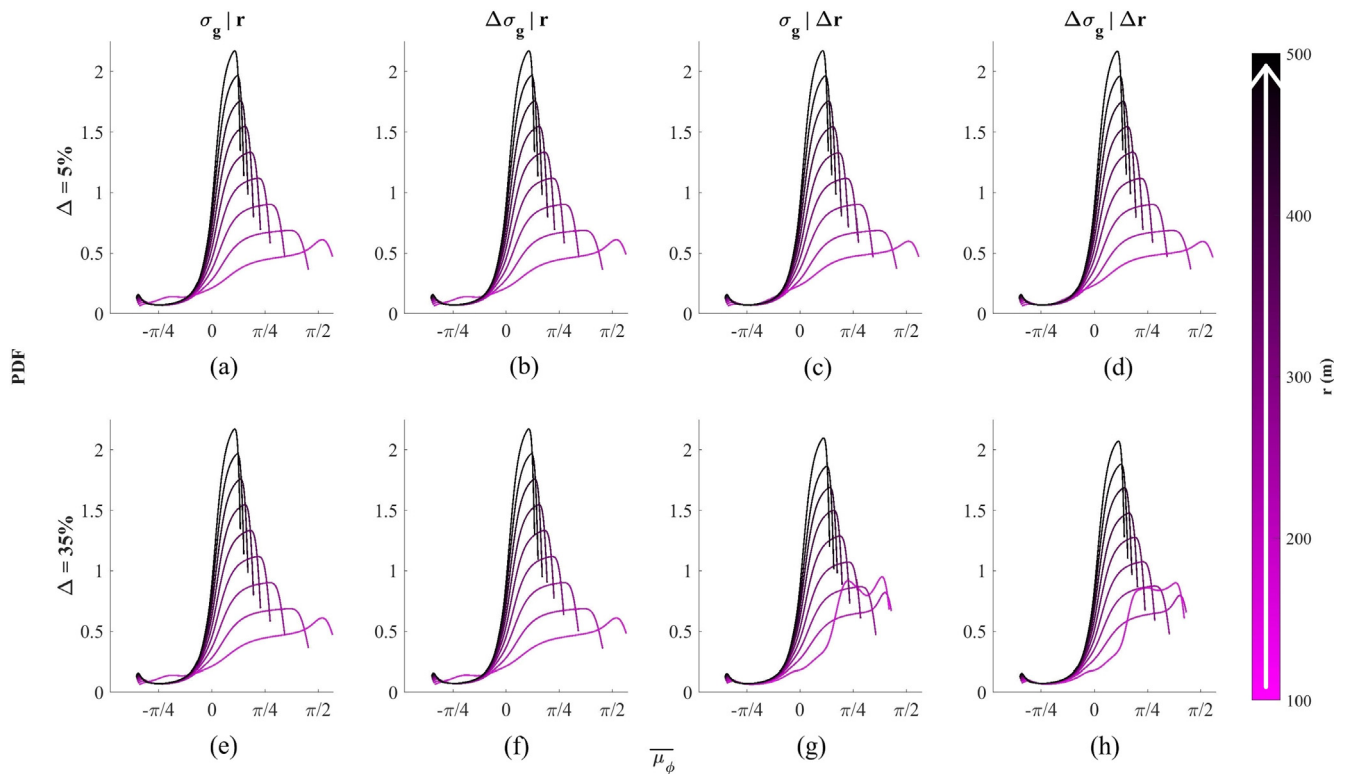


Fig. 9. PDFs for the average phase difference ($\bar{\mu}_\phi$), for an acoustically soft ground ($\sigma_g = 100\text{kPasm}^{-2}$), where each column defining the uncertainty present and range (r) is mapped to colour, from magenta (100m) to black (500m). Uncertainty (Δ) is at 5% in the first row and increased to 35% in the second row. (For interpretation of the references to colour in this figure legend, the reader is referred to the web version of this article.)

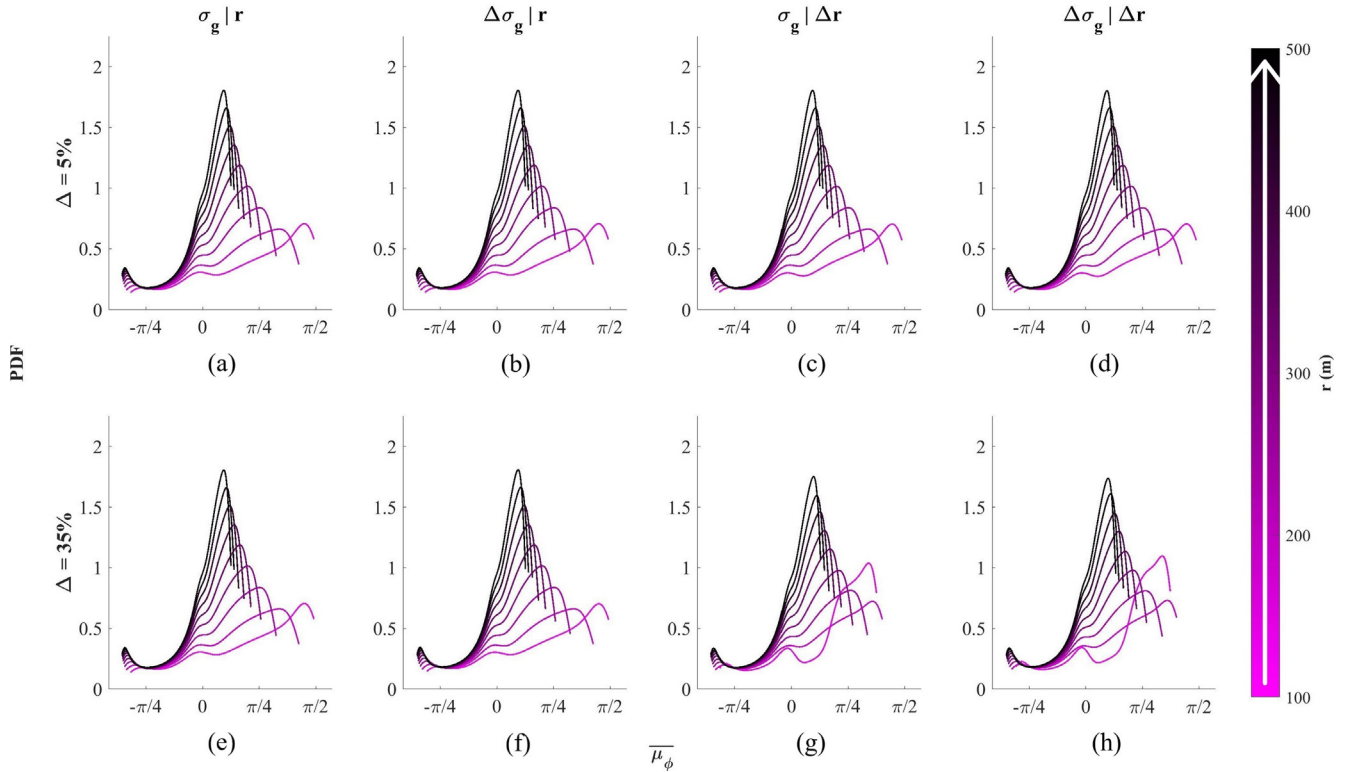


Fig. 10. PDFs for average phase difference ($\overline{\mu_\phi}$), for an acoustically hard ground ($\sigma_g = 2000\text{kPasm}^{-2}$), where each column defining the uncertainty present and range (r) is mapped to colour, from magenta (100m) to black (500m). Uncertainty (Δ) is at 5% in the first row and increased to 35% in the second row. (For interpretation of the references to colour in this figure legend, the reader is referred to the web version of this article.)

tain value of the effective flow resistivity ($\Delta\sigma_g|r$); (iii) uncertain value of the range ($\sigma_g|\Delta r$); and (iv) uncertain values of the effective flow resistivity and range ($\Delta\sigma_g|\Delta r$). Two sets of results are presented: (i) for $\Delta = 5\%$ of the given true value ((a), (b), (c) and (d) in Fig. 5); and (ii) for $\Delta = 35\%$ of the given true value ((e), (f), (g) and (h) in Fig. 5). Fig. 6 presents a similar set of results for the case of hard ground.

The results of these simulations suggest that the variation in the average phase difference spectra ($\overline{\mu_\phi}$) for any combination of small uncertainties ($\Delta = 5\%$) is relatively small, i.e. that this parameter predicted for the chosen microphone locations is relatively immune to the variation in the true value of the range or effective flow resistivity of the ground. The frequency (ω) is the dominant parameter here. Visually, the spectra only show discernible differences from the true spectra, irrespective of the impedance ground (σ_g) ((a) and (e) in Figs. 7 and 8), when the uncertainty in the range (r) is high ($\Delta = 35\%$) and at shorter ranges, i.e. $r \leq 150\text{m}$.

The effect of the effective flow resistivity on the mean of the average phase difference ($\overline{\mu_\phi}$) is more significant than on the average sound pressure amplitude ratio ($\overline{\mu_p}$) (See Appendix A). The mean of $\overline{\mu_\phi}$ seen in Table 1 (See Appendix A) for a soft ground ($\sigma_g = 100\text{kPasm}^{-2}$) starts at ~ 0.8 and reduces to ~ 0.1 at the maximum range of 100 m. These mean values change from 0.65 to -0.015 , respectively, when the impedance of the ground hardens and the effective flow resistivity is increased to $\sigma_g = 2000\text{kPasm}^{-2}$. The standard deviation of the average absolute phase difference ($\overline{\mu_\phi}$) decreases with the increased range (r).

The PDFs for the average phase difference ($\overline{\mu_\phi}$) show a different shape than that of the average absolute pressure ratio ($\overline{\mu_p}$). These

PDFs depend strongly on the range (r), as the peak, and maximum attainable values for average phase difference ($\overline{\mu_\phi}$) of each simulation are directly linked to the range (r), as seen by the evolution between simulations by the colour mapping (Figs. 9 and 10). The lower values of average phase difference are not seemingly affected by the range (r). The change in the impedance ground affects the gradient of the slope of these PDFs, these data show a little ground effect even with the addition of higher uncertainty. When the range is small ($r \leq 150\text{m}$) the PDFs for the average phase difference show a much more complex behaviour than those predicted for greater ranges ((c), (d), (g) and (h) in Figs. 9 and 10). This complex behaviour is exacerbated by an increase in uncertainty in the range parameter.

It is apparent that like in the case of the average absolute pressure ratio ($\overline{\mu_p}$), the PDFs for average phase difference ($\overline{\mu_\phi}$) are not influenced significantly by smaller uncertainties. An increase in the ground impedance reduces the peak in the PDF for the average phase difference at longer ranges, but it does not change the value at which this peak actually occurs. The range and frequency control the PDFs. The range is the most influential parameter, which can be useful for source localisation applications.

4. Conclusions

The two-microphone method is found to be suitable for the characterisation of sound pressure and related measurements. This is said to be true given favourable atmospheric conditions, while early works by the author suggests this assumption holds through varying atmospheric conditions, this conclusion needs further testing in the presence of realistic atmospheric effects such as sound speed gradient and turbulence. The use of the two-microphone method can be helpful in applications related to source localisation

and when the range is greater than 100 – 150m, because the simulations show that this method can be less consistent over the shorter ranges and higher uncertainties. This method seems much more immune to the uncertainties in the range and ground impedance than alternative methods based on single microphone data, e.g. that reported in Ref. [7].

The results suggest that the uncertainty in the ground does not seem to be significant unless the it is relatively high (e.g. $\Delta = 35\%$) and the range is relatively short (e.g. $r \leq 150\text{m}$). In this case, the uncertainty in the range has the dominant effect of the sound pressure ratio spectra and resultant PDFs. Combination of uncertainties in the ground impedance and range results in an increased variability in the predictions of the sound pressure ratio between two microphone positions. This suggests that for applications of the two-microphone method: (i) removal of uncertainty in the range is key for reliably source localisation/inferences, particularly at shorter distances ($r < 150$); and (ii) uncertainty in the effective flow resistivity of the ground is unlikely to affect the behaviour of the PDF for the sound pressure ratio, but relaxing this parameter would result in reduced computational costs with negligible, if any, loss in accuracy.

The frequency has a strong effect on stability of the two-microphone method. For frequencies below 100 Hz the absolute pressure ratio is close to unity and phase difference is close to zero. This small difference between the two sound pressures in this frequency range is likely to affect the quality of inference if this method applied to sources which frequency spectrum is domi-

nated by low frequency components, e.g. gun fire. Larger separations between the two microphones which are comparable with the paths difference and wavelength may be required to enhance the sensitivity of the two-microphone method for applications in this frequency range.

Declaration of Competing Interest

The authors declare that they have no known competing financial interests or personal relationships that could have appeared to influence the work reported in this paper.

Acknowledgements

The author/s acknowledge the support of Defense Science and Technology Laboratory (Dstl) UK and EPSRC CASE studentship award to the University of Sheffield.

Appendix A

Table of statistics

Table 1

Table of means (μ) and std. deviations (σ) for simulation results for average absolute pressure ratio ($\overline{\mu_p}$) and average phase difference ($\overline{\mu_\phi}$) at each combination of given parameters and uncertainty (Δ).

σ_g (kPasm ⁻²)	r (m)	Average absolute pressure ($\overline{\mu_p}$)				Average phase difference ($\overline{\mu_\phi}$)				
		Mean (μ)		Std. Dev. (σ)		Mean (μ)		Std. Dev. (σ)		
		$\Delta = 5\%$	$\Delta = 35\%$	$\Delta = 5\%$	$\Delta = 35\%$	$\Delta = 5\%$	$\Delta = 35\%$	$\Delta = 5\%$	$\Delta = 35\%$	
100	100	1.7279		1.037		0.8282		0.7405		
	150	2.3467		0.6615		0.6182		0.5696		
	200	2.6156		0.5134		0.4401		0.4731		
	250	2.7505		0.4573		0.3322		0.4157		
	300	2.8269		0.4344		0.2599		0.3782		
	350	2.8743		0.4242		0.2082		0.3518		
	400	2.9057		0.4193		0.1693		0.3324		
	450	2.9275		0.4167		0.1391		0.3176		
	500	2.9434		0.4154		0.1148		0.3059		
	$\Delta 100$	1.7302	1.7568	1.0328	0.927	0.8267	0.6842	0.7028	0.5339	
	$\Delta 150$	2.3445	2.2881	0.6628	0.6916	0.6194	0.6367	0.5702	0.5732	
	$\Delta 200$	2.6516	2.5701	0.5134	0.5345	0.44	0.4638	0.473	0.4857	
	$\Delta 250$	2.7499	2.7185	0.4575	0.4686	0.3325	0.3515	0.4159	0.4259	
	$\Delta 300$	2.8257	2.8061	0.4347	0.4398	0.261	0.2737	0.3787	0.3852	
	$\Delta 350$	2.874	2.8607	0.4242	0.4268	0.2085	0.2179	0.352	0.3567	
	$\Delta 400$	2.9056	2.8923	0.4193	0.4212	0.1694	0.1809	0.3325	0.3382	
	$\Delta 450$	2.9274	2.9141	0.4167	0.4182	0.1392	0.1529	0.3177	0.3243	
	$\Delta 500$	2.9434	2.9532	0.4154	0.416	0.1148	0.1231	0.3059	0.3099	
	$\Delta 100$	100	1.7279	1.7277	1.037	1.0356	0.8282	0.8287	0.7404	0.7394
		150	2.3467	2.3464	0.6615	0.6591	0.6182	0.6188	0.5696	0.5684
200		2.6156	2.6153	0.5133	0.5102	0.4401	0.4406	0.4731	0.4718	
250		2.7505	2.7502	0.4572	0.4537	0.3322	0.3327	0.4157	0.4144	
300		2.8269	2.8267	0.4343	0.4306	0.2599	0.2604	0.3781	0.3768	
350		2.8943	2.8741	0.4241	0.4203	0.2082	0.2087	0.3518	0.3505	
400		2.9057	2.9054	0.4192	0.4153	0.1693	0.1698	0.3324	0.331	
450		2.9275	2.9273	0.4167	0.4128	0.1391	0.1396	0.3176	0.3162	
500		2.9434	2.9431	0.4153	0.4114	0.1148	0.1153	0.3059	0.3045	
$\Delta 100$		1.7288	1.7475	1.033	0.9282	0.8251	0.6825	0.7014	0.5324	
$\Delta 150$		2.345	2.2825	0.6624	0.6933	0.6191	0.6417	0.57	0.5755	
$\Delta 200$		2.6149	2.5759	0.5137	0.529	0.4404	0.46	0.4733	0.4825	
$\Delta 250$		2.7497	2.7192	0.4575	0.4653	0.3327	0.3512	0.416	0.4245	
$\Delta 300$		2.8268	2.8031	0.4344	0.4374	0.2599	0.2769	0.3781	0.3857	
$\Delta 350$		2.8742	2.8552	0.4242	0.4246	0.2082	0.2239	0.3518	0.3585	
$\Delta 400$		2.9054	2.8918	0.4193	0.418	0.1696	0.1814	0.3326	0.3372	

(continued on next page)

Table 1 (continued)

σ_g (kPasm ⁻²)	r (m)	Average absolute pressure ($\overline{\mu_p}$)				Average phase difference ($\overline{\mu_\phi}$)			
		Mean (μ)		Std. Dev. (σ)		Mean (μ)		Std. Dev. (σ)	
		$\Delta = 5\%$	$\Delta = 35\%$	$\Delta = 5\%$	$\Delta = 35\%$	$\Delta = 5\%$	$\Delta = 35\%$	$\Delta = 5\%$	$\Delta = 35\%$
2000	$\Delta 450$	2.9272	2.9157	0.4167	0.4147	0.1395	0.1508	0.3178	0.322
	$\Delta 500$	2.9431	2.9329	0.4154	0.4129	0.1152	0.1263	0.3061	0.3101
	100	1.6702		0.9787		0.6473		0.7462	
	150	2.2784		0.7535		0.4345		0.6579	
	200	2.5488		0.704		0.2713		0.569	
	250	2.6876		0.6994		0.1703		0.5146	
	300	2.7678		0.7034		0.102		0.4785	
	350	2.8185		0.7083		0.0528		0.4528	
	400	2.8527		0.7125		0.0158		0.4337	
	450	2.877		0.7159		-0.0131		0.4189	
	500	2.8948		0.7185		-0.0364		0.4072	
	$\Delta 100$	1.6706	1.6846	0.9761	0.8852	0.6399	0.5111	0.7389	0.6153
	$\Delta 150$	2.2779	2.2306	0.7536	0.7632	0.4346	0.4458	0.6579	0.6591
	$\Delta 200$	2.549	2.5052	0.704	0.7078	0.271	0.2918	0.5688	0.5799
	$\Delta 250$	2.6867	2.6548	0.6994	0.6989	0.1708	0.1886	0.5149	0.5243
	$\Delta 300$	2.7677	2.748	0.7034	0.7018	0.102	0.1139	0.4785	0.4847
	$\Delta 350$	2.8181	2.8009	0.7083	0.7063	0.0532	0.0654	0.453	0.4593
$\Delta 400$	2.8529	2.8391	0.7125	0.7106	0.0156	0.0264	0.4336	0.4391	
$\Delta 450$	2.8765	2.8637	0.7158	0.7138	-0.0126	-0.0011	0.4192	0.425	
$\Delta 500$	2.8948	2.8859	0.7185	0.717	-0.0364	-0.0283	0.4072	0.4112	
$\Delta 2000$	100	1.6702	1.671	0.9786	0.9758	0.6473	0.6494	0.7462	0.7447
	150	2.2784	2.2793	0.7534	0.7481	0.4345	0.4366	0.6579	0.6559
	200	2.5488	2.5497	0.7039	0.6975	0.2712	0.2732	0.5689	0.5668
	250	2.6876	2.6884	0.6993	0.6926	0.1702	0.1721	0.5146	0.5123
	300	2.7678	2.7686	0.7033	0.6965	0.102	0.1038	0.4784	0.4761
	350	2.8185	2.8193	0.7082	0.7014	0.0528	0.0546	0.4528	0.4504
	400	2.8527	2.8534	0.7125	0.7056	0.0158	0.0175	0.4337	0.4313
	450	2.877	2.8776	0.7158	0.7089	-0.0132	-0.0114	0.4189	0.4165
	500	2.8948	2.8955	0.7184	0.7116	-0.0364	-0.0346	0.4072	0.4048
	$\Delta 100$	1.6727	1.695	0.9753	0.8778	0.6405	0.5138	0.739	0.6137
	$\Delta 150$	2.2766	2.2218	0.7538	0.761	0.4352	0.4497	0.6583	0.6588
	$\Delta 200$	2.5479	2.5014	0.704	0.7034	0.2716	0.2942	0.5692	0.5794
	$\Delta 250$	2.6872	2.6551	0.6993	0.6942	0.1704	0.1881	0.5147	0.5222
	$\Delta 300$	2.7676	2.7397	0.7034	0.6967	0.102	0.1209	0.4785	0.4865
	$\Delta 350$	2.8184	2.7992	0.7083	0.7016	0.0528	0.0667	0.4528	0.4581
	$\Delta 400$	2.8523	2.8362	0.7124	0.7059	0.0161	0.0294	0.4338	0.4388
	$\Delta 450$	2.8769	2.8661	0.7158	0.7099	-0.0132	-0.0039	0.4189	0.4217
$\Delta 500$	2.8945	2.8839	0.7184	0.7125	-0.036	-0.0258	0.4074	0.4106	

References

- [1] Sabatier JM, Raspert R, Frederickson CK. An improved procedure for the determination of ground parameters using level difference measurements. *J Acoust Soc Am* 1993;94(1):396–9.
- [2] Faranosov GA, Belyaev IV, Kopyev VF, Zaytsev MY, Aleksentsev AA, Bersenev YV, et al. Adaptation of the azimuthal decomposition technique to jet noise measurements in full-scale tests. *AIAA J* 2017;55(2):572–84.
- [3] Hosokawa Y, Hirano Y, Kominami D, Aihara I, Murata M. Implementation of a real-time sound source localization method for outdoor animal detection using wireless sensor networks. *Proceedings of the 13th international conference on signal processing and communication systems*. Gold Coast; 2019.
- [4] American National Standard – Method for Determining the Acoustic Impedance of Ground Surfaces, ANSI/ASA S1.18, 2018.
- [5] Hothersall DC, Harriott JNB. Approximate models for sound propagation above multi-impedance plane boundaries. *J Acoust Soc Am* 1995;97(2):918–26.
- [6] Kruse R, Mellert V. Effect and minimization of errors in in situ ground impedance measurements. *Appl Acoust* 2008;69(10):884–90.
- [7] Parry JA, Horoshenkov KV, Williams DP. Investigating uncertain geometries effect on sound propagation in a homogeneous and non-moving atmosphere over an impedance ground. *Appl Acoust* 2020;160.
- [8] Salomons EM. *Computational atmospheric acoustics*. Kluwer Academic Publishers; 2001.
- [9] Dazel O, Groby JP, Horoshenkov KV. Asymptotic limits of some models for sound propagation in porous media and the assignment of the pore characteristic lengths. *J Acoust Soc Am*. 2016;139(5):2463–74.
- [10] Attenborough K. Outdoor ground impedance models. *J Acoust Soc Am* 2011;129(5):2806–19.

C INVERSE UNCERTAINTY

C.I Outdoor acoustics: Range estimation of gunfire over an acoustically soft impedance ground in a homogeneous atmosphere

Paper III – J. A. Parry, K. V. Horoshenkov and D. P. Williams. “*Outdoor Acoustics: Range Estimation of Gunfire over an Acoustically Soft Impedance Ground in A Homogeneous Atmosphere*”. Proceedings of the International Conference on Statistics: Theory and Applications. (Lisbon, 2019).

Outdoor Acoustics: Range Estimation of Gunfire over an Acoustically Soft Impedance Ground in a Homogeneous Atmosphere

Jordan A. Parry¹, Kirill V. Horoshenkov¹, Duncan P. Williams²

¹University of Sheffield, Department of Mechanical Engineering
Sheffield, England

JAParry1@Sheffield.ac.uk; K.Horoshenkov@Sheffield.ac.uk

²Defence Science and Technology Laboratory (DSTL)
Salisbury, England

DPWilliams@dstl.gov.uk

Abstract – Predicting outdoor sound propagation in uncertain conditions remains a challenge. This increases the complexity of the inverse problem, e.g. parameter recovery in the presence of a particular sound source such as like gunfire. This paper investigates the use of maximum likelihood methods, both frequentist and Bayesian, in inverting true parameters from measured and simulated data. A simple source-receiver acoustic model is used which assumes; a homogeneous atmosphere, soft impedance ground and some medium range sound propagation to predict the deviation in sound pressure at the receiver. A blank firing pistol, Bruni Mod 92, is used to record a realistic sound source spectrum in an anechoic chamber. Gaussian noise is added to model predictions for this type of source to mimic uncertainty of real-life observations. Error analysis is performed by repeatedly generating observations and then evaluating the errors between the true range and recovered range estimate. This analysis is performed in broadband and octave frequency bands. It was found that the frequentist method greatly underestimates the range while the Bayesian method, even with a particularly flat prior, greatly reduces both over- and underestimations, significantly improving the range estimate to within $\pm 5m$ of the true value in the majority of cases. The inclusion of octave band filters in the infrasonic frequency showed these bands were mostly responsible for the accurate range estimates. This paper paves the way for applications of this class of statistical models to real-life acoustic data for source parameter recovery.

Keywords: Acoustics; Sound Propagation; Maximum Likelihood; Maximum A Posteriori; Inference; Error Analysis.

1. Introduction

Unlike other acoustical disciplines, outdoor sound propagation is not well understood in the presence of uncertainty. This complicates the application of the inverse process in which experimental data are used to infer sound source and environmental parameters. Improving the statistical understanding of this problem at the fundamental level will help the development of more robust inversion models and their practical applications.

This paper makes use of the likelihood function, frequentist and Bayesian methodologies to infer an unknown gunshot source range. This is done in the scenario where a simple homogenous atmosphere and soft impedance ground are present, and the remaining key parameters are known. Simulations are done by generating a small set of observations from an established acoustic model with gaussian noise added to simulate uncertainty in experimental data. Parameter estimates are then obtained from the frequentist *Maximum Log-likelihood* [1] and Bayesian *Maximum a Posteriori* methods [2]. The error of the inferred parameters against the true value is studied. This process repeated for over sets of generated observations. The performance of statistical methods is compared for broadband data and data filtered in octave band frequency windows. It is believed that the results obtained from this work will improve current inversion techniques and industrial practices which rely on outdoor sound propagation with uncertainties.

2. Acoustical Methods

2.1. Acoustic Foundations

A typical sound source produces a collection of sound waves, composed of different *frequencies* that propagate through some medium i.e. air in the outdoor case. A *homogenous*, atmosphere removes possible interferences from wind, turbulence and/or temperature gradients. Following this assumption, the sound pressure generated by this source can then be measured at the receiver position as a combination of the direct wave and wave reflected from the ground. These two waves interfere in constructive/destructive way resulting a complicated spectrum of the sound observed at the receiver position. The key parameters that need quantifying to make accurate predictions for this source/receiver/ground

configuration are: sound frequency (ω), source height (s_h), range (r), receiver height (r_h) and impedance of the ground (σ_g). Figure 1 explains this problem schematically.

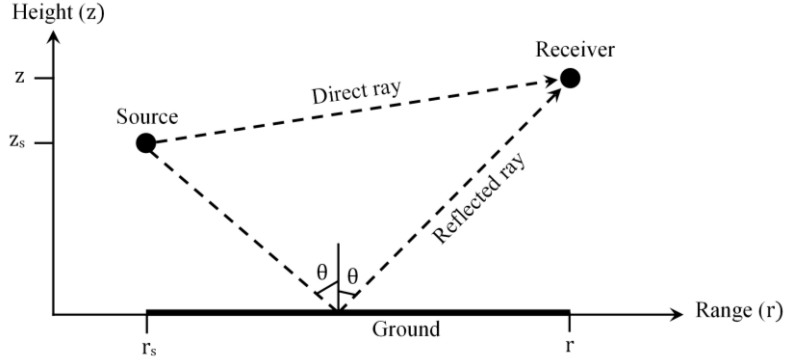


Fig. 1: Acoustic scenario in the (r, z) geometry.

The *excess attenuation* spectrum is a common characteristic of the sound field predicted by this acoustical model. The excess attenuation, ΔL , represents the deviation from the free pressure field now due to the influence of the ground, frequency and geometry, taking positive and negative values due to the constructive or destructive interference between the direct and reflected rays, respectively [3]. ΔL is equated as

$$\Delta L = 10 \log_{10} \left| 1 + Q \frac{R_1}{R_2} \exp(ikR_2 - ikR_1) \right|^2, \quad (1)$$

where

$$R_1 = \sqrt{r^2 + (z - z_s)^2}, \quad (2)$$

$$R_2 = \sqrt{r^2 + (z + z_s)^2}. \quad (3)$$

Parameters k and i are the *wavenumber* and imaginary number, respectively. The parameter Q in eq. (1) is the *spherical wave reflection co-efficient*, describing the relative pressure in the spherical wave reflected by the ground. This is a combination of the *incident angle*, θ , and *normalised impedance* of the ground, Z . Q is calculated as

$$Q = \left(\frac{Z \cos \theta - 1}{Z \cos \theta + 1} \right) + \left(1 - \left(\frac{Z \cos \theta - 1}{Z \cos \theta + 1} \right) \right) F(w), \quad (4)$$

with the *boundary loss factor*, $F(w)$, as

$$F(w) = 1 + iw\sqrt{\pi} \exp(-w) \operatorname{erfc}(-iw), \quad (5)$$

and *error function*, $\operatorname{erfc}(z)$,

$$\operatorname{erfc}(z) = \frac{1}{\sqrt{2\pi}} \int_z^\infty \exp(-t^2) dt. \quad (6)$$

Calculating the acoustic impedance of the ground, Z , can be done by various methods, however assuming the ground to be porous, the method proposed by Horoshenkov et al is used [4] in this paper. This model makes use of the median pore size which relates to the ground impedance. It considers the ground as a porous media with circular pores of non-uniform cross-section. It can be noted however; recent findings suggested the impedance of the ground was not a strongly significant factor inside simple acoustic scenarios while uncertainty was present in the geometry [5].

2.2. Gunshot Evaluation

Acoustical characterisation work on gunfire show that the sound generated can be categorised into three parts; muzzle blast, mechanical action and supersonic projectile [6]. The paper uses data collected from a *Bruni mod 92 blank pistol*, meaning that no supersonic projectile is produced leaving only the muzzle blast and mechanical action of the pistol. Sound recordings were taken of the pistol shots in an *anechoic chamber* at the University of Sheffield. The source and receiver were placed on the hard ground and separated by 3 m. The *Fast Fourier Transform* algorithm was applied

to the time data (left-hand side of Fig. 2) to determine the frequency spectrum of each firing event (right-hand side of Fig. 2).

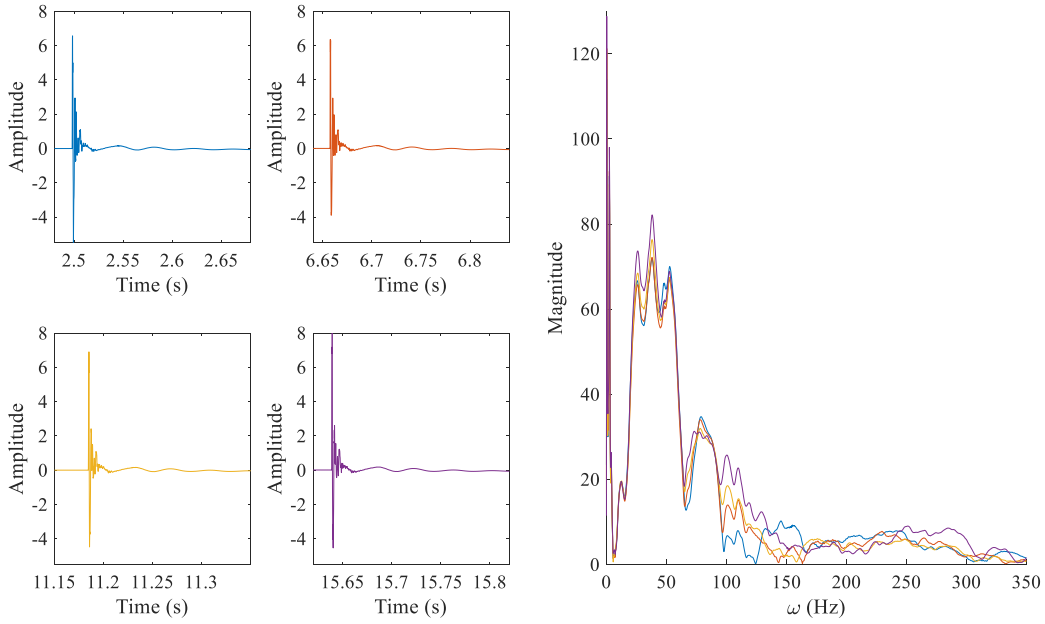


Fig. 2: Selection of gunshot recordings (left) with FFT of each (right).

Problematic mechanical action i.e. the casing being ejected, ricocheting etc is assumed to be the causes of the variation in the higher frequencies in the frequency plot (Fig. 2). It is also logical to assume that at long ranges, the smaller intensity of such sounds would likely dissipate before reaching the receiver. The measured frequency spectra were then averaged, using a cut-off point to remove small amplitudes, to leave a singular array of values which created a broadband frequency spectrum between a minimum of 0.24Hz and maximum of 93.02Hz. These frequencies correspond to the lower and upper octave bands used in this paper as it is common in acoustical practices to study outdoor sound propagation in individual octave bands. Octave filtered bands used in our analyses (Table 1) follow the current international standard set [7]. Bands with an asterisk (*) are described but are not used in analysis since the spectrum recovered did not contain frequencies inside that respective window.

Table 1: Octave band limits, in accordance to ISO 266.

Octave 1/1 Band	Lower Limit (Hz)	Centre Frequency (Hz)	Upper Limit (Hz)
Band 0	0.24	1	1.41
Band 3	1.41	2	2.82
Band 6	2.82	4	5.62
Band 9*	5.62	8	11.2
Band 12	11.2	16	22.4
Band 15	22.4	31	44.7
Band 18	44.7	63	89.1
Band 21	89.1	125	177

2.3. Parameter Selection and Observations

The *known* source and receiver heights were set to $2m$, as higher geometries begin to be highly subject to atmospheric effects, thus keeping our current model fit for use. The ground was considered as *acoustically soft*, which is typical for a field with low growing vegetation with an experimentally measured flow resistivity of at $500Pasm^{-2}$ corresponding to the median pore size of $530\mu m$ [8]. Range, being the *unknown* parameter, will have three true values being; $100m$, $200m$ and $300m$. The excess attenuation spectrum, ΔL for the each set of true values are shown in Fig. 3.

Before collecting observations, it is helpful to rewrite the acoustical model (eq. (1)) as a function of the parameters

$$Y = f(\omega, h_s, r, h_r, \sigma_g). \quad (7)$$

It is assumed that the acoustic model is *perfect* which means that it will predict the exact sound spectra for the input parameters given. To generate observations, the function (eq. (7)) has some gaussian noise added to predicted values, via an error term of $\varepsilon_s \sim N(0, \sigma_\varepsilon^2)$ with the variance σ_ε^2 fixed at 3dB. Thus, dropping constant terms from the notation, observations can be generated by the rewritten function

$$y_s = f(\omega, r) + \varepsilon_s . \quad (8)$$

In relation to the true excess attenuation spectrum, the possible values of the observed excess attenuation are shown to exist between the dashed limits depicted in Fig. 3.

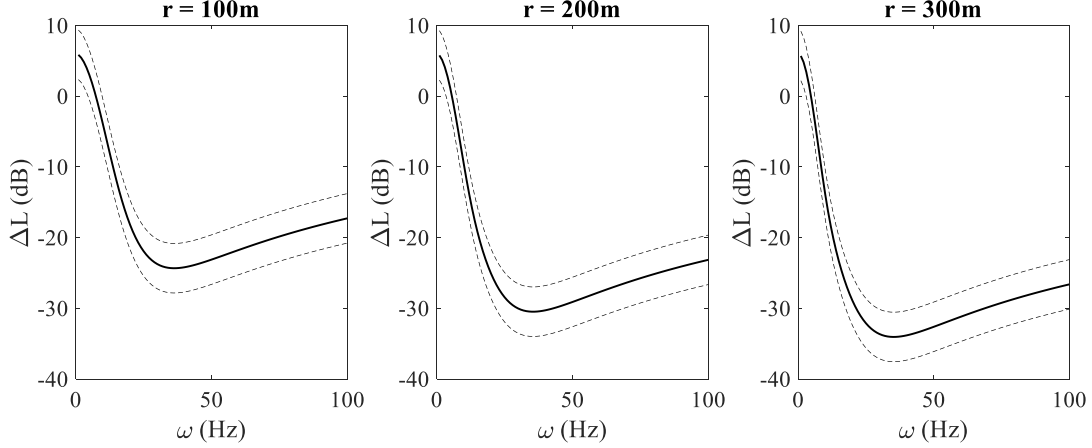


Fig. 3: Excess attenuation spectrum (solid) for true values, for range at 100m (left), 200m (middle) and 300m (right). Limits to observed values due to noise (dashed) are superimposed.

3. Statistical Methods

3.1. Maximum Log-likelihood Estimation (MLE)

The first method will be of the frequentist approach, maximising the likelihood function to estimate a given parameter. It is assumed that the observations generated can be described by some normal distribution, of some give mean and variance $X_s \sim N(\mu, \sigma^2)$, then it has the likelihood function $\mathcal{L}(\theta|X) = \prod_{s=1}^n f_N(x_s; \mu, \sigma^2)$, which can be log transformed to the log-likelihood as

$$\log(\mathcal{L}(\theta|X)) = \ell(\theta|X) = -\frac{n}{2} \log 2\pi - \frac{n}{2} \log \sigma^2 - \frac{1}{2\sigma^2} \sum_{s=1}^n (x_s - \mu)^2 . \quad (9)$$

The above is the log-likelihood [1]. The function in eq. (9) can then, using eq. (7) and eq. (8), be rewritten as

$$\ell(\theta|Y, \omega, r) = -\frac{n}{2} \log 2\pi - \frac{n}{2} \log \sigma^2 - \frac{1}{2\sigma^2} \sum_{j=1}^q \sum_{k=1}^m \sum_{s=1}^n (y_s - f(\omega_j, r_k))^2 . \quad (10)$$

This log-likelihood, eq. (10), uses an n number of generated observations (y_s), to find the best estimate of the range from the source (r_k), from a parameter space of m points, by locating the point in which the function is maximised. This is done for each frequency (ω_j) from an array of q frequency points. Apart from finding the maximised value for r for all the complete frequency spectrum, maximised results inside frequency bandwidths like the defined octave bands (Table. 1), and thus a related estimate for r , can be located to be explored.

3.2. Bayesian Maximum a Posteriori (MAP)

The second method adheres to the Bayesian perspective. Bayes' theorem allows for the likelihood function to be combined with prior beliefs, giving such knowledge statistical weighting in the predictive process. The renown theorem can be written as

$$P(\theta|X) = \frac{P(X|\theta) \times P(\theta)}{P(X)} = \frac{\mathcal{L}(\theta|X) \times P(\theta)}{P(X)} , \quad (11)$$

where $P(\theta|X)$ is *posterior*, $P(X)$ is the *evidence*, $P(\theta)$ is the *prior* and $\mathcal{L}(\theta|X)$ the likelihood described earlier. The posterior probability is computed as a probability distribution of θ given the observed data X . Since the peak of the posterior distribution is the only value of interest to us, as this is the *most likely* estimate of the parameter/s, the normalising constant of $P(X)$ can be dropped greatly reducing computational effort. This results in eq. (3) being modified to

$$P(\theta|X) \propto \mathcal{L}(\theta|X) \times P(\theta) . \quad (12)$$

Eq. (12) allows for the MAP (Maximum a posterior) estimate, or the most likely value given the combination of prior beliefs and observed data, to be found. Like the earlier likelihood function, eq. (12) can be log transformed to

$$\log(P(\theta|X)) \propto \ell(\theta|X) + \log P(\theta) . \quad (13)$$

Priors can be used to import knowledge, or lack of, around the true value. Furthermore, the log of probability is a negative number, thus the value of $\log P(\theta)$ can be interpreted as a penalty term. When the estimated parameters fall outside the interval prior, the penalty becomes $\log(0)$, thus reducing the likelihood to $-\infty$. [2]. The prior probabilities applied in this work are assumed to be proportional to some normal distribution, $P(\theta) \sim N(\mu^*, \sigma^*)$, where the value of μ^* is taken to be equal to the true parameter in each scenario. The standard deviation in the source range is fixed at $\sigma^* = 15m$, as this gives a possible error of up to $\sim \pm 50m$. This is analogous to the observer having an idea where the gunshot was fired yet giving themselves a large window of error, that is also similar to the parameter space of r that is numerically calculated from.

3.3. Computational Error Analysis

Investigating how efficient an estimate of the range is achieved computationally (using MATLABTM) by comparing every simulated estimate to the true value of r in question. This is done by creating 3 observations, using eq. (8), maximising likelihood function for the observations over the (m, q) space detailed in eq. (10) with, and without, a prior belief applied and comparing the related estimate of r to the true range for all the three different true ranges. The process is repeated 1000 times, for each true value of r , so an adequate amount of errors can be investigated. Errors are compared across combinations of each true value for range, statistical method applied and frequency windows.

4. Results

4.1. Broadband Analysis

Comparing the errors from using MLE to the MAP methods (Fig. 4) reveals clear differences in how well the true range of the source was recovered from the simulated observations. The MLE method is not very effective at any range, actually estimating each possible value of r in the parameter space used at least once. There is also a large tendency to underestimate by the minimum possible value. The shortest range ($100m$) was least susceptible to this but the remaining ranges ($200m, 300m$) had over a 50% chance of being out by $-50m$, which is a 50% error in the $100m$ case. In only a small percentage of simulations was the true value recovered, but this was as likely as recovering any parameter from the parameter space for r . There was also a recurrent overestimation ($+\sim 15m$) in the case where $r = 100m$, being the most estimated value, yet this slight overestimation disappeared once the range was increased.

Bayesian MAP method showed that the application of a prior, even the flat one used, greatly reduced the margins of error with 60% + of the simulations approximating the true value of r ($\pm 2m$). Some underestimations of $\sim -50m$ remained present in the shortest range ($100m$), but the occurrence of this was greatly reduced than to their MLE counterparts. For the ranges greater than $100m$, the variance in the error decreases greatly. Some errors of up to $+\sim 20m$ for $r = 200m$ and $+\sim 10m$ for $r = 300m$, yet these results were extremely uncommon. The majority of the results fell within $\pm 5m$, a far more reliable window of error than that of the MLE.

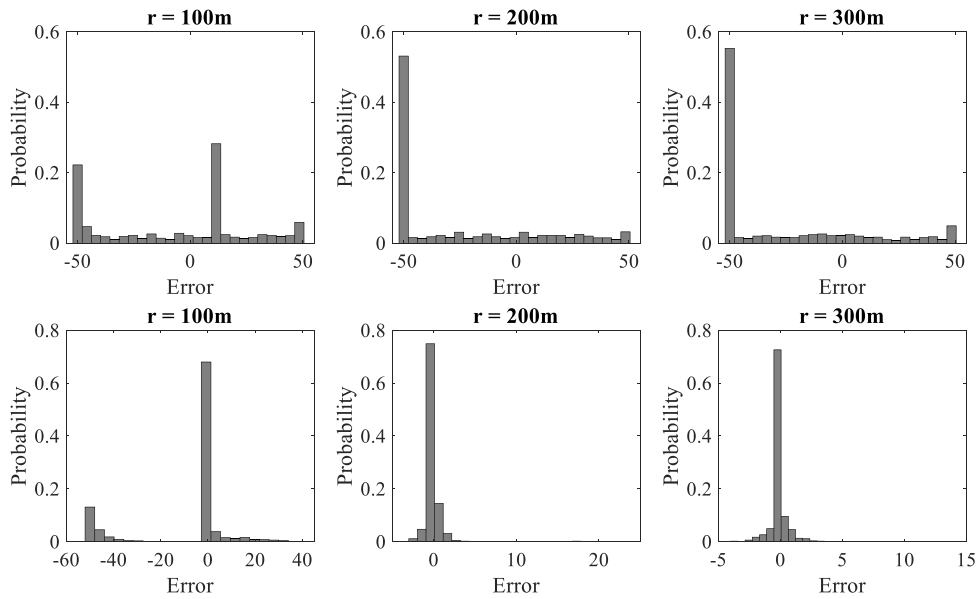


Fig. 4: Errors between estimate and true range across simulations using MLE (top row) and Bayesian MAP (bottom row) methods.

4.2. Octave Filtering

Filtering the excess attenuation data into octave bands and applying the MLE method to data presented in individual octave bands resulted in almost identical errors as in the case of broadband data. However, the application of the MAP method to octave band data proved more successful. Frequency bands deep into the infrasonic range ($< 6\text{Hz}$) were most successful in estimating the true value, with the full variance in errors greatly decreasing as the centre frequency decreased. Application of the MAP method to Band 6 revealed that rarely overestimations were made, and when the exact value wasn't recovered the error was spread between 0m and -50m . Decreasing to Octave band 3 reduced the underestimation, to approximately -20m , with a small likelihood of overestimating by up to $\sim 20\text{m}$. Band 0 was the most efficient, with little to no underestimation, but could overestimate by up to 10m , while it had recovered the true value ($\pm 2\text{m}$) in over 50% of simulations. There were consistent effects of the range, apart from the increase in range to 300m inside Octave band 6 pushed up the maximal underestimations to be the most persistent.

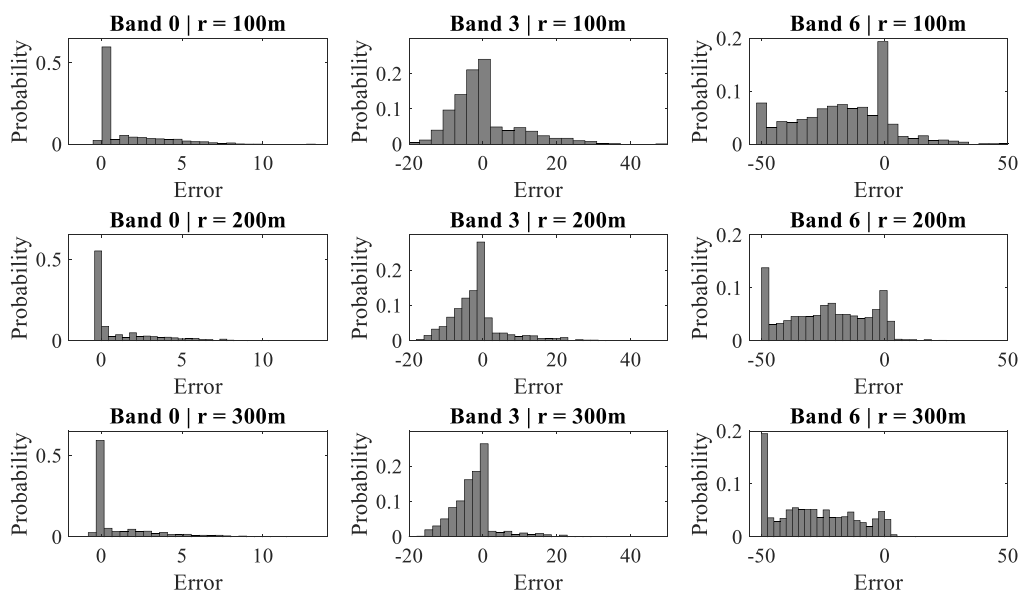


Fig. 5: Error between estimate and true range across simulations for the Bayesian MAP method for each true range (rows) and the lowest three Octaves (columns).

5. Conclusion

Estimating the sound source range solely from the maximising likelihood function does not recover its true value effectively being susceptible to large underestimations. The Bayesian use of a prior was significantly more effective. In the case of a *flatter* prior, it greatly improved the ability of the model to recover the true parameter value within $\pm 2m$. Most other simulations resulted in an error of $\pm 10m$, particularly at longer ranges. At the shorter range of $100m$ the method underestimated the true range value, but the occurrence of this reduced by half. This supports the case of using Bayesian techniques with data that has: a small sample size, not easily replicable or when time constraints may be present around the inference result.

Octave filtering using only the maximisation of the likelihood revealed no significant differences in the error analysis than to the broadband spectrum. However, the application of the Bayesian MAP method to octave band data was shown more successful when some particular frequency bands were adopted. In particular, the infrasonic ($< 20Hz$) frequency bands were found to produce less error. Octave bands higher than Band 6 consistently underestimated the range by $\sim -50m$, akin to that observed with the MLE method. Thus, it is recommended to use a combination of the lower frequency bands and MAP method with priors that allow for more accurate estimations. This supports the idea of relying on infrasonic measurements for a gunfire source when the impedance ground is soft to make accurate predictions while also and may prove useful when trying to invert parameters from higher dimensional problems i.e. inhomogeneous atmosphere.

Acknowledgements

The author/s acknowledge the support of Defense Science and Technology Laboratory (Dstl) UK and EPSRC CASE studentship award to the University of Sheffield. The authors are also grateful to Prof. Jeremy Oakley from the Department of Mathematics and Statistics at the University of Sheffield for his useful comments on the statistical aspects of this work.

References

- [1] M. S. Paoletta, "Likelihood," in *Fundamental Statistical Inference: A Computational Approach*, Oxford, England: Wiley, 2018, pp. 21-27.
- [2] D. Cousineau and S. Hélie, "Improving maximum likelihood estimation with prior probabilities: a tutorial on maximum a posteriori estimation and an examination of the Weibull distribution", *Tut. in Quant. Methods for Psych.*, vol. 9, no. 2, pp. 61-71, 2013
- [3] E. M. Salomons, "Homogenous atmosphere above a ground surface," in *Computational Atmospheric Acoustics*, Netherlands: Kluwer Academic Publishers, 2001, pp. 21-27.
- [4] K. V. Horoshenkov, O. Dazel and J. P. Groby, "Asymptotic limits of some models for sound propagation in porous media and the assignment of the pore characteristic lengths", *J. Acoust. Soc. Am.*, vol. 139, no. 5, pp. 2463-2474, 2016.
- [5] J. A. Parry, K. V. Horoshenkov and D. P. Williams, "On the uncertainties in outdoor sound propagation over a porous ground," in *Proceedings of the Institute of Acoustics 'ACOUSTICS 2019'*, Milton Keynes, UK, 2019.
- [6] R. C. Maher, "Acoustical characterization of gunshots," in *Proceedings of Signal Processing Applications for Public Security and Forensics Workshop 'SAFE 2007'*, Washington, D.C., 2007.
- [7] *Acoustics – Preferred frequencies*, ISO Std. 266, 1997.
- [8] K. V. Horoshenkov, A. Khan and H. Benkreira, "Acoustic properties of low growing plants", *J. Acoust. Soc. Am.*, vol. 133, no. 5, pp. 2554-2565, 2013.

C.II Likelihood maximisation techniques for ranging gunfire over grassland

Paper IV – J. A. Parry, K. V. Horoshenkov and D. P. Williams. “*Likelihood maximisation techniques for ranging gunfire over grassland*”, *Applied Acoustics*, 164 (July 2020).



Likelihood maximisation techniques for ranging gunfire over grassland

Jordan A. Parry^{a,*}, Kirill V. Horoshenkov^a, Duncan P. Williams^b

^a University of Sheffield, Dept. of Mech Engineering, Sheffield, England, UK

^b Defence Science and Technology Laboratory, Salisbury, England, UK



ARTICLE INFO

Article history:

Received 18 December 2019

Received in revised form 15 February 2020

Accepted 18 February 2020

Keywords:

Outdoor sound propagation

Gunfire

Maximum likelihood estimation

Maximum A posteriori

Error analysis

ABSTRACT

A study into acoustic parameter inversion in the presence of a non-moving, homogeneous atmosphere and *grassland* impedance ground is carried out using methods of *likelihood maximisation*. Measured frequency-dependent sound pressure level and power spectra for a blank firing pistol are used to generate simulated data with added Gaussian error to represent variations usually present in real life experiments. Inference is carried out using *maximum likelihood estimation* (MLE) and *maximum a priori* (MAP) where model parameters are either given as known or restricted to some uncertain distribution bounded by realistic conditions. The quality of inference is assessed visually and statistically as the error between the true and inferred predictions for a given propagation range. Application of a prior (MAP) greatly improves inference accuracy compared to the sole maximisation of the likelihood function (MLE). It is shown that the use of a single octave band frequency window does not improve the quality of inference, whereas combinations of several low frequency octave bands do. Exact quantification of the true values of the ground and source height are seemingly less important as range increases beyond 500m. Although the techniques presented in this paper are for military/security applications, they are readily applicable to other acoustical problems, e.g. source characterisation in engineering noise control. The methods adopted are likely to benefit from higher-dimensional models, i.e. inhomogeneous atmospheres, complex terrain or urban environments.

© 2020 Elsevier Ltd. All rights reserved.

1. Introduction

Predicting outdoor sound is a complex problem particularly when there is an uncertainty in the parameters involved. This makes the *inverse problem*, or the *inference* of the non-acoustical parameters affecting outdoor sound propagation from the acoustical data a rather difficult task. This is the situation where an array of statistical concepts and methods can be used to infer a parameter while adjusting for the uncertainty present [1]. Only recently has significant works been published by D. K. Wilson et al, removing some of the ambiguity surrounding uncertainty quantification within outdoor sound propagation [2]. Two cases were studied: a simple homogenous atmosphere then a near-ground propagation in a turbulent atmosphere. It showed which sampling methods proved more accurate, dependant on which parameter uncertainty was more dominant. Citing this work, further research by T. Van Renterghem and D. Botteldooren looked at quantifying the variation in downwind sound propagation over a *grassland* impedance

ground [3]. A large variation was found, strongly dependent on sound frequency, source height, receiver height, and propagation distance. The variation ranges give insight to this systematic uncertainty when performing short-range measurements. However, the effect of the uncertainties and their interactions is still not well understood.

These works suggest to use statistics in combination with outdoor acoustics to understand the uncertainty the problem presents. The art of using statistically justified methods in the already complex outdoor setting usually requires high-level statistical knowledge combined with thorough understanding of acoustical principles. Otherwise, the inference is likely to yield statistically insignificant results. Extending this work to specific sources can complicate matters further, i.e. gun fire sources which spectrum is limited to very low frequencies of sound. Work on gun detection is of obvious importance in defense applications, yet it is still an understudied area particularly in the case of large-scale outdoor situations. There has been works (e.g. [4]) in which methods for localization of small arms fire using acoustic measurements of muzzle blast with, and without, ballistic shock wave arrivals were studied. It was found that accuracy of detection was greatly dependant on the classification of the firearm and bullet

* Corresponding author.

E-mail addresses: JAParry1@Sheffield.ac.uk (J.A. Parry), KHoroshenkov@Sheffield.ac.uk (K.V. Horoshenkov), DPWilliams@dstl.gov.uk (D.P. Williams).

themselves, making wider applicability limited. A more recent paper by one of authors of [4] attempted to expand the model using the *miss angle*, i.e. the angle in which the bullet from a small arms fire passed the acoustic sensor node, to infer the range over a given 2-D space [5]. This method improved by only having to know a known approximate range for the acoustic impulses i.e. gun barrel length, caliber, rather than requiring exact classification of the firearms and components as in the authors former study. It was shown that the error greatly increased with the increase in miss angle, and it was suggested that the method would be relatively accurate for known stationary geometric areas, i.e. counter-sniper zone. This is an improvement for stationary 3D capture, but there was lot of inherent reliance on known parameters, like impedance ground, and a fair amount of information about the firearm source. More recent work by J. A. Parry et al. used a simple *excess attenuation* model, with and without *a priori* knowledge to infer the source range and simulated data for sound propagation from a blank firing pistol [6]. The ground in this instance was assumed to be *vegetative*, creating an *acoustically softer* ground. It was found that errors could be reduced when a *priori* was applied. A greater accuracy ($\sim \pm 5$ m) of range detection was achieved when the likelihood space was filtered in octave bands in the infrasonic frequency range. It was noted that *measuring* the value of excess attenuation directly would require some extra mathematical computation, but this study still showed the powerful accuracy of this method specifically and also how these statistical techniques could be expanded directly to other models.

This paper aims to study the effect of geometrical uncertainties on outdoor sound propagation of a gunshot and performance of some parameter inversion methods. We show that a relatively simple outdoor propagation model and maximum likelihood method can be applied effectively to infer the location of the gunshot with limited prior knowledge at a short and medium range. The study assumes a *grassland* impedance, more similar to wilder areas of United Kingdom. The methods applied also aim to show the effect of specific interactions of uncertainties in the parameters of the model. This paper makes use of two differing statistical ideologies to maximise the *likelihood function*: frequentist and Bayesian. The frequentist method of *maximum likelihood* (or *log-likelihood estimation* (MLE) makes use of the likelihood function in combination with the mean and variance to gather estimates of given parameters [7]. MLE methods have been successfully used in acoustical research, with good examples in the forward case to evaluate models for impulsive noise propagation [8] or for acoustic source localisation in wireless sensor networks [9]. These works are a good example of how MLE methods can be applied to given uncertain scenarios and used to improve understanding of the effects of a given uncertainty on sound propagation, while also being used for direct parameter inference.

The Bayesian *Maximum a Posteriori* (MAP) method also makes use of the likelihood function, but it also incorporates a *prior*, which is the quantification of beliefs or known knowledge [10]. The use of Bayesian methods is more novel in outdoor sound propagation. A recent study successfully used Bayesian inference to optimise the selection of parameters in models used for sound propagation outdoors [11] and in porous media [12]. They however did not successfully detail the uncertainty itself, perhaps because some departure from model simplicity in their approach [11]. The work by Xiang and Fackler [12] defines the power of Bayesian statistics in application to acoustics in general rather than for outdoor sound propagation. This work demonstrates how Bayesian statistics can be used to improve model selection and parameter inference techniques in acoustics. This work suggests that Bayesian methods have their advantages when applied correctly, but they can easily be misused or overcomplicated meaning that intricacies of the physical effects can be overlooked.

Our paper aims to illustrate how these statistical ideas can be effectively applied to study the uncertainty in outdoor sound propagation and how two different statistical approaches can influence the effectiveness of the inference process and quantified in terms of the inversion error. Simulations are used to mimic the repeated measurement to inform the inference process. It is assumed that sound propagates in a non-moving homogenous atmosphere over a *grassland* impedance ground. The impedance ground, and other source geometry parameters are studied under known and uncertain conditions, solely and in combination, to establish whether or not some particular uncertain conditions have a significant influence on the inference process.

Observed data are synthesised using a popular model for short-/mid-range sound propagation that is assumed to be *perfect*, i.e. given a set of geometrical, ground and source parameters this model would predict the exact true value of the sound pressure at the receiver position. Gaussian (normal) noise is then added to simulate the uncertainties present in the measurements. Observation sample size is kept small ($n = 10$) to test the effects of limiting information on the performance of the model. Estimates of the range are gathered from each sample data set either solely from the *maximisation of the log-likelihood* or via *Maximum a Posteriori* by applying some *prior beliefs* as a statistical function. Estimations are performed for a combination of the parameters being given as known, or uncertain. The uncertainty here is some flat *uniform distribution* where no information on which parameter values are more likely is given. The prior considered here is chosen selectively around the true parameter value with a *normal distribution*, $N(\mu, \sigma^2)$, with a mean (μ) and constant variance (σ^2). Prior beliefs are only applied to the range parameter. The function will also have its frequency range restricted to specific *octave bands* to further assess whether inference or parameter interactions change compared to the initial broadband frequency range.

The primary question of this paper is: *How well can a simple method recover an unknown range in an outdoor sound propagation setting?* We are also asking: (i) Which, if any, combinations of uncertainty inside parameters cause more errors than others? (ii) What is the effectiveness of simple statistical techniques in inferring the source range? (iii) How effectively the source of a gunshot could be detected, over a grassy floor, using these methods? The answer to the primary question is likely to have an immediate impact on current practices while the other specific questions will help improve the basic understanding of the uncertainty in outdoor sound propagation. This work will also pave the way to further statistical improvements to acoustic inversion methods in the presence of uncertainties, with direct application to improving gunshot detection practices.

This paper is structured in the following manner. [Section 2](#) describes the acoustical model and source characterisation. [Section 3](#) details the statistical likelihood methodologies. [Section 4](#) reviews the results from the simulations, firstly for broadband sounds and then at octave filtered frequency bands. Finally, [Section 5](#) is the conclusions from this study.

2. Research methods

2.1. Gun source evaluation

Acoustical characterisation of gunfire shows it has three main components: (i) muzzle blast, (ii) mechanical action; and (iii) supersonic projectile [13]. The gun used in this study is a *Bruni Mod. 92 Top Venting 8 mm Blank Pistol*. A blank pistol must be used due to the obvious security issues and to obey with the statutory gun law in the UK. This means that the third contributing sound source of the projectile is not present in this experiment. Acoustic

recordings of the gunfire are taken in the *anechoic chamber* at the University of Sheffield. The hilt of the gun is placed on the floor and 3m away from a GRAS 46AN 1/2" Microphone which is also placed on the floor. The frequency range of this microphone is 0.5–10000 Hz. The microphone is connected to a NI DAQ PC and digitised at 1 kHz without any filtering except the anti-aliasing filter provided as standard in the NI DAQ PC. The level of background noise in the chamber was negligibly small in comparison with the level of the gunshot (with the SNR > 100 dB). Recordings made were narrowed down to four *clean* recordings to study the reproducibility of the source spectrum with minimum interference. Fig. 1 presents the Fourier spectra plotted against the frequency (ω) in Hertz of the four *clean* (i.e. without unwanted sounds heard during recording) gunshots. The frequency spectra show strong peaks around < 50Hz and 50Hz which level is consistent within ± 1 dB between individual gunshots. Frequencies over 500 Hz were omitted due to their lack of energy. The time and Fourier spectra look remarkably alike to other experimental data recorded for other types of gunfire [14,15].

An important quantity that can be established from these recordings is the *sound power level* (SWL or L_w for hereon) of the gunshot. The SWL of the source placed on the ground can be defined as

$$L_w(\omega) = L_{\bar{p}}(\omega) + 10 \log(2\pi\bar{r}^2) \quad (1)$$

where \bar{r} is the range from the sound source and $L_{\bar{p}}$ is the *sound pressure level* (SPL from hereon). The range from the source is known to be 3 m, resolving the second term in Eq. (2). The SPL is a measure of the frequency-dependent pressure measured against the reference pressure ($p_{ref} = 20 \times 10^{-6}$ Pa). The SPL is calculated from

$$L_{\bar{p}}(\omega) = 10 \log\left(\frac{p_{av}^2(\omega)}{p_{ref}^2}\right) \quad (2)$$

where $p_{ref} = 20\mu Pa$ is the reference sound pressure. The mean is taken from the measured pressures (p_{av}), as seen in the left of Fig. 1, to then obtain a given SPL. This gives us a representative

frequency dependent SWL of the gunshot (see RHS of Fig. 1) ready to be used to generate long range observations.

2.2. Acoustical predictions

Acoustical predictions are made with one receiver across a 2-D plane as shown in Fig. 2. Ignoring problems, such as angle detection for a 3-D sound propagation case allows for better investigation into the underlying uncertainties. In practical applications the measured quantity at the receiver is the SPL. The calculated SWL is used to simulate the SPL (L_p) that would be measured at a given range. According to the constraints from the assumptions of the homogenous atmosphere and from impedance ground, the frequency dependent SPL at a given range r can be calculated as [16]

$$L_p(\omega) = L_w(\omega) - 10 \log(4\pi r^2) + \Delta L(\omega) \quad (3)$$

where ΔL is the *excess attenuation*. *Atmospheric absorption* is omitted due to its negligible effect at the given lower frequencies. The excess attenuation for a non-moving, homogeneous atmosphere is a measure of the ground effect only and it is calculated as [17]

$$\Delta L = 10 \log \left| 1 + Q \frac{R_1}{R_2} \exp(ik(R_2 - R_1)) \right| \quad (4)$$

where k and Q are the wavenumber and spherical wave reflection coefficient, respectively. The distances R_1 and R_2 can be defined as

$$R_1 = \sqrt{r^2 + (z - z_s)^2} \quad (5)$$

$$R_2 = \sqrt{r^2 + (z + z_s)^2} \quad (6)$$

for given source (z_s) and the receiver (z) heights. The spherical wave reflection coefficient (Q) accounts for the effect of the impedance ground on the acoustic pressure amplitude and phase. The equation for the spherical wave reflection coefficient is

$$Q = \left(\frac{Z \cos \theta - 1}{Z \cos \theta + 1} \right) + \left(1 - \left(\frac{Z \cos \theta - 1}{Z \cos \theta + 1} \right) \right) F(\omega) \quad (7)$$

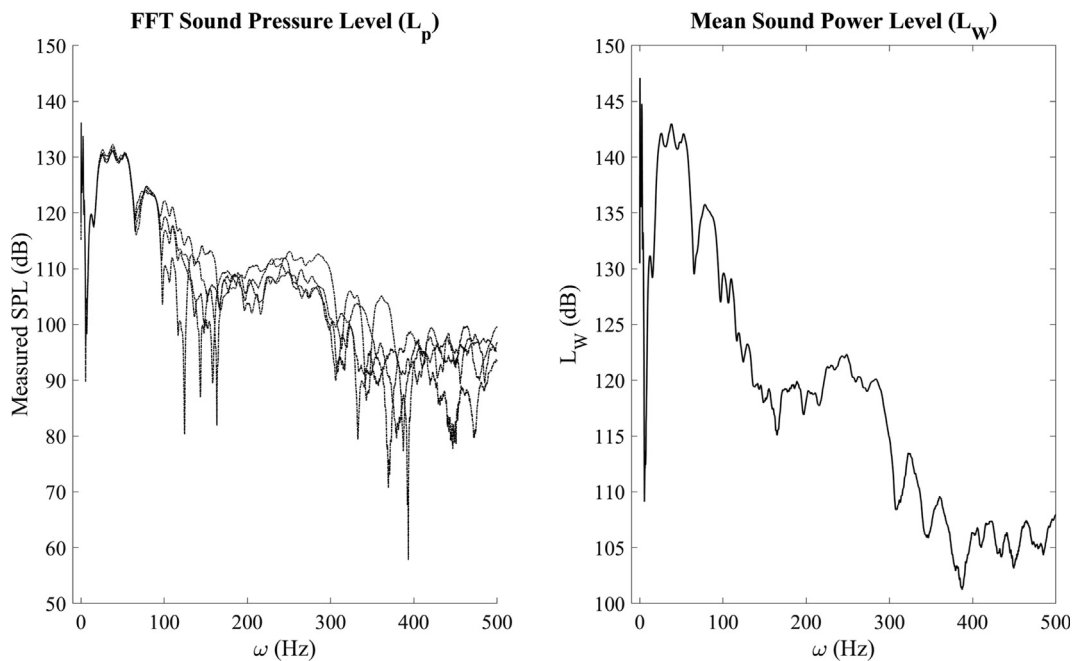


Fig. 1. Sound pressure level spectra ($L_{\bar{p}}$) of the gunshot recordings (left) and the mean sound power level (L_w) spectrum (right).

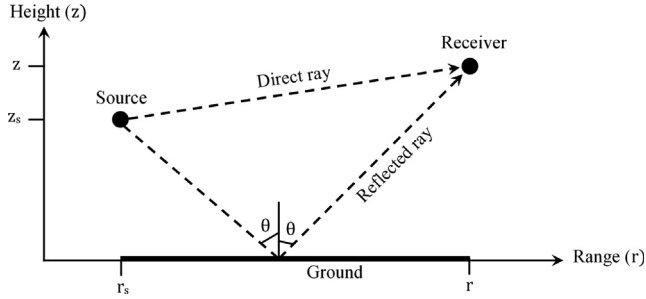


Fig. 2. Acoustic scenario in the (r, z) geometry.

The angle θ is the incident angle as shown in Fig. 2. The function $F(w)$ accounts for the boundary loss factor and it is defined as

$$F(w) = 1 + iw\sqrt{\pi} \exp(-w) \operatorname{erfc}(-iw) \quad (8)$$

with $\operatorname{erfc}(-iw)$ being the complimentary error function

$$\operatorname{erfc}(z) = \frac{1}{\sqrt{2\pi}} \int_z^{\infty} \exp(-t^2) dt. \quad (9)$$

The parameter Z in Eq. (7) is the normalised impedance of the ground, which depends greatly on the ground characteristics. The impedance Z is determined using the model proposed by Horoshenkov et al. [18]. This model calculates the acoustic properties of the impedance ground by considering the ground as a porous media with pores of non-uniform cross-section with the median radius \bar{s} .

In outdoor sound propagation studies, it is common to refer to the effective flow resistivity of the ground (σ_g). The acoustic impedance model proposed in [18] relates the effective flow resistivity to the median pore size as

$$\sigma_g = \frac{8\eta\alpha_{\infty}}{\bar{s}^2\phi} e^{6(\sigma_s \log 2)^2} \quad (10)$$

where η is the dynamic viscosity of air. In the above equation it is common to set the values of porosity (ϕ) and tortuosity (α_{∞}) to unity and standard deviation in pore size (σ_s) to zero, because for a majority of outdoor ground types their influence on the value of effective flow resistivity is relatively small in comparison with that of the median pore size.

Examples of the excess attenuation spectrum for the given true values, the varying range and grassland impedance, of the input

parameters are shown in Fig. 3. It is seen how the value of excess attenuation (ΔL) varies across frequency (ω), exhibiting an oscillatory behaviour with the increase of frequency (ω). The initial geometry effects the interaction pattern, with more oscillations occurring as the range is decreased.

2.3. Generating observed SPL

Observations are generated by assuming that our acoustical model is *perfect*, or that with given parameters the model would predict the exact observable value i.e. SPL measurement. This assumption allows observations to then be generated by using the predictive model itself with some given *noise*. Initial observations are generated using the SPL model (Eq. (3)) with the true heights of the source (h_s) and receiver (h_r) set to 2 m and the impedance ground has the effective flow resistivity (σ_g) of 100 kPasm⁻², which is the typical for *grassland* [19]. The range (r) is assessed at either 250 m or 500 m. The predicted SPL spectrum for the set parameters including the range (r), are shown in Fig. 4 as black lines. These predicted SPL show a strong resemblance with the experimental data recorded for similar settings using a 9 mm handgun [20], with the differences expected to be due to 1 mm decrease in the pistol calibre and lack of projectile in the case of our pistol. The sound propagation model, Eq. (3), can be expressed as a function of the input parameters

$$y = f(\omega, h_s, r, h_r, \sigma_g, L_W(\omega)) \quad (11)$$

Simulated observations are then repeatedly generated by adding a random, but *controlled*, artificial error to mimic noise within data collection, thus observations, y , are generated via

$$y = f(\omega, h_s, r, h_r, \sigma_g, L_W(\omega)) + \varepsilon_s \quad (12)$$

The error applied at every simulation is randomly drawn from the distribution $\varepsilon_s \sim N(0, \sigma_{\varepsilon}^2)$, with a fixed variance (σ_{ε}^2) set to 5dB. This error term remains constant across frequency (ω). Normal (Gaussian) error is an acceptable error term to use being supported by the central limit theorem. The added term creates observations that can be ± 5 dB away from the true value. However, the probability of observing data with such an error decreases the further it moves from the true value. This error value is approximately equal to 10% of the difference between the highest and lowest observable SPL. The range for which the generated observations can be measured are seen via the dashed limits in the plots of the true SPL (dashed lines in Fig. 4).

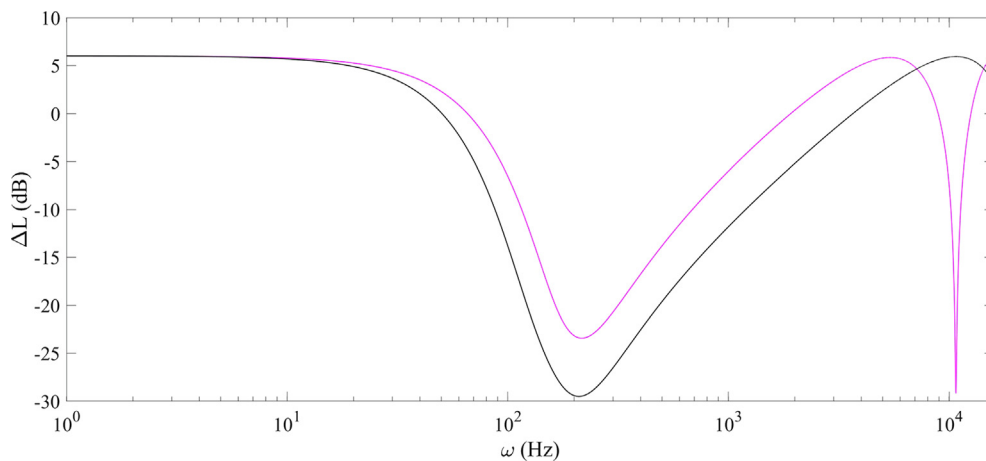


Fig. 3. Excess attenuation (ΔL) spectra of due to each combination of parameters and impedance ($\sigma_g = 100 \text{ kPasm}^{-2}$) over a logarithmic scale up to a frequency (ω) of 16kHz. The ranges given are 250m (black line) and 500m (magenta line). (For interpretation of the references to colour in this figure legend, the reader is referred to the web version of this article.)

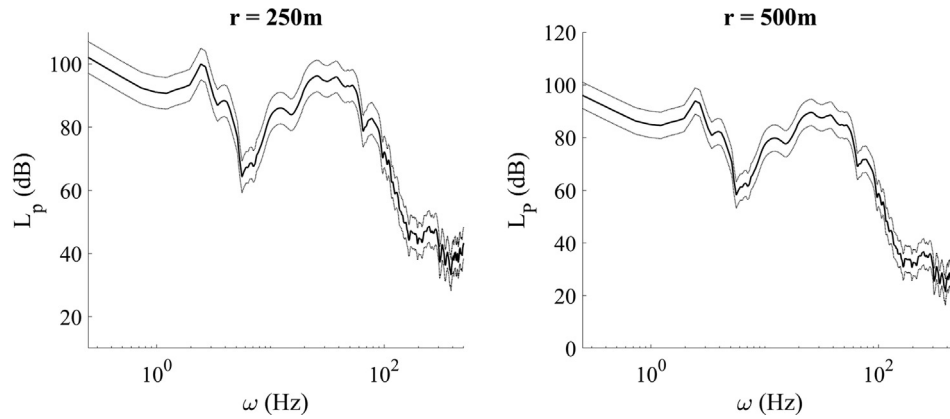


Fig. 4. Predicted SPL (L_p) against frequency (ω) for the different ranges (r) over a logarithmic scale (solid line). Error margins for observation generation are superimposed (dashed lines).

For our investigations a small amount of observations ($n = 10$) are used to test how effective the parameter estimation can be using each statistical technique and little information present in the model. It is known that smaller sample sizes increase the uncertainty present in the estimation techniques. This is a key part in the investigation to compare how applicable this methodology is in practice in the presence of such systematic uncertainty.

In practice it is common to analyse the sound pressure level in octave bands. This analysis will become useful as shown in the following sections. The octave bands used in our analysis are defined in Table 1 in accordance with the ISO 266 [21]. Each band is denoted as B with a relevant subscript. This is merely to improve ease during visual analysis and scission.

3. Statistical techniques

3.1. Maximum log-likelihood estimation (MLE)

The first statistical method uses the frequentist ideology of maximising the *likelihood function* at a given parameter. For this, we assume that the observations are distributed *normally*. This allows us to describe the observations with a normal probability density function (PDF for hereon), the familiar bell-shaped curve, defined as

$$f_N(x_j|\mu_o, \sigma_o^2) = (2\pi\sigma_o^2)^{-\frac{1}{2}} \exp\left(-\frac{1}{2\sigma_o^2}(x_j - \mu_o)^2\right) \quad (13)$$

The mean (μ_o) and variance (σ_o^2) in this case are the true and known values that describe how the observations, e.g. sound pressure or sound pressure level, are distributed. The set of parameters then define a normal distribution, $\theta = (\mu, \sigma)$, are the values that objective variables the likelihood function attempts to maximise

simultaneously. The remaining information required by the likelihood function is the *observables*, i.e. recorded data. Each new observable brings information into the function, allowing for the likelihood to define a better set of θ that describes the likelihood's of new data [7]. If we define our sample group of observations as $\mathbf{x} = (x_1, \dots, x_j)$ the likelihood function can be written as

$$\mathcal{L}(\theta|\mathbf{x}) = \prod_{j=1}^n f_N(x_j|\mu, \sigma^2) \quad (14)$$

where n is the total number of observables (x). The function in Eq. (14) can be further simplified with some manipulation to

$$\mathcal{L}(\theta|\mathbf{x}) = \prod_{j=1}^n (2\pi\sigma^2)^{-\frac{1}{2}} \exp\left(-\frac{1}{2} \frac{(x_j - \mu)^2}{\sigma^2}\right) \quad (15)$$

$$\mathcal{L}(\theta|\mathbf{x}) = (2\pi\sigma^2)^{-\frac{n}{2}} \exp\left(-\frac{1}{2\sigma^2} \sum_{j=1}^n (x_j - \mu)^2\right) \quad (16)$$

Taking the log transform $\log(\mathcal{L}(\theta|\mathbf{x})) \rightarrow \ell(\theta|\mathbf{x})$, gives the *log-likelihood function*, a better-defined function which is also algebraically easier to compute. The log-likelihood $\ell(\theta|\mathbf{x})$ can be rewritten as

$$\log(\mathcal{L}(\theta|\mathbf{x})) = \ell(\theta|\mathbf{x}) = -\frac{n}{2} \log(2\pi) \dots \dots -\frac{n}{2} \log(\sigma^2) - \frac{1}{2\sigma^2} \sum_{j=1}^n (x_j - \mu)^2 \quad (17)$$

It is important to note at his stage the key relationship, and differences between likelihood and probability. The following relationship is known to be true

$$P(\mathbf{x}|\theta) \equiv \mathcal{L}(\theta|\mathbf{x}) \quad (18)$$

While colloquial in use, the terminology is equally misused as the same thing in daily life whereas each function is doing something different. For any given distribution, $P(\mathbf{x}|\theta)$ defines the *probability* for observing data \mathbf{x} , for given set of parameters θ . Meanwhile, $\mathcal{L}(\theta|\mathbf{x})$ describes the how *likely* taking the set of parameters inside θ is for given values of the observables \mathbf{x} . The important difference is that each function is asking question about the data or parameters values. Manipulation of these statistical ideas is what allows us to perform inferences on our observables and thus study the effects of error and uncertainty on our given, or in a matter of fact any, acoustical scenario.

Our study manipulates the θ set in combination with the model that generates \mathbf{x} , to infer parameters from inside the later model. The variance (σ^2) is given as known being assumed equal to the initial variance inside our observations. Thus, the variance of

Table 1
Octave bands, in keeping with ISO 266.

Octave 1/1 band(B_n)	Lower limit(Hz)	Centre frequency(Hz)	Upper limit(Hz)
B_0 (Band 0)	0.24	1	1.41
B_1 (Band 3)	1.41	2	2.82
B_2 (Band 6)	2.82	4	5.62
B_3 (Band 9)	5.62	8	11.2
B_4 (Band 12)	11.2	16	22.4
B_5 (Band 15)	22.4	31	44.7
B_6 (Band 18)	44.7	63	89.1
B_7 (Band 21)	89.1	125	177
B_8 (Band 23)	177	250	355
B_9 (Band 25)	355	500	710

$\ell(\theta|\mathbf{x})$ is equal to σ_e^2 which was set to 5 dB in Eq. (12). The mean (μ) is also given as known, but uses the given acoustical model in *perfect* conditions. The mean (μ) is calculated using the same method that generates our sample data, requiring the situation-dependant true values of frequency (ω), source geometry (h_s, r) and effective flow resistivity of the ground (σ_g), but no noise added. This can be used as it is still assumed that, given a set of parameters, the model would predict the *perfect* result which would also be equivalent to the mean of a data set containing noise. The inference process then relies on the values inside our predictive model (Eq. (3)) would maximise the likelihood to these given set of θ , i.e. which set of parameter values would be most likely.

It is well understood that Bayesian methods become equivalent to frequentist methods as the number of observations becomes *large*. Limiting the initial information available to the likelihood function allows for investigation into the performance of the MLE (and soon to be discussed MAP) method. The increase in observation size, albeit small, will assess if any improvements can be detected with such a smaller addition of initial information.

The $\omega - r$ space is generated by using given values of each parameter. Frequency points (ω) cover the frequency range for sound generated by the gunshot (see Section 2.2), usually $1 \leq \omega \leq 500\text{Hz}$. The r space covers the range of $100\text{m} \leq r \leq 650\text{m}$. The definition of the r space should not be confused with the application of a *prior* previously discussed in Section 3.2. Other parameters, specifically the source height (h_s) and effective flow resistivity of the ground (σ_g), are allowed to be distributed, i.e. incorporate uncertainty, for further study into their interactions. In the most uncertain case, with both parameters unknown, draws are taken from a *uniform distribution* for each parameter for every individual simulation run. A *uniform distribution*, $U \sim [a, b]$, creates a distribution between a lower bound (a) and upper bound (b) with an equally weighted probability of drawing any number between these limits. This allows for the physical constraints of reality to be applied without any *a priori* knowledge, while simulating complete uncertainty around the parameter. The distributions drawn from are

$$\tilde{h}_s \sim U[0.1, 10] \quad (19)$$

$$\tilde{\sigma}_g \sim U[20000, 200000] \quad (20)$$

The distribution of the height (Eq. (19)) has its upper bound at 10 m as higher source heights are also known to be subjected to atmospheric influences [17] which the model adopted here does not account for. The distribution of the flow resistivity of the impedance ground (Eq. (20)) is chosen to encompass variations in the experimental data recorded for this type of grassland [19] we are assuming to be present.

The values of the $\omega - r$ space that best maximise the given combination of likelihood parameters (θ) can now be located. According to the most uncertain case, Eq. (17) can be rewritten as

$$\begin{aligned} \ell(\theta|\mathbf{y}, \omega, h_s, r, \sigma_g) = & -\frac{n}{2} \log(2\pi) - \frac{n}{2} \log(\sigma_e^2) \dots \\ & - \frac{1}{2\sigma_e^2} \sum_{a=1}^{n_\omega} \sum_{b=1}^{n_r} \sum_{j=1}^n \left(y_j - f\left(\omega_a, \tilde{h}_s, r_b, \tilde{\sigma}_g\right) \right)^2 \end{aligned} \quad (21)$$

In the case when the source height (h_s) and/or impedance (σ_g) are known they simply have the distributions $(\tilde{h}_s, \tilde{\sigma}_g)$ replaced with the respective true, and unchanging, values $(2\text{m}, 100\text{kPasm}^{-2})$. This likelihood function uses n observations to generate a $n_\omega \times n_r$ space over n_ω and n_r points for frequency (ω)

and range (r), respectively. In simple terms, the maximised value is located in the space related to the *best estimate* of r , at a specific frequency for given or unknown source height and impedance.

3.2. Semi-bayesian maximum a Posteriori (MAP)

The second method requires the understanding of *Bayes' theorem*. Bayes' theorem is defined as [10]

$$P(\theta|\mathbf{x}) = \frac{\mathcal{L}(\theta|\mathbf{x}) \times P(\theta)}{P(\mathbf{x})}, \quad (22)$$

where $P(\theta|\mathbf{x})$ is the *posterior*, $P(\mathbf{x})$ is the *evidence*, $P(\theta)$ is the *prior* and $\mathcal{L}(\theta|\mathbf{x})$ is the *likelihood function*. The likelihood function is defined the same way as in Section 3.1, while the prior is the PDF of beliefs about θ . The application of a prior is used to import knowledge, or the absence, into the given statistical procedure. The posterior is the PDF that uses these beliefs in combination with the likelihood to generate a probability function of θ for a given set of data. The evidence term normalises the function to a true PDF, however is generally difficult and expensive (computational) to compute. The MAP procedure avoids this by disregarding this term. The only value of interest to us in the posterior is the *best estimate* which happens to be the easily-obtainable peak of the distribution, which is *proportional* to the combination of the prior and likelihood. This method reduces Eq. (22) to

$$P(\theta|\mathbf{x}) \propto \mathcal{L}(\theta|\mathbf{x}) \times P(\theta) \quad (23)$$

Removal of the evidence term greatly reduces computational time, without removing the ability to gather a best estimate of a parameter. Similar to the MLE method, the reduced Bayes equation (Eq. (23)) can be log-transformed to

$$\log(P(\theta|\mathbf{x})) \propto \ell(\theta|\mathbf{x}) + \log P(\theta) \quad (24)$$

The log-transformed prior can be better interpreted here as a penalty term. The log of a probability is always negative, increasing in magnitude for a decreasingly small probability. The application of log here reduces the likelihood function at positions where the prior is less-confident. It also reduces the likelihood to $-\infty$ in areas outside of the coverage of the prior, due to the log of zero [10].

The prior applied in this instance is a normal, centred around the mean ($\mu_0 = 250\text{m}, 500\text{m}$) with a standard deviation of 15m, thus the distribution covers approximately $\pm 50\text{m}$ either side of the given mean. A completely flat prior could have been used in principle, especially in situations where reality constraints motivate it i.e. a uniform distribution that installs cut-offs at values that are known physical impossibilities. However, a flat normal is already applied, thus uniform priors are deemed unnecessary to the narrative of this paper.

3.3. Performance metrics

To investigate the effectiveness of the inference process and the effects of uncertainties in parameters, we study the *errors* in relation to the predicted values and the true value. We make use of MATLAB™ (and the ShARC supercomputer facilities at the University of Sheffield) to repeatedly simulate a small set of observations ($n = 10$), maximise the likelihood over the $\omega - r$ parameter space for given parameter values, either known or randomly drawn from given distributions, then find the *best-estimate* before and after a prior is applied. The ω space is also analysed in the octave band bounds defined in Table 1.

The error (ϵ_r) is then found as the difference between a simulation's estimate of the range and the true value of range

$$(\epsilon_r)_i = (r)_i - r^* \text{ for } i \in [1 \ 1000] \quad (25)$$

The error is investigated in both *relative* and *absolute* terms. The relative error will allow insight into the *direction* of the incorrect estimations (i.e. whether an under or over estimation was made) while the absolute error is independent of direction.

A substantial number of errors ($n_e = 1000$) are generated to allow the error set to be explored visually and numerically and to minimise the error from the sampling process. Additionally, two more statistics can be investigated: (i) mean absolute error (MAE); and (ii) root mean squared error (RMSE). Both use the previously defined ϵ_r to analyse the inference process across the entire set of errors. The MAE is the arithmetic mean of the modulus of the errors (Eq. (26)), while the RMSE is the root of the arithmetic mean of the square of the errors (Eq. (27))

$$MAE = \frac{1}{n_e} \sum_{i=1}^{n_e} |(\epsilon_r)_i| \tag{26}$$

$$RMSE = \sqrt{\frac{1}{n_e} \sum_{i=1}^{n_e} ((\epsilon_r)_i)^2} \tag{27}$$

The MAE allows for an insight into the overall average error, while the RMSE is another way of calculating the average error, but it is far more punishing to larger errors, i.e. more *weight* is given to larger errors. Both errors are *independent* of direction, i.e. whether the average estimate overestimates or underestimates the given true value. Visual analysis will be used to assess the under and/or overestimations that may occur

4. Results

4.1. Inference using broadband data

The results of the analysis of errors using broadband sound pressure level data is presented in Table 2. This table shows the MAE, RMSE and absolute maximum error for the simulations for the combinations of known or unknown parameter. These data were drawn from the respective error distribution. The results from each statistical method are also compared.

Overall errors estimated while using MLE alone are relatively large, being on average 50% and 60% of the true range when the true range (r^*) is 250 m and 500 m, respectively. Application of a priori, using the MAP method, greatly reduced errors to within 10% of the true range.

The differences in the MAE and RMSE are negligibly small ($< 0.05m$) between most simulations where the true range (r^*) is 250 m. In addition, the difference between error statistics when

the true range is 500 m are also negligibly small ($< 0.1m$) when using the MAP method in all conditions. However, when the true range is 250 m, and both the flow resistivity of the ground (σ_g) and source height (h_s) where initially unknown, a large jump in error can be seen when the MAP method is used. The MAE increased by ~ 15 m, the RMSE by ~ 20 m and the absolute maximum error increased by ~ 100 m. It is likely that the increase in extreme outliers has dragged the average errors particularly in the case when both the source height (h_s) and flow resistivity of the ground (σ_g) have varied due to the uncertainty present. This effect is not seen when the true range (r^*) is increased to 500 m, which indicates the interaction effects of these uncertainties may either be increased by reducing range, or the opposite, the interfering effects of the uncertainties being reduced as the true range (r^*) is increased.

The negligible differences between the statistics of error when uncertainties are imported to various parameters, may be influenced by a relatively small sample of observed data ($n = 10$) in the model. Studying interactions with various levels of initial data in the model is outside the scope of this paper, and it would require repetition of the methods used here with such variations present. They also would inherently be affected by the distribution choice, specifically the effective flow resistivity of the ground (σ_g) being a distribution that covers various recorded values for *grassland*. More acoustically harder grounds *urbanised areas, water*, can have different effects.

4.2. Visualisation of errors

Visualisation of errors (ϵ_r) is done using three different plots: (i) a PDF of estimates; (ii) a PDF of the absolute errors; and (iii) the *cumulative distribution function* (CDF from hereon) of the absolute errors. The first allows for insight into the general distribution of where estimates were made in relation to the true value and differences in over and underestimations. The second plot of absolute error defines the probability of the error, no matter whether it is over or under. The CDF of absolute error can be used to visualise the cumulative probability of the defined error. Kernel density estimation (ksdist function in MATLAB™) is used to produce smoothed curves that are visually easier to assess. This is deemed acceptable due to the large sample size in each case ($n_e = 1000$).

Visualisations are presented in Fig. 5 ($r^* = 250m$) and Fig. 6 ($r^* = 500m$). Each subplot of a given PDF/CDF contains multiple lines, each representing the results for simulations with the varying input uncertainty, i.e. either only r is unknown, or r and σ_g are unknown or r , σ_g and h_s are unknown. The results presented

Table 2

Collated statistics of error (ϵ_r) from each simulation. Each row follows the selection of initial parameters, known or drawn from a given distribution, then for the given statistical method used.

r^* (m)	h_s (m)	σ_g (kPasm ⁻²)	Method	MAE(m)	RMSE(m)	Abs. max.(m)	
250	2	100	MLE	124.74	127.26	150	
			MAP	23.53	30.1634	96.05	
		$\tilde{\sigma}_g$	MLE	122.55	125.64	150	
			MAP	23.53	30.16	96.05	
		\tilde{h}_s	100	MLE	123.24	126.48	150
				MAP	23.58	30.21	96.05
	$\tilde{\sigma}_g$	100	MLE	120.89	124.71	150	
			MAP	37.85	48.25	202.9	
	500	2	100	MLE	294.43	300.21	500
				MAP	44.63	57.81	211.71
			$\tilde{\sigma}_g$	MLE	295.1	301.21	399.45
				MAP	44.67	57.83	211.72
\tilde{h}_s			100	MLE	295.9	302.47	400
				MAP	44.72	57.87	211.72
$\tilde{\sigma}_g$		100	MLE	300.29	306.63	400	
			MAP	44.77	57.91	211.71	

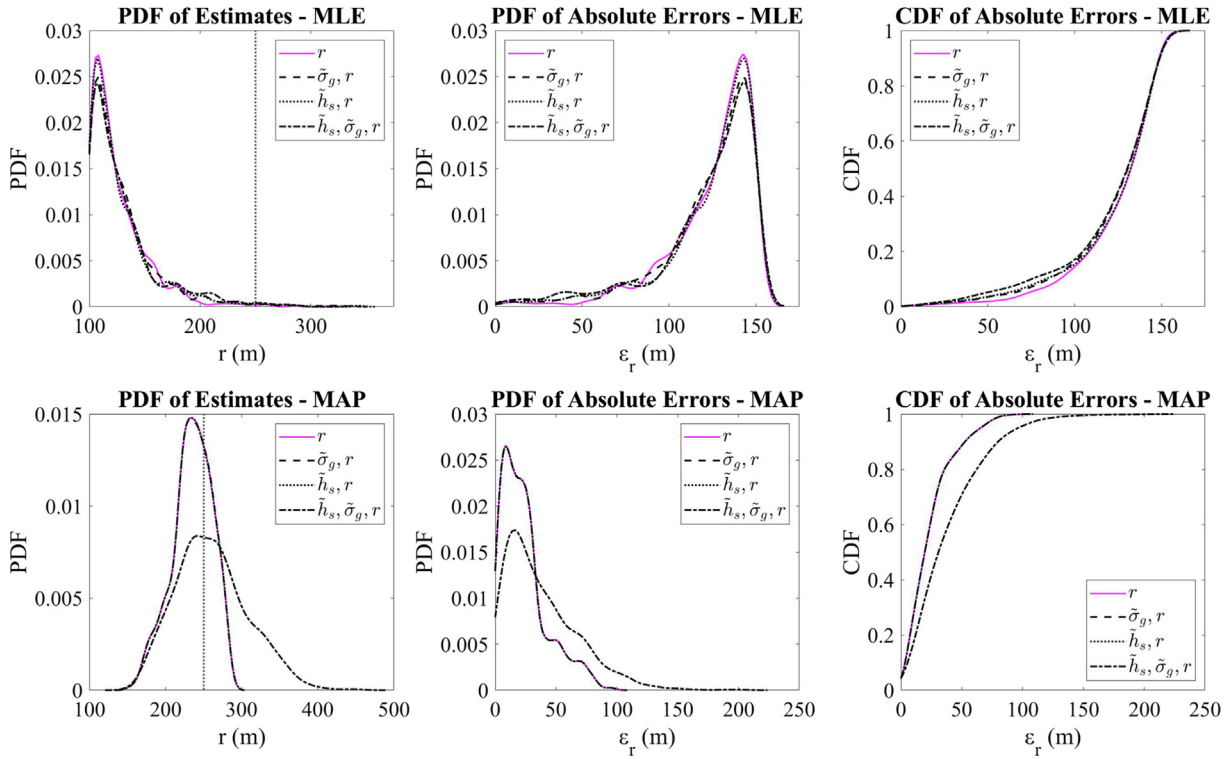


Fig. 5. Kernel distributions for the PDF of estimates (first column), PDF of absolute errors (second column) and CDF of absolute errors (last column) for each simulation of varying uncertainty at $r^* = 250m$. Top and bottom rows show the results from using the MLE and MAP methods, respectively. The true range value is superimposed (dashed line) in the PDF plot of estimates. Each line represents which initial parameters were uncertain as defined in each legend.

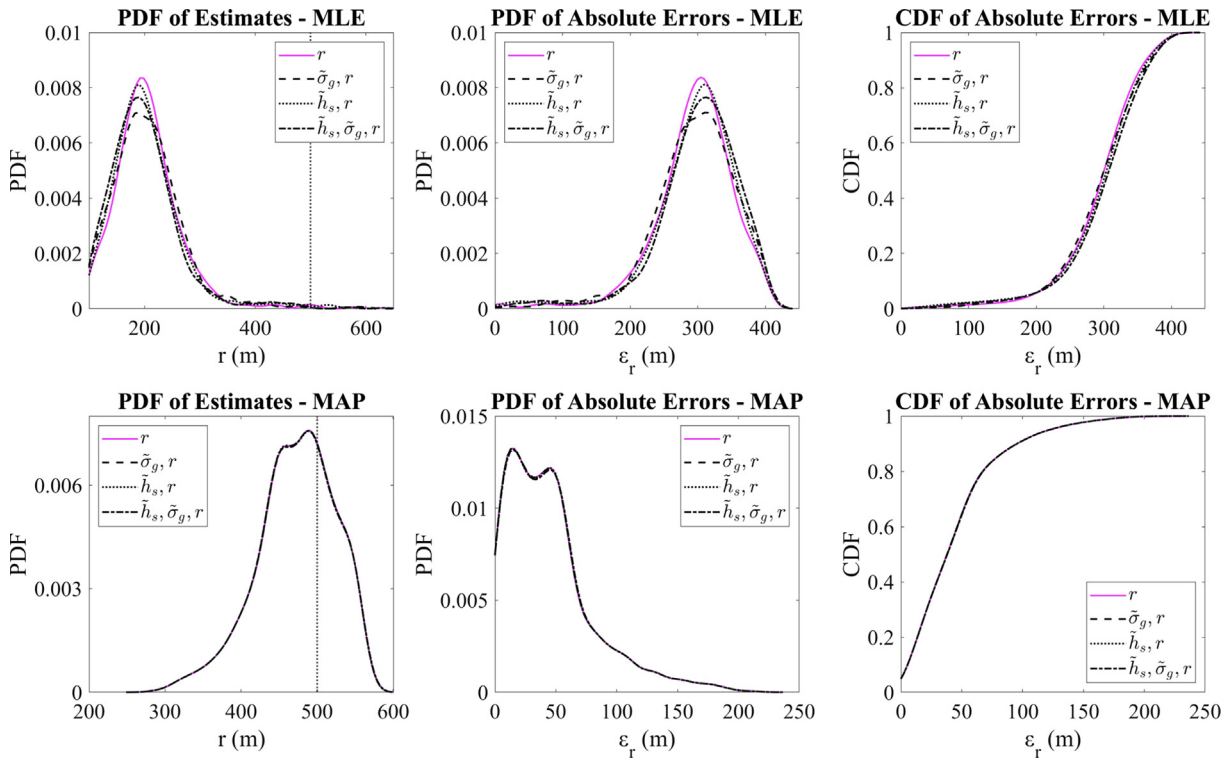


Fig. 6. Kernel distributions for the PDF of estimates (first column), PDF of absolute errors (second column) and CDF of absolute errors (last column) for each simulation of varying uncertainty at $r^* = 500m$. Top and bottom rows show results from using the MLE and MAP methods, respectively. The true range value is superimposed (dashed line) in the PDF plot of estimates. Each line represents which initial parameters were uncertain as defined in each legend.

in Fig. 5 suggest that in the short-range case ($r^* = 250\text{m}$) the ineffectiveness of the sole maximisation of the likelihood (MLE) is obvious (as also seen in Table 2). Estimates are centred around the minimum possible value of r set in the model, with a positive skew allowing for a smaller proportion of better estimates, as well as over-estimations (top-left in Fig. 5). The PDF of absolute error (top and mid rows in Fig. 5) shows that the majority of errors are greater than 100 m, which is confirmed by the CDF of absolute error (top-right in Fig. 5) where there is a 20% chance of getting an error of less than ~ 100 m and 80% chance of getting an error of smaller than ~ 140 m. The differences between the simulations when all to none of the initial parameters are known are not clear for the MLE method for the true range (r^*) of 250 m (top row in Fig. 5). However, there is some indication that allowing the effective flow resistivity of the ground (σ_g) to vary may decrease the error slightly, but the magnitude in which the peak (and distributions generally) is flattened here is too small to state as fact.

The application of a prior (MAP method) greatly improves estimations (bottom row of Fig. 5). The spread of estimates (bottom-left of Fig. 5) is more symmetric around the true range ($r^* = 250\text{m}$), with a negative skew away from this value. When the source height (h_s) and effective impedance of the ground (σ_g) are unknown, the distribution of estimates is far flatter, yet more symmetric around the true value, showing tails containing more overestimations than the related simulations while using the MLE. This confirms the findings (see Table 2) that the error is increased in the most uncertain simulation due to the allowance of larger overestimations rather than underestimations. The MAP method leads to the PDF of absolute error (bottom and mid row in Fig. 5) becoming flipped, peaking around zero error with tail decreasing toward larger errors. The most uncertain case is less strongly peaked leading to an increase in size and frequency of large errors. All other simulations seem to be highly probable to be less than ~ 30 m, with a large drop to a *step* appearing to around ~ 50 m. The likelihood of an error larger than 50 m lower substantial, before tailing out to the maximum error. The CDF (bottom-right of Fig. 5) shows the reduction in error compared to the MLE, with a 20% chance of error of less than ~ 5 m and 80% chance of an error less than ~ 40 m. These probabilities are weakened by the case where initial parameters are unknown, with only an 80% chance of less than ~ 55 m, yet this is substantially better than the MLE case with the least uncertainty. Practical application shows how effective a single simulation could be for inference, giving a user with data ready a value within seconds, with great confidence while using the MAP method. More simulations would be needed for confident predictions with the MLE.

All MAP simulations (see bottom row in Fig. 5) show far less difference between each distribution, with each plot being smoother and almost exactly alike when compared to the MLE results (see top row in Fig. 5) where each plot *oscillates* over one other i.e. each distribution is higher and lower than the others at multiple points. This indicates that the MAP method may itself smooth out small artefacts from varying the uncertainty in other parameters in the model that are not the direct object of the inference. The MAP method does highlight a reduction in likelihood in the most uncertain case (see blue plot at the bottom row in Fig. 5), which is not seen in any other simulations. It is not clear what causes this simulation to be so different, but it seems that the increase in degree of uncertainty is the most likely reason for this difference.

Increasing the true range to $r^* = 500\text{m}$ leads to the results shown in Fig. 6. The performance of the MLE method is similar to that observed in the case of $r^* = 250\text{m}$ (see top-left graph in Fig. 5) with a similar distribution of the range and error estimates (see top-left graph in Fig. 6). There is a strong peak at the lowest range that the model accepts, with a decreasing probability as

the estimate value increases. The distribution of absolute error (top-mid rows in Fig. 6) shows a strong peak around 300 m tailing off with some negative skew towards small errors. The CDF of absolute error (see top-right in Fig. 6) shows that an increase in range reduces performance, where now there is only a 20% chance of the range being less than ~ 250 m out and 80% chance of being greater than ~ 250 m. Differences between simulations in the three plots (see top row in Fig. 6) are due to the fact that the uncertainties present are less erratic (or less oscillatory). The peak in each of distribution becomes increasingly flatter as more uncertainty is present (from initial parameters).

The MAP method at this range improves the estimation and reduces the discrepancies between the differing levels of uncertainties from initial parameter selection. The distribution of estimates (see bottom-right graph in Fig. 6) shows a distribution around the true value (r^*) close to normal with a negative skew. There is evidence of another peak in the distribution around 450 m range. The distribution of the absolute error (see bottom-middle graph in Fig. 6) is strongly centred around 5 m, with the second peak around 50 m. There is a long tail in the distribution showing that larger errors (100 m+) are highly unlikely in this case. The CDF (bottom-right graph in Fig. 6) shows the effectiveness of the MAP method for errors with a 20% chance of being within 5 m and an 80% chance of being within 50 m. All of the simulations, of any given initial uncertainty, are near-identical (see bottom row in Fig. 6). Even the most uncertain case (source height (h_s) and impedance ground (σ_g) being uncertain) is now no longer a visible different distribution, unlike when the true range was less ($r^* = 250\text{m}$) (bottom row in Fig. 5). A recent study by the authors highlighted how the impedance in particular uncertain geometries and statistical behaviour can affect inferences using certain methods [21]. This is likely why the simulations with multiple uncertainties are more strongly affected in the MAP methods at the shorter range ($r^* = 250\text{m}$), yet the increase in range reduces this effect.

4.3. Interactions of uncertainties

Since draws were taken from distributions for the unknown parameters, source height (h_s) and/or effective flow resistivity of the ground (σ_g), they can be compared to the final estimate determined via the inference. This will enable us to study the sensitivity of such parameter/s while using MLE/MAP methods with the given conditions, i.e. differing range, low initial data source, *grassland* impedance ground against the final inferred range. Scatter plots are used to compare when either the flow resistivity of the ground (σ_g) or source height (h_s) are uncertain to their relevant error from the inference (see Figs. 7 and 8). The dots shown in Figs. 7 and 8 correspond to the realisations simulated with the proposed statistical methods. When both the effective flow resistivity of the ground (σ_g) and source height (h_s) are uncertain, a grayscale surface plot is used (see Fig. 9) to show maps for the error as a function of the range and flow resistivity. These graphs highlight behaviour patterns in the uncertainty that are affecting such inference processes.

The first parameter investigated is the effective flow resistivity of the ground (σ_g) taken across all possible values ($\tilde{\sigma}_g$) against its related absolute error (ϵ_r). This is achieved by taking the absolute difference from the inferred value and true value while using a drawn value of σ_g (see Fig. 7). The MAP method is shown to be far more effective than the MLE method in terms of the value of error. This is true for the both true ranges (r^*) studied in this work. The results presented in Figs. 7 and 8 show that the error is not sensitive to the initial draw of σ_g . Although, the MLE results for a

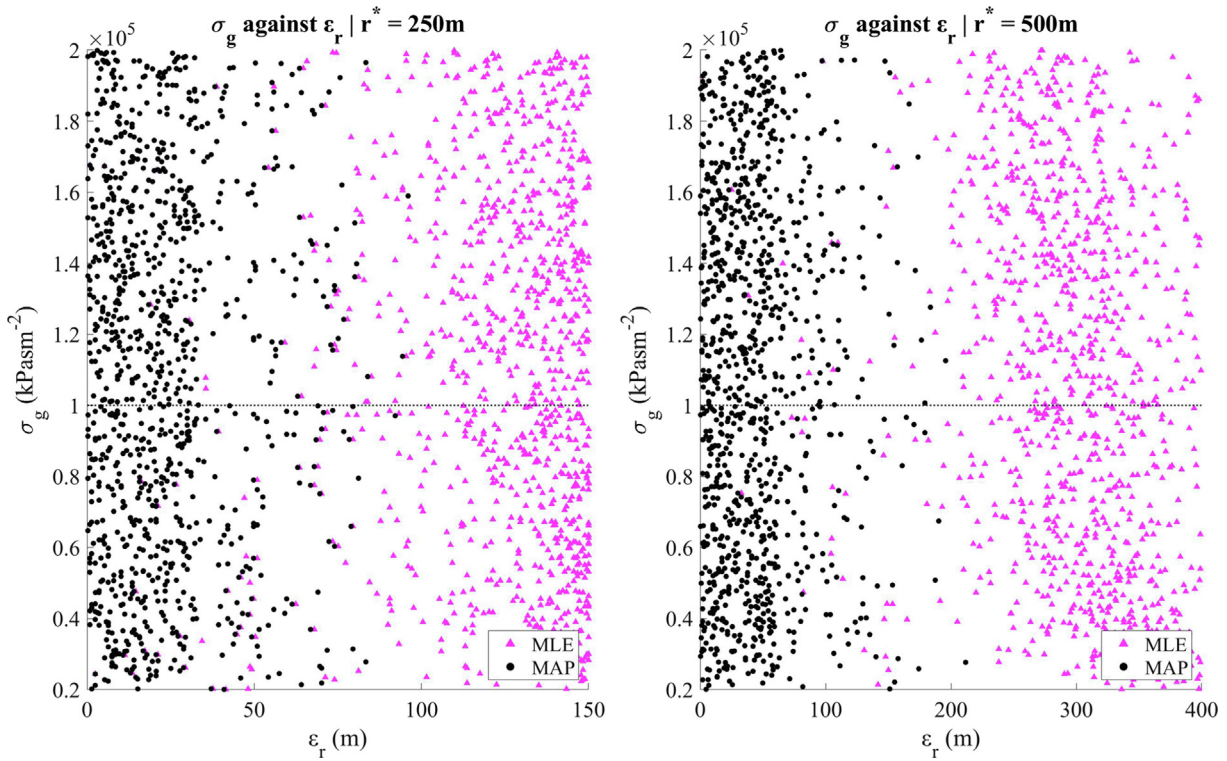


Fig. 7. Draws from $\tilde{\sigma}_g$ against their related ϵ_r for both statistical methods for $r^* = 250m$ (left) and $r^* = 500m$ (right). The true value of the effective flow resistivity ($\sigma_g = 100kPasm^{-2}$) is superimposed (dashed line).

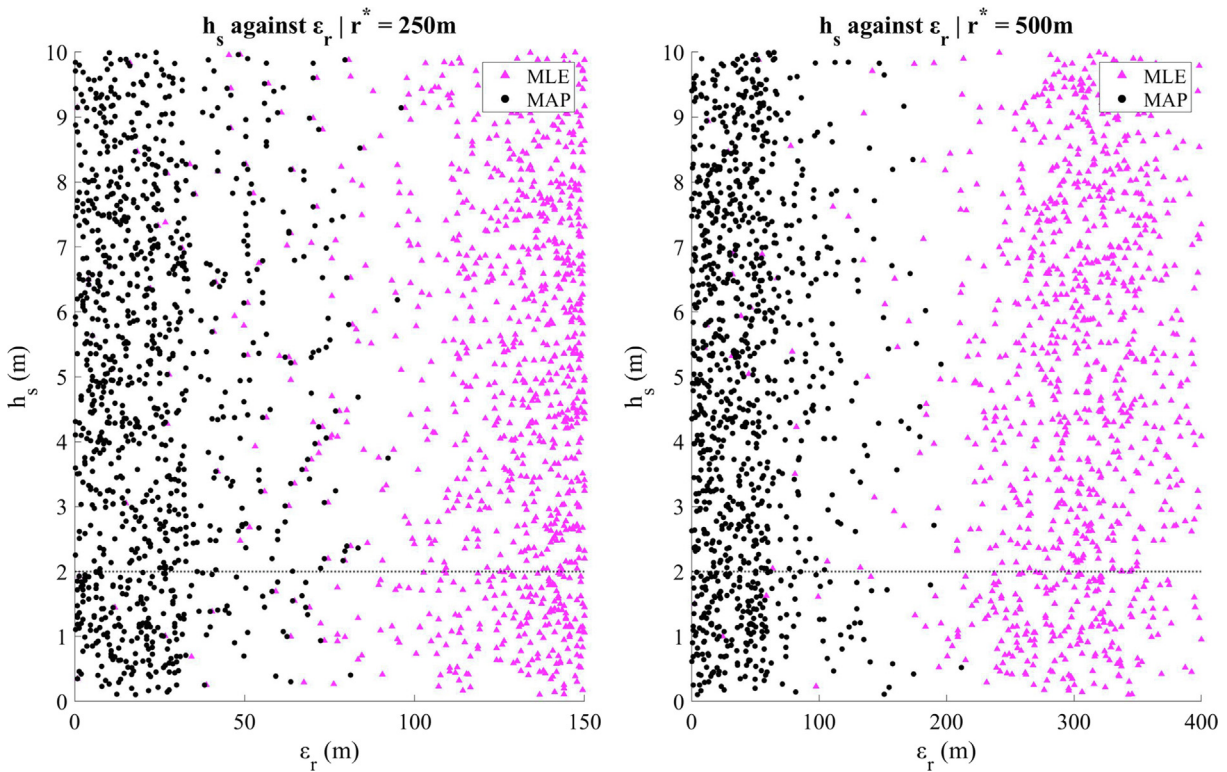


Fig. 8. Draws from \tilde{h}_s against their related ϵ_r for both statistical methods for $r^* = 250m$ (left) and $r^* = 500m$ (right). The true value of the source height ($h_s = 2m$) is superimposed (dashed line).

true range $r^* = 500 m$ tend to have smaller errors when a higher value of the effective flow resistivity (σ_g) is drawn (see right plot in Fig. 7). It is not thoroughly clear why this would be the case.

Plotting the draws from the source height (h_s) instead of the flow resistivity of the ground (σ_g) shows similar behaviour (see Fig. 8). The MAP method again has greater accuracy than the

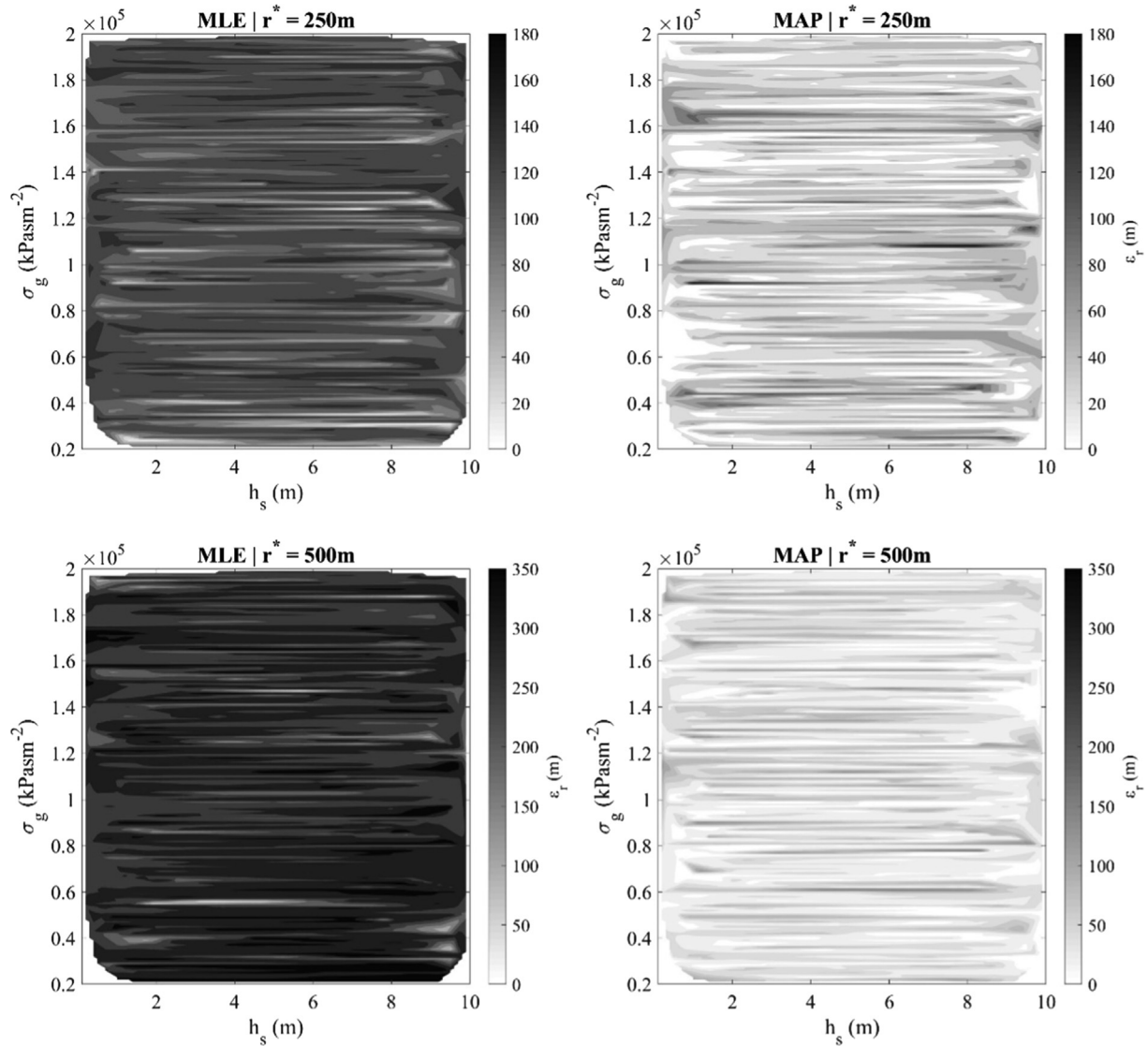


Fig. 9. The absolute error plotted as a function against the draws of source height (h_s) and effective flow resistivity of the ground (σ_g) for the two ranges. Error is depicted using a colour gradient. Top and bottom rows show r^* as 250 m and 500 m, with left and right columns the MLE method and MAP method respectively.

MLE, with no obvious sensitivity to the draw of the source height (h_s) at initialisation. There is some indication that at the range of 500 m the MLE method performs slightly worse as the drawn value of source height (h_s) increases. It is known that the increased height would greatly affect the ground interference patterns, yet an overestimation of 8 m (as 10 m is the maximum overestimated source height allowed) does not seem to prevent the model from inferring the true range (and close to it).

The interactions between the draws and the given error (ϵ_r) are harder to visualise. Fig. 9 plots the error against the source height and effective flow resistivity of the ground. The absolute error is depicted using a colour map with white being no error and black being the maximum error of 180 m and 350 m for the true range of 250 m and 500 m, respectively. Horizontal bands can be seen in the surface plots in Fig. 9. This means that small variations in the source height (h_s) for a given effective flow resistivity of the ground (σ_g) do not strongly affect the quality of inference, whereas small variations in the effective flow resistivity of the ground (σ_g) for a selected source height (h_s) do. This hints that quantification of the ground impedance may be more important than the source height in situations where both are unknown quantities. These

findings are supported by the fact that the so-called “ground effect” is more important for low-height sources than sources at higher altitude, a well-known fact in acoustics, with greatly developed definitions and reasoning explained in well by Solomons [17].

4.4. Inference using octave band data

Additionally, inference is studied in octave frequency bands and compared against that obtained for the broad band spectrum. This enables us to assess the effect that specific frequency restrictions would have on the inference quality. Table 3 presents the error statistics for each combination of known or unknown (and therefore drawn from the respective distribution) parameters. Only the best and worst performing bands (using bandwidths defined in Table 1) are shown. Best and worst are taken to be the smallest and largest values of error respectively. Unlisted bands are only assessed visually later.

As expected, for both the MAE and RMSE, the equally worst performing bands are B_8 and B_9 for all the cases considered in this study. These are higher frequency bands in which the sound power of the gun shot is relatively low (see Fig. 1). At the shorter range

Table 3
Collated statistics of error ($\hat{\epsilon}_r$) from each simulation, portraying the best and worst performing octave bands. Each row follows the selection of initial parameters, known or drawn from a given distribution and for the given statistical method.

r^* (m)	h_s (m)	σ_g (kPasm ⁻²)	Method	MAE (m)		RMSE (m)			
				Best	Worst	Best	Worst		
250	2	100	MLE	B_0 : 55.3	$B_{3,7,8,9}$: 150	B_0 : 70.96	$B_{3,7,8,9}$: 150		
			MAP	B_0 : 34.16	$B_{3,7,8,9}$: 150	B_0 : 41.66	$B_{3,7,8,9}$: 150		
			MLE	B_0 : 55.04	$B_{3,7,8,9}$: 150	B_0 : 70.82	$B_{3,7,8,9}$: 150		
		$\tilde{\sigma}_g$	MAP	B_0 : 55.04	$B_{3,7,8,9}$: 150	B_0 : 41.67	$B_{3,7,8,9}$: 150		
			\tilde{h}_s	100	MLE	B_0 : 56.42	$B_{3,7,8,9}$: 150	B_0 : 72.18	$B_{3,7,8,9}$: 150
					MAP	B_0 : 56.42	$B_{3,7,8,9}$: 150	B_0 : 41.67	$B_{3,7,8,9}$: 150
	MLE	B_0 : 56.73			$B_{3,7,8,9}$: 150	B_0 : 72.55	$B_{3,7,8,9}$: 150		
	$\tilde{\sigma}_g$	MAP	B_0 : 56.73	$B_{3,7,8,9}$: 150	B_0 : 48.24	$B_{3,7,8,9}$: 150			
		500	2	100	MLE	B_0 : 190.21	$B_{7,8,9}$: 400	B_0 : 233.66	$B_{7,8,9}$: 400
					MAP	B_0 : 62.63	$B_{8,9}$: 400	B_0 : 76.7	$B_{8,9}$: 400
					MLE	B_0 : 188.27	$B_{8,9}$: 400	B_0 : 231.83	$B_{8,9}$: 400
				$\tilde{\sigma}_g$	MAP	B_0 : 62.63	$B_{8,9}$: 400	B_0 : 76.7	$B_{8,9}$: 400
\tilde{h}_s					100	MLE	B_0 : 187.06	$B_{8,9}$: 400	B_0 : 230.16
	MAP					B_0 : 62.63	$B_{8,9}$: 400	B_0 : 76.7	$B_{8,9}$: 400
	MLE		B_0 : 189.02	$B_{8,9}$: 400		B_0 : 232.57	$B_{8,9}$: 400		
$\tilde{\sigma}_g$	MAP		B_0 : 62.64	$B_{8,9}$: 400	B_0 : 76.7	$B_{8,9}$: 400			

($r^* = 250m$), bands of B_3 and B_7 are also relatively poor performing. Band B_7 also appears as the worst for the least uncertain MLE in the longer range ($r^* = 500m$). All of these are the result of the model choosing the lowest value possible, the lowest value for r that was used in the computation of the likelihood, a problem that was also seen in the MLE for broadband.

The best performing band is the infrasonic band B_0 , no matter which method is used or error statistic analysed. In this range the MAP method remains mostly effective. In general, the same bands (B_3, B_7, B_8, B_9) underperform as in the MLE, albeit with some small differences. Unlike for the broadband results, the MAEs for the MLE and MAP methods are equivalent when either the effective flow resistivity (σ_g) or source height (h_s) is unknown. The RMSE data suggest that the MLE is underperforming against the MAE and that outlying inferences are present in simulated data.

Comparing the broadband results (see Table 2) to the octave band results (see Table 3) suggests that overall the broadband inference is likely to outperform inference via specific octave bands for the considered acoustic and statistical models. This does not however rule out that combinations of octave band windows would allow for better inferences for some types of sources, specifically B_0, B_1 and B_2 for gunshot sources.

4.5. Octave band visualisations

Visualisations are completed to assess more in-depth the effects of filtering to octave bands (see Figs. 10–13). Each figure is for a particular statistical method and value of the true range. Each subplot is for a given octave band where each of the plots follow the same rules as before, with each representing the given initial uncertainties. The PDF of estimates are used to assess the octave bands, so both under and over estimates can be detected.

Fig. 10 depicts the PDFs for the MLE method when the true range (r^*) is 250 m. Octave bands B_3, B_7, B_8 and B_9 perform poorly picking up estimates at the minimum value entered into the model. Bands B_4 and B_6 also perform poorly but have tails extending towards to true value (r^*). The distributions created for bands B_2 and B_5 have their peaks at slightly above the minimum value, but their tails have no coverage of the true range ($r^* = 250m$). The remaining bands, B_0 and B_1 cover much more accurately the true range (r^*) with band B_0 being the best choice for having the most likely point close to the true value. Interestingly, there is a bimodal (i.e. double peaked) PDF present for B_0 , with an earlier

peak around 120m which can be associated with strong variations in the gunshot spectrum (see Fig. 1). B_1 has the majority of estimate below the true value but extends to the true value also. It is seen that while using the MLE method (see Fig. 5) inferences can be improved by choosing the best estimates from these top-performing bands (B_0, B_1). Variation between simulations of differing input uncertainty is negligible in the case of the MLE method.

Fig. 11 presents the PDFs for the error estimated using the MAP method for the true range $r^* = 250$ m. These results follow the same behaviour as seen in the case of the MLE (see Fig. 10) but with some improvements. The poor performing bands remain the same as in the case of the MLE, while the better performing bands (B_0, B_1) have larger probabilities of capturing the true range (r^*). In comparison with the MLE, the PDF for band B_1 is shifted closer to the true range. The PDF for band B_0 is accurately centred around the true value, but the bimodality observed in the case of MLE is now removed. The increased accuracy in the lower bands could be due to the physical interactions, i.e. excess attenuation, remaining constant at the lower frequency ranges.

Increasing the true range to $r^* = 500$ m changes the PDFs considerably especially when using the MLE (see Fig. 12). The PDFs for bands B_0, B_1 and B_2 exhibit bimodality. The two bands that can cover well the true estimate (B_0, B_1) exhibit relatively strong bimodality. In the case of band B_0 the dominant peak is around 200m whereas the secondary peak is close to the true range. This behaviour can hinder the convergence to the true estimate.

The application of a prior in the MAP addresses the issues experienced with the MLE method. Fig. 13 illustrates that the use of limited prior knowledge removes the bimodality and leaves only one peak in the PDF for bands B_0 and B_1 close to the true estimate. The great increase in accuracy is even more likely to be due to the physical interaction patterns, which become even more constant at the extended range. The application of the MAP to other bands does not offer any improvement and results in a relatively large error.

The existence of the bimodal distribution is believed to be created by the generation of two distinct normal distributions, from the normal likelihood function (not the uncertainty – as a data doped with uniform uncertainty most times still produce normally distributed data) that are interfering with each other. Their appearance is likely due to strong interactions present at such combinations of parameters in the model.

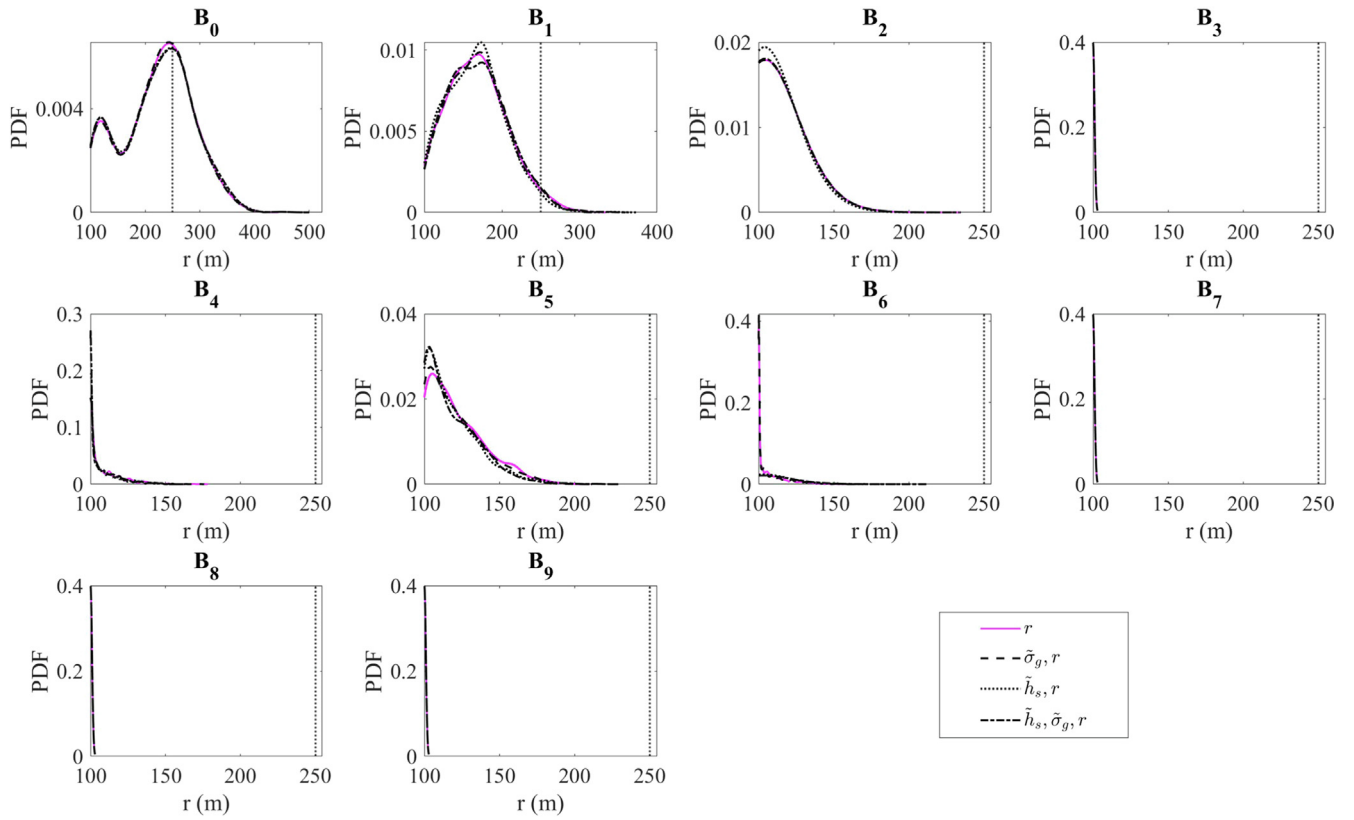


Fig. 10. Kernel distributions for the PDF of estimates, using the MLE method at each octave band from smallest (top-left) to largest (bottom-right) for each simulation of varying uncertainty at $r^* = 250m$. The true range value is superimposed (dashed line) in the PDF plot of estimates.

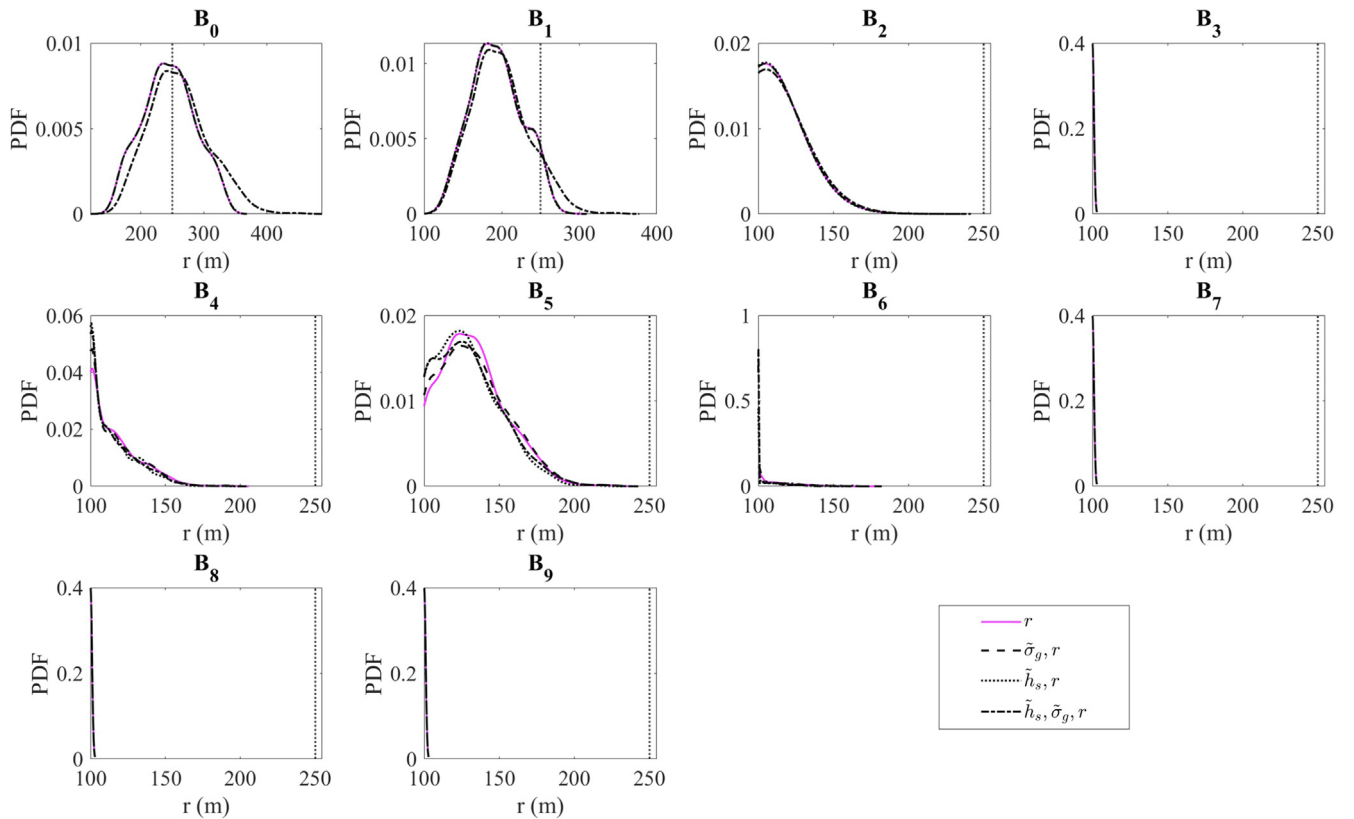


Fig. 11. Kernel distributions for the PDF of estimates, using the MAP method at each octave band from smallest (top-left) to largest (bottom-right) for each simulation of varying uncertainty at $r^* = 250m$. The true range value is superimposed (dashed line) in the PDF plot of estimates.

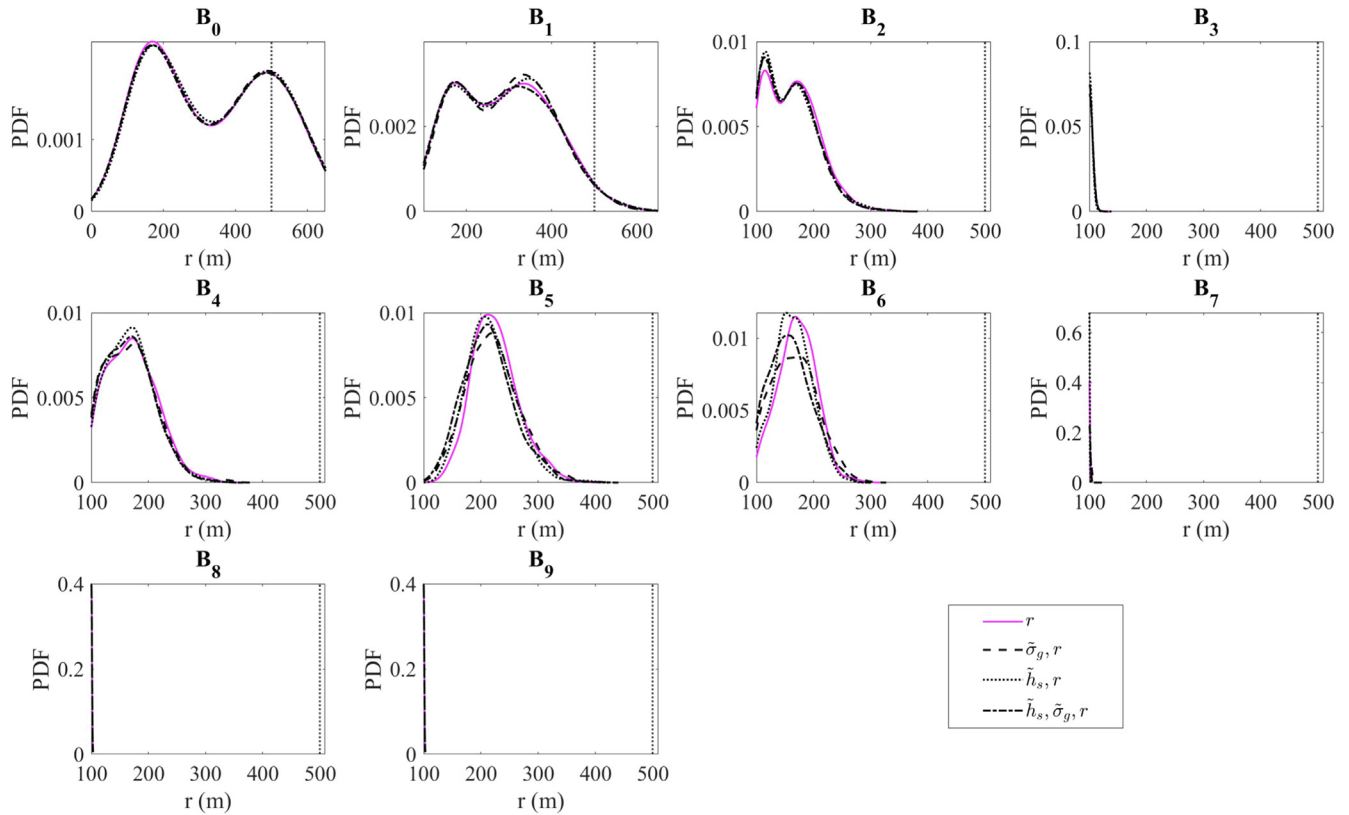


Fig. 12. Kernel distributions for the PDF of estimates, using the MLE method at each octave band from smallest (top-left) to largest (bottom-right) for each simulation of varying uncertainty at $r = 500m$. The true range value is superimposed (dashed line) in the PDF plot of estimates.

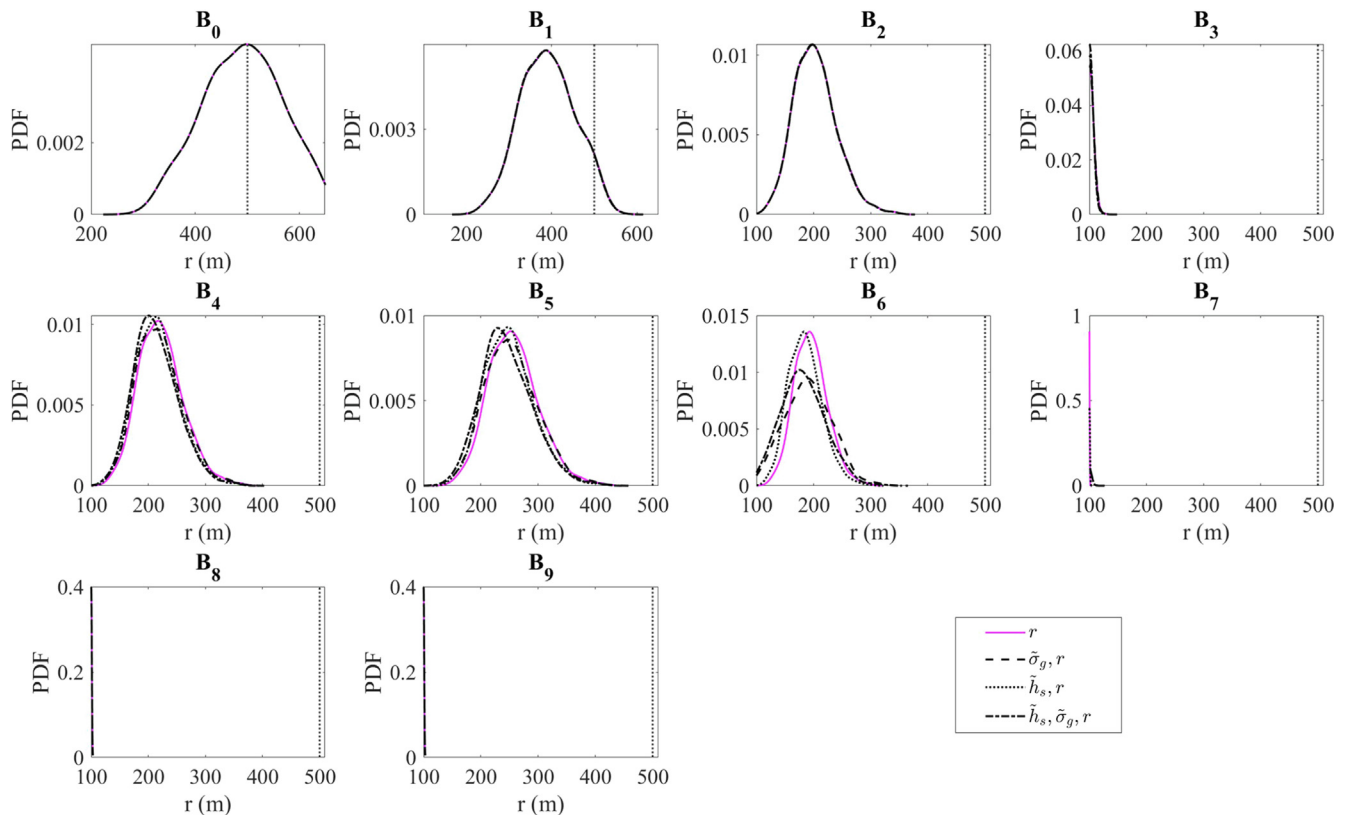


Fig. 13. Kernel distributions for the PDF of estimates, using the MAP method at each octave band from smallest (top-left) to largest (bottom-right) for each simulation of varying uncertainty at $r = 500m$. The true range value is superimposed (dashed line) in the PDF plot of estimates.

5. Conclusions

The application of a prior to infer the true range from the sound pressure level data of a gunshot recorded on a single microphone in the presence of porous ground reduces the average error from almost 50% to within 10% of the true range event when initial information is limited to a small number of observations, e.g. $n = 10$. The MLE performs poorly because it has the tendency to choose repeatedly the smallest range possible in the model. There is a possibility for this method to become more accurate as more data for a wider range of porous grounds is made available. Application of a prior, even a flat one like in this study, greatly reduces the hindrance of parameter uncertainties. Although at the shorter range ($r^* = 250m$), the average error was only reduced to $\sim 15\%$ when all parameters were uncertain, indicating that shorter ranges are still more influenced by high uncertainty. Both the MLE (as long as the observation size was greatly increased) & MAP techniques are widely applicable to other acoustical settings, yet would provide a substantially effective basis to methods that incorporate *learning algorithms*.

The study of the interactions between uncertain parameters reveals that exact quantification of individual unknown parameters is not always necessary. Only at the shorter range ($r^* = 250m$) either the source height (h_s) or impedance ground (σ_g) needs quantifying to improve the inference quality as it was shown that when the both parameters (h_s, σ_g) were uncertain a notable increase in error could be observed. Further investigation into this dual uncertainty shows that the effective flow resistivity of the ground would be the preferential parameter to be quantified. This parameter seems more significant. An increasing degree of uncertainty in the adopted acoustical model becomes more influential as the range shortens.

Use of octave filtering reveals those bands which are responsible for poor or more efficient inferences. In general, limiting the analysis to a single octave band results in poor performance in terms of the MAE and RMSE in comparison with a broadband spectrum analysis. However, the PDFs of the infrasonic bands (see B_0, B_1 in Table 1) exhibit strong likelihoods on, and closely around, the given true range, especially for the MLE method, than when using the broadband spectrum. Combinations of these octave bands would likely be more effective for the inference. A large portion of energy output of a firearm exists in the infrasonic frequency range. As highlighted in recent works [6], there is strong evidence to suggest that combining octave windows between in the low and infrasonic, frequency range will greatly improve parameter inference for firearms. Usual techniques try to use information from the supersonic projectile (bullet) which is good for 3D problems (location via miss angle), but may not actually be the best method. The lower frequency output of the firearm going off is likely to be less affected by possible interferences that can generate mid and high frequency noises. This could also improve detection in more realistic environments (i.e. inhomogeneous atmosphere).

The real-life application to small arms fire is apparent. Unlike current practices [4,5], this technique does not rely on the make, model, barrel rifling etc. This makes it appropriate to such defensive security programs where quantification of the firearm would likely be implausible, but prior information of the detection zone would be readily accessible. Study into larger firearms, and other small arms fire, will help confirm the best combination of octave bands suitable for specific purposes. The main benefit of this approach is that it relies on a single receiver which can be a smartphone or low-cost microphone connected to a basic microcontroller. It should also be stated that these methods would be effective for other low frequency sources, such as the natural occurrences of earthquakes, volcanic eruptions and thunder, or

man-made sources like windfarms. Further study of applications to a broader range of sources would be beneficial to test this idea further and expand it to cases where an array of receivers is used.

This study was limited to grassland. Other harder grounds can have different effects on the quality of inference methods proposed here. These proposed inference methods are not specifically exclusive to application to firearms. These can be extended to other low frequency sources such as drones and sources of environmental noise. Higher frequency sources deserve more extensive studies to assert such claims.

CRedit authorship contribution statement

Jordan A. Parry: Data curation, Writing - original draft, Visualization, Investigation. **Kirill V. Horoshenkov:** Supervision, Writing - review & editing. **Duncan P. Williams:** Supervision.

Declaration of Competing Interest

The authors declare that they have no known competing financial interests or personal relationships that could have appeared to influence the work reported in this paper.

Acknowledgments

The author/s acknowledge the support of the UK's Defense Science and Technology Laboratory (Dstl) and Engineering and Physical Sciences (EPSRC) CASE studentship award to the University of Sheffield. The authors are also grateful to Prof. Jeremy Oakley from the Department of Mathematics and Statistics at the University of Sheffield for his useful comments on the statistical aspects of this work, and to fellow PhD student, Liam Grimmett (Department of Physics and Astronomy) for assistance in using the ShARC computing facilities at the University of Sheffield.

References

- [1] D. Colton, H. W. Engl, A. K. Louis, J. McLaughlin and W. Rundell. *Surveys on Solution Methods for Inverse Problems*, Springer Science & Business (Dec 2012).
- [2] Wilson DK, Pettit CL, Ostashev VE, Vechev SN. Description and quantification of uncertainty in outdoor sound propagation calculations. *J Acoust Soc Am* 2014;136(3):1013–28.
- [3] Van Renterghem T, Botteldooren D. Variability due to short-distance favorable sound propagation and its consequences for immission assessment. *J Acoust Soc Am* 2018;143(6):3406–17.
- [4] Lo KW, Ferguson BG. Localization of small arms fire using acoustic measurements of muzzle blast and/or ballistic shock wave arrivals. *J Acoust Soc Am* 2012;132(5):2997–3017.
- [5] Lo Kam W. A ballistic model-based method for ranging small arms fire using a single acoustic sensor node. *J Acoust Soc Am* 2019;145(4):2409–17. <https://doi.org/10.1121/1.5098772>.
- [6] J.A. Parry, K.V. Horoshenkov, D.P. Williams. "Outdoor Acoustics: Range Estimation Of Gunfire Over An Acoustically Soft Impedance Ground In A Homogeneous Atmosphere." *Proceedings of the International Conference on Statistics: Theory and Applications*. (Lisbon, 2019.)
- [7] Paoletta MS. *Likelihood*. In: *Fundamental Statistical Inference: A Computational Approach*. Oxford, England: Wiley; 2018. p. 21–7.
- [8] Pena D, Lima C, Dória M, Pena L, Martins A, Sousa V. Acoustic impulsive noise based on non-gaussian models: an experimental evaluation. *Sensors* 2019;19(12):2827–45.
- [9] Sheng X, Hu YH. Maximum likelihood multiple-source localization using acoustic energy measurements with wireless sensor networks. *IEEE Trans Signal Process* 2005;53(1):44–53.
- [10] Cousineau D, Hélie S. Improving maximum likelihood estimation with prior probabilities: a tutorial on maximum a posteriori estimation and an examination of the Weibull distribution. *Tut Quant Methods Psychol* 2013;9(2):61–71.
- [11] D. Caviedes-Nozal and J. Brunskog, "Parameter optimization of forward sound propagation models using Bayesian inference for sound field control purposes" in *Proceedings of Euronoise 2018*, Crete, Greece, 2018.
- [12] Xiang N, Fackler CJ. Objective bayesian analysis in acoustics. *Acoust Today* May 2015;11(2):54–61.

- [13] R.C. Maher Acoustical characterization of gunshots", in Proceedings of Signal Processing Applications for Public Security and Forensics Workshop 'SAFE 2007 2007 Washington D.C.
- [14] Ylikoski ME, Pekkarinen JO, Starck JP, Pääkkönen RJ, Ylikoski JS. Physical characteristics of gunfire impulse noise and its attenuation by hearing protectors. *Int J Audiol* 1994;24(1):3–11.
- [15] Tsiatis NE. Understanding distance shooting and the type of firearm from the analysis of gunshot sounds. *Euro Police Sci Res Bulletin* 2016;15.
- [16] Salomons EM. Computational atmospheric acoustics. Kluwer Academic Publishers; 2001.
- [17] Dazel O, Groby JP, Horoshenkov KV. Asymptotic limits of some models for sound propagation in porous media and the assignment of the pore characteristic lengths. *J Acoust Soc Am* 2016;139(5):2463–74.
- [18] Attenborough K. Outdoor ground impedance models. *J Acoust Soc Am* 2011;129(5):2806–19.
- [19] T.E. Nikolaos. (2010). "Recording and Calculating Gunshot Sound—Change of the Volume in Reference to the Distance", Proceedings of the AIP Conference, 1203(1), 846-85, (Jan 2010).
- [20] Acoustics – Preferred frequencies, ISO Std. 266, 1997.
- [21] Parry JA, Horoshenkov KV, Williams DP. Investigating uncertain geometries effect on sound propagation in a homogeneous and non-moving atmosphere over an impedance ground. *Appl Acoust* 2020;160:107–22.

D CONCLUSIONS

D.1 Key conclusions

The aim of this thesis has been to explore the effects of uncertainty in outdoor sound propagation, with attempts to simplify methodologies where possible. While there are a wide range of methodologies concerning the prediction and quantification of outdoor sound propagation. These studies have maintained direct focus on the understanding of the foundational behaviours. While the possible limitations highlighted in each paper have been discussed, the understanding of statistical behaviours, both in the theoretical and practical aspects, are widely misunderstood. This thesis has made progress towards providing the insight into and highlight the use of understanding statistical behaviours, both forward-wise and inverse, of outdoor sound propagation. This has been collectively done by the papers presented in this thesis, where now the overall impact of this research is discussed.

The initial aims of this thesis, to establish a thorough foundation in the understanding of the statistical behaviour in outdoor sound propagation in relation to the uncertainties present, were addressed in **Paper I**. Most studies assume behaviours from the interactions seen at a foundational level, yet this work shown that there are significant behaviours in the statistical moments that relate directly to the strength of the uncertainty, acoustical hardness of the ground and the geometry of the scenario, which are commonly not employed in the most effective manner. The predicted mean is shown to hardly vary, yet the mode is sensitive to the manipulation of the geometric ratio between the receiver height and range. This greatly effects which parameter estimation methods will and will not be effective. Since the geometric ratio of range and receiver height is also found to be the dominant parameter in shaping the distributions, this would be the most effective parameter for both use for in inverse and forward sampling, especially in combination with Bayesian methods using the distributions detailed in **Paper I**. The acoustical hardness of the ground is found not be greatly influential with the presence of geometric uncertainty, with only minimal evidence of differences in the jump from a soft ground ($\sigma_g = 500 \text{ kPasm}^{-2}$) to a very hard ground ($\sigma_g = 20,000 \text{ kPasm}^{-2}$). This does hint that the quantification of the ground is not crucial in outdoor sound propagation studies, which is corroborated by the results from the later studies.

The results of **Paper I** helped navigate towards further research ideas regarding forward-wise uncertainty studies. **Paper II** looked at implemented a differing physical method, inspired by current standard practices in related acoustic measurements, to understand more greatly the statistical behaviour of common acoustical quantities. As highlighted in the results from **Paper I**, the acoustical hardness of the ground was found to be minimally influential, even at large uncertainties ($\Delta = 35\%$) in the simulated data. This uncertainty was only found to be influential when there was uncertainty in the geometry. The physical implication of this method are promising, as with ranges of greater than 150m, the uncertainty present seems to be completely nullified, giving rise to more accurate measurements with recording of acoustical data with this method at the given ranges. There is a direct relationship highlighted between the results and frequency however, with lower frequencies being unable to be determined efficiently. This is believed to likely be due to the distance of separation chosen between the microphones.

Paper III and **Paper IV** complete the research of this thesis, reversing the direction of the uncertainty, to assess methods to be efficiently used in general and for a defined small firearm source. Each paper is separate in their study, but the implementation of reversing the likelihood function, in combination with simple engineering models, to invert parameters from given acoustical data from differing simple acoustical models is shown to be highly effective when considering computational costs, and accuracy when Bayesian methodology is applied. The explicit defining of the likelihood function, and ways it can be implemented with common engineering models and user-defined uncertainties, while not revolutionary in statistical terms, allows for any acoustician to apply such methods to their given problems with ease, aiming to improve studies of uncertainty within acoustics, even to the most complex cases. The results directly related to specific firearm sound source also serve to be novel. While most detection methods for gunfire rely on the bullet, which is complex supersonic problem, it has been shown in **Paper III** and **Paper IV** that isolating the sound waves from the infrasonic explosion of the bullet leads to far greater accuracy. The application to the development and/or improvement security and military applications is greatly apparent. It was found to be true again that only the geometric uncertainties effect the accuracy of the results, with the ground being non-influential and confirmed to be the non-dominant parameter when both the geometry and the acoustical hardness of the ground were uncertain, just as presented in **Paper I** and **Paper II**. It should be pointed out however, that in this instance it could be a direct relation

to the specific low-frequency sound source of a firearm, but it is interesting that this behaviour would arise again.

D.II Future works

Each of the papers presented in this thesis has contributed scientific advances towards the understanding of, and the ability to overcome, the problems faced due to uncertainties in outdoor sound propagation. While interesting progress has been made, the research has raised further questions that future research should answer. While each paper did discuss aspect for future works, this section reflects on the compiled research and outlines several key examples where this work could be extended and built upon.

Mimicking the studies of **Paper I** and **Paper II** to other acoustical models is the next important step. The models used in this research were intentionally simple for computational costs and clarity of understanding, however there are additional parameters that can effect outdoor sound propagation. Preliminary studies have shown complex models that account for metrological effects, in the case of non-extreme but uncertain atmospheres, are simply not worth the computational costs and do not greatly improve the accuracy that can be obtained using the statistical and/or simpler methods outlined in this thesis. This however does need further study to expand the validity of this claim and to improve the knowledge of statistical behaviours of these effects in the literature.

Using the two-microphone method experimentally to build a substantial knowledge database, defining its effectiveness in relation to the separation of the receiver array in relation to the frequency of the source and geometry should be established. Quantification of the optimal array for a given scenario gives rise to improving recording techniques for acoustical research and for immediate applications in industry.

The development of an advanced neural network (ANN) was investigated briefly, based on the results from **Paper III** and **Paper IV**. Due to the computational cheapness of the methods applied, and the further understanding of what frequencies can be efficiently used to detect and locate gunfire, an extremely powerful ANN could be developed for use in military and security applications. The cheapness of its initial development allows for either the development of a mobile instate-response model, or mounting to a receiver to which more power can be used to greater depth in the network without losing speed in response time. There

are also opportunities to apply such statistical (and related) methods to other cases, yet the effectiveness of the ANN would be greatly influenced by the understanding of the architect who designs the learning algorithm, in relation to the characteristics of the acoustic problem.

D.III Closing remarks

This thesis presents research that has provided insight into the application of statistical methodologies, both with uncertainty present in prediction and in inversion, to outdoor sound propagation problems. Consistent, although not revolutionary, improvements are made in the characterisation of parameters and development of complex engineering models thought to be useful in outdoor sound propagation. Yet this research has highlighted gaps in the foundational understanding of the methodology being employed, for which with some intuitive statistical thinking, could bring vast improvements to outdoor sound propagation.

The importance of effectively employing statistical methodologies into outdoor sound propagation problems, along with understanding of the resultant statistical behaviour, is evident, especially with the successes highlighted while using simpler engineering models. The expansion into more complex statistical methods, now that more understanding of the foundational statistical behaviours has been established, can only serve to improve the results seen in this thesis and likely outperform the methods that expend their computational costs on the engineering models.

E BIBLIOGRAPHY

- [1] J. A. Parry, K. V. Horoshenkov and D. P. Williams. *“Investigating Uncertain Geometries Effect on Sound Propagation in a Homogeneous and Non-Moving Atmosphere over an Impedance Ground”*, Applied Acoustics, 160. (March 2020).
- [2] C. L. Pettit and D. K. Wilson. *“Uncertainty and stochastic computations in outdoor sound propagation”*, Journal of the Acoustical Society of America, 135(4). (May 2014).
- [3] C. L. Pettit, D. K. Wilson, V. E. Ostashev and S. N. Vecherin. *“Description and quantification of uncertainty in outdoor sound propagation calculations”*, Journal of the Acoustical Society of America, 136(3). (September 2014).
- [4] K. Attenborough, K. M. Li and K. V. Horoshenkov. Predicting Outdoor Sound. CRC Press. (2006).
- [5] D. C. Hothersall and J. N. B. Harriott. *“Approximate models for sound propagation above multi-impedance plane boundaries”*, Journal of the Acoustical Society of America, 97(2). (Feb 1995).
- [6] R. Kruse and V. Mellert. *“Effect and minimization of errors in in situ ground impedance measurements”*, Applied Acoustics, 69(10). (October 2008).
- [7] E. M. Salomons. Computational Atmospheric Acoustics, Kluwer Academic Publishers. (2001).
- [8] O. Dazel, J. P. Groby and K. V. Horoshenkov. *“Asymptotic limits of some models for sound propagation in porous media and the assignment of the pore characteristic lengths”*, Journal of the Acoustical Society of America, 139(5). (May 2016).
- [9] K. Attenborough. *“Outdoor ground impedance models”*, Journal of the Acoustical Society of America, 129(50). (May 2011).
- [10] D. W. Scott. *“On Optimal and Data-Based Histograms”*, Biometrika, 66(3). (Decemeber 1979).
- [11] A. Ghasemi and S. Zahediasl. *“Normality tests for statistical analysis: a guide for non-statisticians”*, International Journal of Endocrinology Metabolism, 10(2). (April 2012)

- [12] P. J. Curran, J. F. Finch and S. G. West. *“Structural Equation Modeling: Concepts, Issues, and Applications”* in Structural equation models with nonnormal variables: Problems and remedies, Sage Publications Incorporated. (1995)
- [13] A. Field. *Discovering Statistics Using SPSS*, London: Sage Publications Ltd. (2009).
- [14] M. A. Stephens. *“EDF Statistics for Goodness of Fit and Some Comparisons”*, Journal of the American Statistical Association, 69(346). (September 1974).
- [15] A. H. Elhan, D. Oztuna and E. Tuccar. *“Investigation of four different normality tests in terms of type 1 error rate and power under different distributions”*, Turkish Journal of Medical Sciences, 36(3). (January 2006).
- [16] “ISO 9613-2:1996”. ISO, 12 June 2017, <https://www.iso.org/standard/20649.html>.
- [17] “European Commission”. CORDIS, <https://cordis.europa.eu/project/rcn/57829/factsheet/en>.
- [18] J. A. Parry, K. V. Horoshenkov and D. P. Williams. “Pressure ratio and phase difference in a two-microphone system under uncertain outdoor sound propagation conditions.” *Applied Acoustics*, 170 (December 2020).
- [19] J. M. Sabatier, R. Raspet, and C. K. Frederickson. *“An improved procedure for the determination of ground parameters using level difference measurements”*, Journal of the Acoustical Society of America, 94(1). (1993).
- [20] G. A. Faranosov, I. V. Belyaev, V. F. Kopiev, M. Y. Zaytsev, A. A. Aleksentsev, Y.V. Bersenev, V. A. Chursin and T. A. Viskova, *“Adaptation of the azimuthal decomposition technique to jet noise measurements in full-scale tests”*, American Institute of Aeronautics and Astronautics, 55(2). (2017).
- [21] Y. Hosokawa, Y. Hirano, D. Kominami, I. Aihara and M. Murata, *“Implementation of a real-time sound source localization method for outdoor animal detection using wireless sensor networks”*, Proceedings of the 13th International Conference on Signal Processing and Communication Systems. (Gold Coast, 2019).

- [22] American National Standard – Method for Determining the Acoustic Impedance of Ground Surfaces, ANSI/ASA S1.18. (2018).
- [23] J. A. Parry, K. V. Horoshenkov and D. P. Williams. “*Outdoor Acoustics: Range Estimation of Gunfire Over An Acoustically Soft Impedance Ground In A Homogeneous Atmosphere*”, Proceedings of the International Conference on Statistics: Theory and Applications. (Lisbon, 2019).
- [24] M. S. Paoella, “*Likelihood*”, in *Fundamental Statistical Inference: A Computational Approach*, Oxford, England: Wiley. (2018).
- [25] D. Cousineau and S. Hélie, “*Improving maximum likelihood estimation with prior probabilities: a tutorial on maximum a posteriori estimation and an examination of the Weibull distribution*”, *Tutorials in Quantitative Methods for Psychology*, 9(2). (2013).
- [26] J. A. Parry, K. V. Horoshenkov and D. P. Williams, “*On the uncertainties in outdoor sound propagation over a porous ground*”, in *Proceedings of the Institute of Acoustics ‘ACOUSTICS 2019’*, (Milton Keynes, 2019).
- [27] R. C. Maher. “*Acoustical characterization of gunshots*”, in *Proceedings of Signal Processing Applications for Public Security and Forensics Workshop ‘SAFE 2007’*, (Washington D.C., 2007).
- [28] Acoustics – Preferred frequencies, ISO Std. 266, 1997.
- [29] J. A. Parry, K. V. Horoshenkov and D. P. Williams. “*Likelihood maximisation techniques for ranging gunfire over grassland*”, *Applied Acoustics*, 164. (July 2020).
- [30] K. V. Horoshenkov, A. Khan and H. Benkreira, “*Acoustic properties of low growing plants*”, *Journal of the Acoustical Society of America*, 133(5). (2013).
- [31] D. Colton, H. W. Engl, A. K. Louis, J. McLaughlin and W. Rundell. *Surveys on Solution Methods for Inverse Problems*, Springer Science & Business (Dec 2012).
- [32] T. Van Renterghem, D. Botteldooren. “*Variability due to short-distance favorable sound propagation and its consequences for immission assessment*”, *Journal of the Acoustical Society of America*, 143(6). (June 2018).

- [33] K. W. Lo and B. G. Ferguson. "Localization of Small Arms Fire Using Acoustic Measurements of Muzzle Blast and/or Ballistic Shock Wave Arrivals", *Journal of the Acoustical Society of America*, 132(5). (November 2012)
- [34] Lo, Kam W. "A Ballistic Model-Based Method for Ranging Small Arms Fire Using a Single Acoustic Sensor Node", *Journal of the Acoustical Society of America*, 145(4). (April 2019)
- [35] D. Pena, C. Lima, M. Dória, L. Pena, A. Martins and V. Sousa. "Acoustic Impulsive Noise Based on Non-Gaussian Models: An Experimental Evaluation", *Sensors*, 19(12). (Jun 2019).
- [36] X. Sheng and Y. H. Hu, "Maximum likelihood multiple-source localization using acoustic energy measurements with wireless sensor networks", in *IEEE Transactions on Signal Processing*, 53(1). (Jan 2005).
- [37] D. Caviedes-Nozal and J. Brunskog. "Parameter optimization of forward sound propagation models using Bayesian inference for sound field control purposes", in *Proceedings of Euronoise 2018*, (Crete, 2018).
- [38] N. Xiang and C. J. Fackler. "Objective Bayesian Analysis in Acoustics", *Acoustics Today*, 11(2). (May 2015).
- [39] M. E. Ylikoski, J. O. Pekkarinen, J. P. Starck, R. J. Pääkkönen and J. S. Ylikoski. "Physical Characteristics of Gunfire Impulse Noise and Its Attenuation by Hearing Protectors", *International Journal of Audiology*, 24(1). (April 1994).
- [40] N. E. Tsiatis. "Understanding distance shooting and the type of firearm from the analysis of gunshot sounds", *European Police Science and Research Bulletin*, 15. (Dec 2016).
- [41] T. E. Nikolaos. "Recording and Calculating Gunshot Sound—Change of the Volume in Reference to the Distance", *Proceedings of the AIP Conference*, 1203(1). (Jan 2010).